Nonlinear Wave Propagation in Brass Instruments

by

Janelle Resch

A thesis
presented to the University of Waterloo
in fulfillment of the
thesis requirement for the degree of
Master of Mathematics
in
Applied Mathematics

Waterloo, Ontario, Canada, 2012

I hereby declare that I am the sole author of this thesis. This is a true copy of the thesis, including any required final revisions, as accepted by my examiners.

I understand that my thesis may be made electronically available to the public.

Abstract

The study of wave production and propagation is a common phenomenon seen within a variety of math and physics problems. This thesis in particular will investigate the production and propagation of sound waves through musical instruments. Although this field of work has been examined since the late 1800s, approaching these types of problems can be very difficult. With the exception of the last fifty years, we have only been able to approach such problems by linearizing the necessary equations of gas dynamics. Without the use of a computer, one can only get so far in studying nonlinear acoustic problems. In addition, the numerical theory for nonlinear problems is incomplete. Proving stability is challenging and there are a variety of open problems within this field.

This thesis will be examining the propagation of sound waves specifically through brass instruments. However, we will not be able to fully examine this problem in a masters thesis because of the complexity. Instead, the objective is to provide a foundation and global picture of this problem by merge the fields of nonlinear acoustics as well as computational and analytical gas dynamics.

To study the general behaviour of nonlinear wave propagation (and to verify previous findings), experiments have been carried on a trumpet. The purpose of these experiments is take measurements of the sound pressure waves at various locations along the instrument in order to understand the evolution of the wave propagation. In particular, we want to establish if the nonlinear distortion is strong enough to have musical consequences; and if there are such outcomes, what prerequisites are required for the observable behaviour. Additionally, by using the discontinuous Galerkin numerical method, a model of the system will be presented in this thesis. It will then be compared with the experimental data to verify how well we were able to describe the nonlinear wave motion within a trumpet.

Acknowledgements

Firstly, I would like to thank my supervisors for all their support and guidance throughout my masters degree. Thank you Lilia Krivodonova for being so open about this project from the very beginning; I appreciate how much you did for me in order for me to obtain this position. To John Vanderkooy, I thank you for being so positive, patient and motivating throughout this whole process; your Feynman-like energy and enthusiasm was very inspiring. Also, despite the fact that you were not officially one of my supervisors, I would like to thank you Kevin Krauel for your constant assistance in the lab, continuous contributions in discussions, and your unconditional support and positivity.

I would also like to thank the following people for all their helpful discussions and support: David McKinnon, Michael Waite, Conrad Hewitt, J.P. Pretti, Francine Vinette, Dong-Eui Chang, Achim Kempf, Sue-Anne Campbell, Marek Stastna, Brian Ingalls, Eddie Dupont, Scott Mallais, Noel Chalmers, Dale Connor, Eric Ocelewski, Nathan Zavaglia, Kevin Liu and my family and best friend Keehan Koorn for her constant support and mathematical comic relief.

I also want to thank the following long-distance professors and students from other parts of Canada, the United States and Europe for sending me papers, theses, and just answering general questions: Chris Waltham, Orlando Richards, Stefan Bilbao, Johnathan Kemp, Joe Wolfe, Gary Settles, Brian Pandya, and William Strong. The fast replies, suggestions and motivation was very much appreciated.

Finally, I would also like to thank the Applied Mathematics Department at the University of Waterloo, especially the secretaries Helen Warren and Rina Salazar (without you, we would all be lost), for the great opportunity. Last but not least, I would also like to thank the SJU Mathematics Department and staff for all their support and kindness over the last couple years.

Dedication

This is dedicated to my fiancé, for all your love, help, patience and support. Never forget that my information will always love your information.

Table of Contents

List of Tables

List of Figures

Chapter 1

Introduction

1.1 Historical Background

The scientific study of sound is known as acoustics and began in the sixth century when Pythagoras became interested in the problem of a vibrating string [20, p. 10]. Although music has been an integral part of human experience for thousands of years, the scientific advances of acoustic theory have been rather slow. For instance, the concept that sound and wave motion are deeply related was not recognized until the 1600s [20, p. 1]. Almost no progress took place until the 1700s when the theory of sound propagation was connected with the basic theory of continuum physics by Leonard Euler [8, p. 5], [20, p. 2]. Through this relationship, scientists have been able to model linear acoustics by d'Alembert's equation (the wave equation). This equation was first derived for one-dimensional string motion. The wave equation was also a necessary stepping stone for the advancement of fluid mechanics and elasticity theory [20, p. 2]. However, from early on in the development of acoustic theory, it was realized that not all problems could be explained using the linear framework. For some problems nonlinear effects cannot be neglected. In general, linear acoustic theory is applicable for waves with sufficiently small amplitude. We refer to waves with non-negligible amplitude as finite amplitude waves. These waves must be described by nonlinear acoustic theory [8, pp. 2, 73].

The field of nonlinear acoustics has only drastically expanded in the last fifty years [8, p. 1]. The lack of progress is partly due to the fact that the majority of audible sound waves can be successfully described using linear acoustic theory [8, p. 1]. By taking a small amplitude linearization of the equations of gas dynamics, very reasonable approximations

can be obtained for audible sound waves [39, pp. 1-2]. Secondly, and more importantly, modeling waves in nonlinear acoustic theory is very difficult. The nature of this problem is complex and even with all the "good enough" approximations, it is computationally irreducible. Here, simulation itself cannot be avoided by any means of any shortcut. The only way to determine the solution to such a problem is to perform (i.e. simulate) the computation. This implies that computers are required to make significant progress [8, p. 2].

A few important properties of finite amplitude sound waves have been considered since the 1800s [8, p. 7]. In particular, large amplitude mechanical vibrations as well as the formation of shock waves were examined shortly after the one-dimensional wave equation was derived. George G. Stokes was the first person to identify the difficulty associated with the discontinuities arising in the nonlinear wave propagation [20, p. 3]. He also recognized that viscosity needs to be taken into account to accurately describe the observed discontinuities [8, p. 14]. Shortly after, William J.M. Rankine and Pierre H. Hugoniot were the first to attempt to find a solution. They successfully derived the expressions for conservation of mass, momentum and energy for the flow field in front and behind a shock wave [8, p. 8].[1] Then, in the 1900s, Lord Rayleigh (John W. Strutt) and Geoffrey I. Taylor were able to express the shock formation and propagation by taking viscosity into account. [8, p. 17], [20, p. 3].

Simultaneously, the study of sound production and propagation within musical instruments began. Research in the first half of the 1900s was focused on how the geometry of the instruments influences the sound production and propagation [6, p. 320], [46]. Brass instruments particularly are considered to be fascinating since they are the most difficult to understand given their geometry and length. For instance, they are much longer than woodwind instruments. Brass instruments are constructed with bends and coils as well as a large flare (called a bell) at the end of the instrument. Also, they have a mouthpiece compared to a reed or double-reed (which is usually used for woodwind instruments). Trying to incorporate the mouthpiece into a model for brass instruments is very difficult [24, pp. 429-432].

In the second half of the century the focus shifted to understanding the effects of nonlinear wave propagation [8, pp. 14-17]. Even though the importance of nonlinear effects was acknowledged, it was assumed that sound production and linear propagation within musical instruments could be properly described using small amplitude sound wave

[1] George G. Stokes was actually the first person to describe shock waves as 'surfaces of discontinuity'. He was actually the first person who derived the conservation laws over a discontinuity but received no credit (but his analysis did not have the proper tools from thermodynamics) [8, pp. 7-8].

models [20, p. 2]. Recently, it has been claimed that depending on the range and loudness of the notes being played on brass instruments, nonlinear effects may play a significant role in the acoustical wave propagation [8, p. 72]. In particular, it has been suggested that nonlinear wave propagation could be strong enough to cause the strengthening of higher harmonics and the formation of shock waves [29, p. 1754]. It has also been suggested that the nonlinear wave propagation is responsible for producing the elephant-like timbre heard when a player generates either very loud or high notes. [2] Therefore, in order to accurately describe sound production and propagation in brass instruments, the model should be nonlinear. [3]

1.2 Objective of the Thesis

The purpose of this thesis is to investigate sound production and propagation of finite amplitude sound waves within brass instruments. To accomplish this, experimental data has been collected to further understand the nonlinear behaviour associated with finite amplitude sound waves. By then using this information and incorporating it into a mathematical model, we performed a series of numerical simulations. The intention behind this was to verify if the observed nonlinear effects could be accurately described (in the mathematical sense). Although examining the complexity of the problem in its entirety will not be possible, the objective of this thesis is to obtain

* a deeper understanding of the current depiction of how these instruments function and

* to construct a foundation for further research in this area.

As a quick remark to the reader, although several musical instruments will be mentioned throughout the discussion, the focus will be on brass instruments. Moreover, this thesis will particularly be investigating the trumpet.

We will now quickly outline the presentation of this thesis. Chapter 2 will review the acoustic properties of brass instruments that are responsible for influencing the production

[2] In the literature, it is also very common for researchers to describe this timbre as the brightness of the sound [29, p. 1754]. The term *brassiness* is also used to describe this distinctive sound quality [29, p. 1754], [15, p. 1].

[3] It should be noted that although there also exists nonlinear behaviour in the wave propagation for woodwind instruments, because of the geometry of the bore as well as the mouthpiece, wave steepening is not experienced (which will be discussed later [29, p. 1755], [26]).

and propagation of sound waves. Firstly, section 2.1 will discuss how sound is produced by musical instruments assuming the amplitude of the sound wave is reasonably small. The limitations of neglecting the two different types of nonlinear effects [8, p. 19] will also be considered in this section. Secondly, specific brass instrument features such as the bell, mouthpiece or how the player controls aspects of the airflow will be examined in section 2.2. Finally, section 2.3 will provide an overview (from previous and current literature) of possible acoustic consequences associated with nonlinear wave propagation in musical instruments. For example, it is possible for shock waves to be generated at a certain distance called the shock distance (denoted by x_s) [8, p. 71], [29, p. 1755].

The next chapter will focus on developing the ideas within the language of mathematics. All prerequisite mathematical fundamentals will therefore be presented in chapter 3. Section 3.1 will discuss the necessary fluid dynamics (specifically gas dynamics) and its relation to sound. The equations of motion for small and large amplitude sound waves will be examined in section 3.2.

Before continuing on to construct a model however, further insight to the effects of nonlinear wave propagation is needed. Verification of previous findings is crucial. In chapter 4, we will present a series of experiments that were carried out in Dr. J. Vanderkooy's acoustics lab. The purpose of these experiments was to gather information regarding the acoustic properties of brass instruments and of finite amplitude wave propagation. The experimental set up and procedure can be found in section 4.1 and 4.2. In several experiments sound pressure measurements were taken at the mouthpiece, bend and bell of a trumpet. This allows one to determine how the frequency components of the sound waves interact and change as the waves propagates further through the instrument. Section 4.3 will examine the results to establish if the nonlinear effects become more influential at higher sound pressure levels or at higher frequency notes. This will enable us to verify if these nonlinear effects lead to only wave steepening or the generation of shock waves.

Chapter 5 will introduce the model and the numerical method that was used for a series of numerical experiments. The purpose of this is to determine how well the mathematical model fits the experimental data. The model was simulated using a discontinuous Galerkin numerical method implemented by Dr. L. Krivodonova. In section 5.1, the numerical method will be introduced, its formulation, and the discretization of the conservation laws. Furthermore, the initial and boundary conditions will be examined, including the meshes used in the simulations. Section 5.2.5 will discuss how neglecting the third dimension could potentially influence the outcomes since all simulation for this thesis were done in two dimensions.

The simulations that were carried out for this thesis will be illustrated in chapter 6. Section 6.1 provides an overview of two sets of experiments performed: *pulse experiments* and *waveform experiments*. The pulse experiments presented in section 6.2 were carried out for a group of small and large amplitude pulses to acoustically verify the numerical method; determine the propagation behaviour of loud, short wavelength pulses, and the shock distance inside the trumpet. Section 6.2 will also consider the influences the trumpet's geometry by simulating varying amplitude pulses in three different meshes. One mesh is a trumpet shape that includes a bend and a flare, the second mesh only considers a flare, and the third mesh is a straight tube. This is to establish the significance and necessity of considering a bend. This knowledge will be useful because the other numerical experiment will simulate particular musical notes measured in the lab. Ideally, if we could neglect the bend, it would result in less computation time. The outcomes of the waveform experiments are discussed in section 6.3. More specifically, section 6.3.1 begins by reconstructing the sound pressure waveforms, depicted in chapter 4 using Fourier analysis. This is to determine the importance of the harmonic components, and how many terms are needed to reproduce each measured tone. In addition, different expressions which relate the mouthpiece pressure to velocity will be examined. The results of the simulated notes will help establish how well simulated data fits the experimental data. Section 6.3.6 will briefly consider the importance of losses (and neglecting them). Finally, in section 6.3.7, we will verify if shock waves can be formed in a trumpet within a particular distance, known as the shock distance.

The chapter concluding this thesis, chapter 7, will evaluate and compare the findings from the experimental and simulated results. In particular, in section 7.1 we will determine how well the model described and approximated sound production and propagation within the trumpet given by a two dimensional mesh. Finally, section 7.2 will discuss possible future work and the limitations of the work presented within this thesis.

Chapter 2

Sound Production in Musical Instruments

Before approaching the mathematical formalism of wave propagation inside brass instruments, it is important that the conceptual aspects of such phenomena are understood. The purpose of this chapter is to describe how sound is produced by musical instruments and how the characteristics of musical instruments, such as the bell or mouthpiece, influence sound production. While the majority of the discussion will be focused on brass instruments, woodwind instruments will be introduced for comparative purposes.

2.1 Description of Sound Production in Brass Instruments

The subject of acoustic waves inside a horn [4] was discussed as far back as the eighteenth century. In particular, around 1770, Daniel Bernoulli, Leonhard Euler and Joseph Lagrange were the first to consider the equations of motion for waves inside of a horn. However, the theory that was developed became more useful when further applications were developed the 1920s [5, p. 405]. In this section we will introduce the physics that describes sound production inside musical instruments. The mathematical details will be presented in chapter 3.

When a player blows air into a musical instrument, the lungs of the player are considered as a source of air at constant pressure. The air from their lungs travels through a pressure

[4] A horn can also be referred to as a duct.

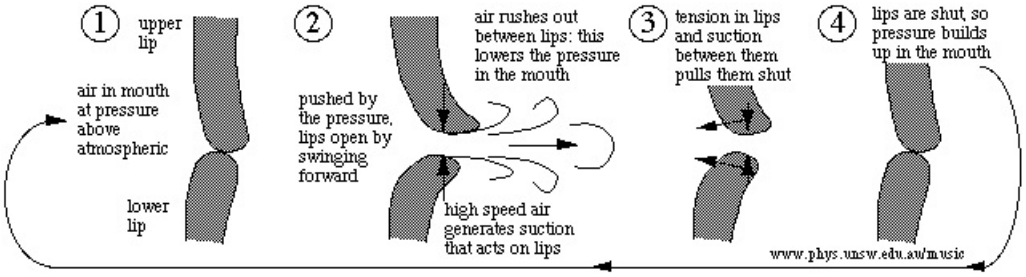

Figure 2.1: Lip behaviour when playing a brass instrument (from [55]).

control valve; which is the reed for woodwind instruments and the player's lips for brass instruments. The control valve is coupled to the air column of the instrument [5, p. 395] and can also be referred to as a mechanical oscillator [12, pp. 415-416]. [5] [6]

It is important to note that for reed instruments, the oscillations within the air column affect the oscillations of the reed. This results in the fundamental frequency (see footnote 9) being very close to the resonant frequencies of the instrument. For brass instruments however, the vibration of the lips is controlled by the acoustic pressure established in the mouthpiece in response to the airflow [5, p. 391]. Furthermore, this flow behaviour in the brass instrument may not be simply proportional to the acoustic pressure that controls it; this is referred to as nonlinear behaviour and is necessary in order for the sound to be transferred from the instrument to the listener (this will become apparent shortly) [29, p. 395].

Then, as the air travels through the mechanical oscillator modulating a flow disturbance produced by the source, a pressure wave is created that travels through the instrument. The opening and closing of the player's lips is basically periodic allowing the fluctuating volume flow of air (which itself is roughly periodic) to move into the air column (also called a resonator) [12, p. 416]. In addition, the air being blown into the instrument can cause acoustic pressure measurements which are a few tenths of a percent of one atmosphere [55], [12, p. 428].

[5]The control valve is analogous to a flow-control function that happens to be a complicated nonlinear process that is still not fully understood [5, p. 395]. Furthermore, it is coupled to the instrument's mechanical oscillator which can be treated as a linear vibrating system for woodwinds, but sometimes linearity breaks down for brass instruments [12, p. 428].

[6]If the reed-valve is nonlinear this means the flow through it changes such that the flow is not simply proportional to the acoustic pressure which controls it [5, p. 295]. Furthermore, if the reed-valve is nonlinear, then oscillation is favored if the air column has one or more natural frequencies that correspond to one or more of the higher partials of the tone being produced (from [5, p. 295]).

As mentioned, for both brass and woodwind instruments the puffs of air excite the air column of the instruments causing them to oscillate such that longitudinal pressure waves are created [24, p. 397]. Once the air within the instrument vibrates, some of the energy is radiated as sound out of the bell. In addition, there are energy losses in the instruments due to viscous friction and the transfer of energy in the form of heat from the wave to the wall of the instrument [5, p. 397], [12]. For instance, in the case of woodwind instruments most of the higher frequency harmonics lose energy due to viscous friction at the walls [8, p. 19], [12]. Comparatively, for brass instruments the radiated power (or energy output) can go up with frequency in a certain playing range. In other words, there tends to be a maximum radiation (i.e., a maximum energy output) at moderately high frequencies but less power at the lowest and highest frequencies. Consequently, there is a specific range in which the trumpet can transmit energy as sound [12, p. 428]. [7]

Once the pressure disturbance reaches the junction of the instrument (or the bell) and room, it is almost completely reflected with a change of sign [5, p. 397]. The reflection occurs because of the discontinuity in the wave impedance (which is the sound pressure divided by the product of the particle velocity and surface area), since the room has a much bigger cross-sectional area, the wave impedance is very small [5, p. 397]. Continuing, as the returning pulse travels back up the pipe, it combines with a new incoming disturbance to produce standing waves with amplitude ratios that depend on the relative strength of the reflection. Once the standing waves are sustained inside the instrument, a large pressure disturbance is generated in the pipe [5, p. 391]. [8]

It is important to point out that the reflections of the pressure disturbances also depend on the frequency of the note being played. In general, the air column of an instrument responds (so the air inside vibrates) stronger to waves of certain frequencies compared to others; these special frequencies are called resonant frequencies [5, p. 399]. [9]

For brass instruments, the lower frequency sound waves travelling from the mouthpiece towards the bell are mostly reflected further inside the bell, around the junction of the

[7] When a sustained note is heard, this implies the player is constantly blowing into the instrument supplying energy to maintain the oscillation of the air column [55], [12, p. 416].

[8] In other words, if the disturbances excite the air column at one of it's characteristic frequencies, the corresponding vibrational shape builds up in the horn. At other specific frequencies, the returning pressure wave arrives out of phase and the overall response of air column is minimal (from [5, p. 399]).

[9] A musical tone can be written as the sum of simple harmonic functions (waves) of time for each of the various harmonic frequencies. If the period of the vibration is T, the fundamental angular frequency will be $\omega = \frac{2\pi}{T}$ and the harmonics will be 2ω, 3ω , etc. [21, s. 50-2]. The magnitude of each harmonic wave is what gives the tone a certain timbre (i.e. quality of sound) [55]. In order to play different tones, the player must adjust the length of the instrument to produce new resonant frequencies by using the valves [55].

cylindrical tube and bell. This is why one can auditorily perceive low frequencies as soft notes, because only a small amount of energy initially emits from the bell [42, pp. 251-254], [5, p. 397]. Conversely, higher frequency waves penetrate the regions of greater flare; this area is known as the *acoustically forbidden region* [5, p. 406]. According to literature, frequencies over 1500 Hz mostly propagate out of the bell. This is why high frequency notes are perceived to be so much louder, because more of the initial energy propagates out the bell to the listener in a range sensitive to our ears [42, pp. 251-254], [5, p. 406]. This means at high frequencies the air column can be considered as a sort of megaphone rather than a resonator, propagating the majority of the frequency spectrum into the space without reflection [5, p. 404]. Nonetheless, assuming an acoustic pressure disturbance is generated in the instrument, it will propagate up and down the tube until the disturbance in the air spreads out as a travelling sound wave (the number of vibrations per second is what we have been referring to as frequency) [5, p. 391], [42, p. 246]. Once the longitudinal waves are emitted from the bell, they propagate outward with spherical symmetry and are composed of multiple frequencies. The sequence of multiple frequency waves gives each note its tone colour or character [21, s. 50-2], [24]. The vibrations in the air will propagate until they reach the little hairs in our ears which send a signal to the brain allowing one to recognize these vibrations as sound (in very simple terms) [42, pp. 242-246], [24].

2.1.1 Limitations of Small Amplitude Sound Wave Description

The amplitude of most audible sound waves is only a small fraction of atmospheric pressure. In such cases, it can be assumed that the sound pressure waves in the air will exhibit linear behaviour and in regards to the mathematics, this implies a small amplitude linearization of the equations of motion from gas dynamics can be made [8, pp. 14-15]. The description in section 2.1 is based on this linearized framework. However, for brass instruments, the previous explanation is accurate only for low volume and low frequency notes. These simplifying assumptions start to break down once loud or high frequency notes are played [8, pp. 71-74].

In the cylindrical part of the instrument, where the cross-sectional area is the smallest, the sound pressure will be highest. As the pressure wave propagates from the mouthpiece towards the bell, the majority of the harmonic components below a certain frequency are reflected to generate standing waves. The energy of the low frequencies is confined by the boundary of the tube, providing an exaggerated amplification effect to the waves within the instrument. Thus, the pressure variations can be a significant fraction of atmospheric pressure in the narrow tubing [42, pp. 251-252]. This can potentially allow the nonlinear

behaviour from the high amplitude propagating waves to escalate having considerable consequences [8, p. 19], [48].

However, before continuing and in order to avoid confusion (and to be consistent with previous literature), it is important to distinguish that for finite amplitude sound waves, there are two types of nonlinear effects, *cumulative* and *local* [8, p. 19]. Cumulative nonlinear effects are usually more influential, especially in the case of progressive waves [8, p. 73]. In particular, these effects are caused by variations in the propagation speed of the waveform. This results in wave distortion that builds up with distance [8, p. 19]. [10] [11] Local nonlinear effects also cause distortion, however the difference is these nonlinearities do not develop with distance [8, p. 73]. Therefore, this type of nonlinearity can usually be ignored. An example of a local effect is the pressure-particular velocity (impedance) relation [8, p. 10]. However, one local nonlinear effect that is important is the local distortion that is caused near the source (i.e. the nonlinear vibration of the lips.) [8, p. 73].

Overall, the significance of nonlinear effects for finite amplitude sound waves can lead to: the development of shock waves; converting power from low to high frequencies and possibly producing other frequencies [8, p. 19], [48]. In general, it is possible for a wave to develop other frequencies (rather than just integer multiples of the fundamental) within a brass instrument because of how the instruments are designed. The resonances for cylindrical pipes that are closed at one end are odd harmonics of its fundamental frequency. But for brass instruments, except for the fundamental, the second and all higher resonances have risen such that the frequency ratios form a complete harmonic series. Furthermore, these higher resonances merge allowing the lips to more easily produce a nonlinear vibrations (i.e. nonsinusoidal) at the frequency of the missing fundamental [55],[19, p. 181].

Thus, it is reasonable to assume that nonlinear effects can influence acoustic wave propagation. However, before discussing how to take these effects into account, it is important to consider how the physical properties of brass instruments, such as the bell or mouthpiece (i.e. the geometry), influence the production of sound.

[10] Fay described in the 1930s that "wave distortion generally tends to enrich the higher harmonic components at the expense of the lower ones (energy transfer effect), while viscosity damps out the higher components more rapidly than the lower ones. He reasoned that a balance should be reached in which a given component loses as much energy by absorption as it gains from nonlinear distortion [8, p. 19]."

[11] "Convection and nonlinearity of the pressure-density relation are classified as cumulative nonlinear effects because they case waveform steepening [8, p. 73]."

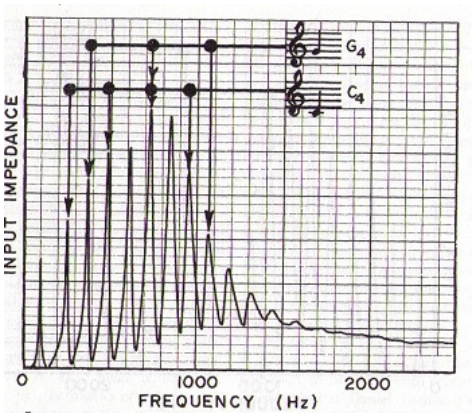

Figure 2.2: Resonance curve of a B^b trumpet showing the regimes of oscillation for C_4 and G_4. Shows relative amplitude of the initially measured partials belonging to C_4 and indicates the strength of the first 11 partials produced when the trumpet is played at forte (from [5, p. 206]). [12]

2.2 Properties of Musical Instruments that Influence Sound Production

2.2.1 The Difference between Playing Loudly and Softly

In music, dynamics usually refers to the volume of a sound or note. This term is also used to refer to the printed musical notation in a composition to indicate a note's (or section of notes) volume. However, this terminology can be confusing, so from now on we will just refer to the loudness of a note as either piano, denoted *p*, for a soft note (which is the literal meaning in Italian) or forte, denote *f*, for a loud note (again, the literal meaning in Italian) [42, p. 35]. [13]

In general, the volume of a musical tone is important because the loudness of a note changes the timbre (quality of sound). In the case of musical instruments, the player is partially able to control the volume of a note by manipulating the lip movement [55]. For instance, in the case of brass instruments, if a player wants to produce a low frequency musical tone at *p*, the waveform of the sound wave is almost completely sinusoidal [5, p. 418]. This implies that the fundamental of the wave will be strong (specifically only the

[13] It is important to note that these terms are not defined as certain decibel levels.

second mode of the pipe is maintaining oscillation). Furthermore, the higher harmonic components will be weak meaning the timbre of the tone played will be rather mellow [55].

However, as the musician plays the note increasingly louder, the player's lips not only move more abruptly but the lips also close. This means that the physical movement of the lips does not have a sinusoidal pattern but moreover, this produces a sound wave where the waveform is not sinusoidal (i.e. the waveform is distorted and this is characterized as nonlinear behaviour) [19, p. 181], [29, p. 1756]. As the lip movement becomes more irregular and the distortion of the sound wave becomes more prominent with volume, the sound spectrum develops and the harmonics (starting with the lower partials) become more significant [5, p. 418]. In other words, stronger harmonics are generated which interact and reinforce each other [14] such that the resonance frequencies influence the region of oscillation in order to stabilize the tone [5, p. 393]. [15] Thus, the upper harmonics do not contribute to maintain oscillation but rather influence the oscillation to make it stable. This implies the timbre of the note will be brighter, but the sound will also be louder since more energy escapes from the bell [55]. It is interesting to note that for loud tones, even if the player was able to control the opening/closing lip movement to make it roughly sinusoidal, the airflow through the lips is not usually sinusoidal due to the nonlinear behaviour of the control valve and mechanical oscillator (see footnote 5) [5, p. 394].

2.2.2 Effects of the Bell

One of the most important properties and effects of the bell is the way it influences the reflections of the sound pressure waves. Recall that where a pressure wave is reflected in the bell of a brass instrument depends on the frequency of the wave. Aside from the discontinuity of the wave impedance at the bell, this is because the wavelengths of lower notes are not short enough to propagate through the bell effectively (especially because of the curvature). Since shorter wavelengths (i.e. higher frequency notes) can travel further into the acoustically forbidden region, it is more likely that they will either completely escape from the bell or lose part of their energy [5, p. 406]. This implies that the higher frequency waves are more efficiently radiated as sound outside the instrument [55], [5, p.

[14] For example, according to literature, this can particularly be seen for the 4, 6, and 8 harmonic [5, p. 418].

[15] As a remark to the reader: a regime of oscillation is that state of the collective motion of an air column in which the reed or lips collaborate with a set of air column modes to maintain a steady oscillation containing several harmonically related frequency components, each with its own definite amplitude. And this is the other and greater component that drains energy from the system, inefficiency in the mouthpiece (from [5, p. 395]).

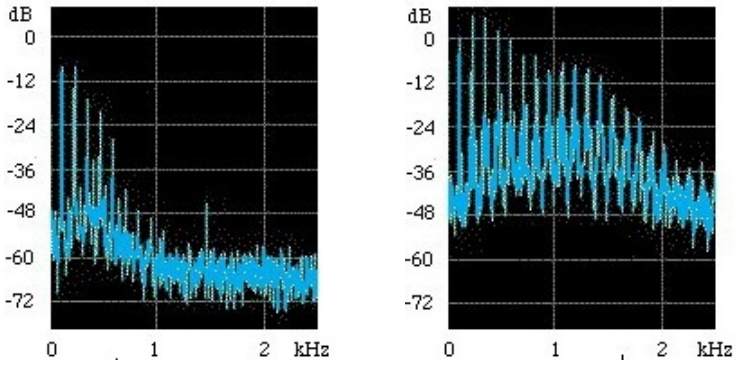

Figure 2.3: Pressure waveform for C_4 being played at (left) p and (right) at f (from [55]).

411]. The improved sound emission at the bell (for short enough waves) is done so well that the power of the harmonics does not decrease with frequency as strongly as it does in the woodwinds [48], [5, pp. 411-414].

The disadvantage however is that high transmission implies low reflection; and low reflection means weak standing waves, weak resonances and rather flexible notes. Obviously, total absence of reflection would presume no standing waves. Although, this can happen when the wavelength becomes comparable with the radius of curvature of the bell. In this incredibly high range, the trumpet acts just like a megaphone for the player's lips [55].

In figure 2.4, one can see how the bell influences the input impedance curves. The lower figure demonstrates that resonance peaks lose amplitude at excitation frequencies above 1500 Hz [5, p. 399]. The majority of these components sent down toward the bell propagate almost completely into the room with very little of the sound returning to form standing waves [5, p. 399]. The resonance peaks become shorter as the frequency increases because of frictional losses and thermal dissipation at the pipe walls increase with frequency [5, p. 399]. Furthermore, the peaks overall are lower in the bottom figure compared to the top figure. This is because the waves spread out (without a reduction of energy) as they enter the bell due to the dramatic increase of the cross-sectional area [5, p. 399]. Also, if there is a higher dampening affect due to frictional losses, the peaks broaden and the curve becomes smoother [5, p. 400].

Figure 2.5 also demonstrates how the bell manipulates the characteristic shapes of the pressure distribution in a flare horn. In particular, the mode shapes are like sinusoids that are progressively stretched out in the parts closest to the open end. The shape will be most deformed nearest to the bell because of the reflection behaviour in this region (from

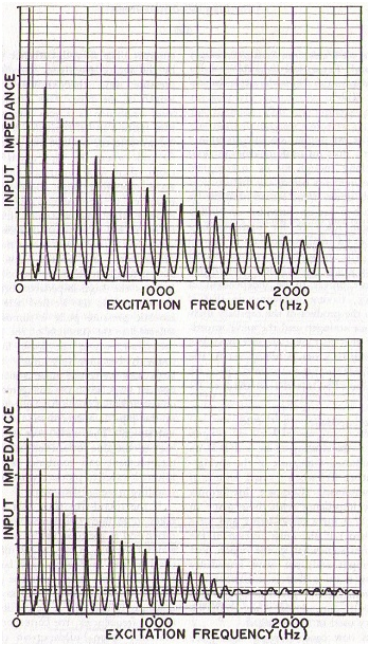

Figure 2.4: Input impedance curves for a piece of cylindrical tubing only (top) and for a piece of tubing with a normal bell (bottom). Notice that when the bell is added, the peaks become negligible after 1500 Hz (from [5, p. 398].)

[5, p. 407]).

2.2.3 Effects of the Mouthpiece

The mouthpiece is an important part of a brass instrument for two reasons. First, the mouthpiece allows the lips to be comfortably connected to the instrument. This permits the player to have more control over the sound production (for instance, playing at a specific volume). Secondly, the structure of the mouthpiece, influences the sound production. For example, a mouthpiece that has a deep funnel promotes less steep waveforms compared to a shallower shape [55], [44].

It is also interesting to note that a brass instrument mouthpiece has its own natural frequency. This frequency can be adjusted depending on the volume of the bowl of the mouthpiece. In particular, the larger the volume, the lower the first natural frequency is [55]. Although, in general, a brass mouthpiece has its first natural frequency near 875 Hz [5, p. 401]. In figure 2.6, it is evident how the natural frequency of the mouthpiece biases

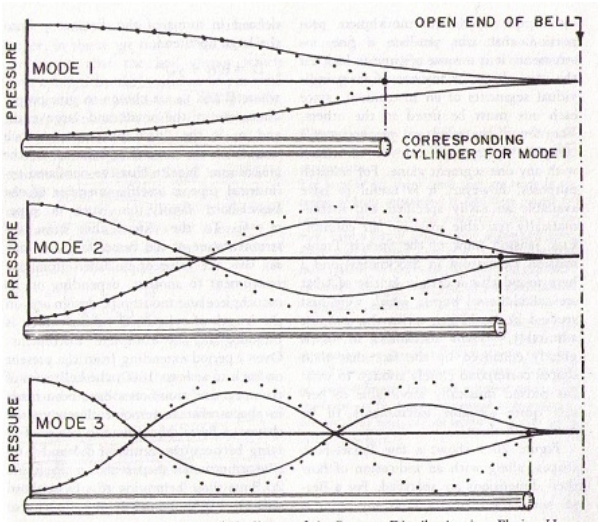

Figure 2.5: The first three characteristic shapes of the pressure distribution in a flaring horn (solid lines) and the sinusoidal shapes (dots) (from [5, p. 407]).

the input impedance of the trumpet. When the mouthpiece is added to the instrument, the highest input impedance peak shifts from approximately 150 Hz to 875 Hz.

2.3 Consequences of Nonlinear Wave Propagation inside Musical Instruments

The speed with which a finite amplitude wave propagates in the air column of the instrument depends on the amplitude of the pressure disturbance. If the pressure pulse leaving the mouthpiece of an instrument has a large enough amplitude, the crest of the pulse will travel noticeably faster than the trough. This will cause the waveform to steepen, and eventually, a shock wave will form. This will occur if the air column in the instrument is long enough and the nonlinear effects are strong enough [8, p. 8]. Although wave propagation is nonlinear in both woodwind and brass instruments, the formation of shock waves only occurs in brass instruments such as the trombone and trumpet (or so literature says) [29, p. 1756], [26].

There are two reasons why nonlinear effects are more apparent in brass instruments. Firstly, the wave entering the tube of the instrument is steeper when produced by a mouthpiece compared to a reed. Secondly, since brass instruments are longer, the waves travel a

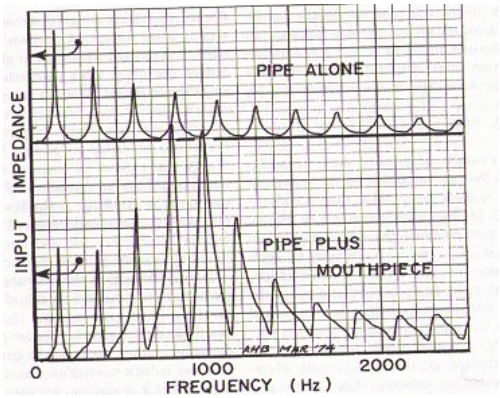

Figure 2.6: The input impedance curves for a piece of cylindrical trumpet tubing (top) and the tubing with mouthpiece attached at input end (bottom) (from [5, p. 402]).

longer distance before reaching the bell. In other words, the waves have a longer time to steepen further. Below we discuss this in more detail [29, p. 1756], [26], [34].

The paper [29], was the first (and only) article to argue (using experimentally obtained images) that shock waves develop in trombones. The authors also provided a rationalization for this hypothesis coming up with two main conclusions from their investigation. One reason brass instruments exhibit stronger nonlinear behaviour compared to woodwinds is because of the geometry of the mouthpiece [29, pp. 1755-1756].

For brass instruments, a player has to direct the airflow precisely into a tiny hole in the centre of a cone-like metal mouthpiece. Also, the aperture between the lips is much larger than the neck of the mouthpiece. Since the neck controls the flow, this means when a player closes their lips (which is usually the case when playing loud or high frequency notes), the lip movement is more vigorous in a short period of time generating a more erratic acoustic pressure [29, p. 1755], [5, pp. 390-395]. So if low frequency pulses are considered, the player's lips do not need to oscillate nearly as much, and they usually do not close. This implies that the pressure pulse created is fairly constant [16] and the oscillatory pressure pulse is close to the player's driving pressure of air [5, p. 402]. However, for high frequency pulses (or loud ones), the irregularity of the fluctuating pressure associated with the airflow becomes stronger at higher playing levels. This generates a highly non-sinusoidal pressure pulse at the mouthpiece [5, p. 402], [29]. [17]

In comparison, the clarinet has a smaller neck relative to the cross-sectional area of

[16] Within this context, a constant pressure pulse means it is sinusoidal, it is not erratic and the higher frequency components have a negligible amplitude.

[17] Consequently, the acoustic pressure in that relatively narrow pipe ceases to be tiny in comparison with

its pipe with the reed controlling the airflow. More importantly, the mouthpiece of most woodwind instruments (which is where the reed is attached) is curved unlike the mouthpiece for brass instruments. Because of this geometry, when the lips close, the flow is not completely cut off as it is for brass instruments. Instead, the reed closes at the opening of the mouthpiece rather slowly. This implies that the mouthpiece pressure for all dynamics is close to sinusoidal. Thus, the nonlinear effects due to wave propagation for the clarinet are not nearly as strong as in the trumpet or trombone [29, p. 1755], [24].

The air column length of instruments is another feature that influences the production of shock waves. This is because a certain distance is necessary for a pressure wave to steepen into a shock wave. The typical equilibrium length (i.e. when the slide/valves are not being used) of a B^b trombone is 2.74 m (B^b trumpet is 1.48 m), whereas a B clarinet is only around 0.6m. Since the trombone is composed with more tubing, it is more likely that a shock wave can develop. Additionally, the airflow of brass instruments is more susceptible to stronger nonlinear effects (because the pressure associated with the airflow at the mouthpiece is nonsinusoidal). This further implies that pressure waves inside a trombone are more likely to steepen compared to a clarinet [12, p. 428], [29, pp. 1755-1756].

This description leads to a natural question, how much length in the tube of an instrument is needed in order to produce a shock wave? Hirschberg, Msallam and Wijnands pursued to answer this question by using the classical method of characteristics to derive an expression for what is known as the *shock distance*. That is, the distance required for a shock wave to be produced inside an instrument [29, p. 1755]. However, it is important to note that this derivation was done assuming a simple wave propagates through a uniform region. This assumption is based on the fact that most of the high frequencies produced in a brass instrument are radiated into the room instead of being reflected [5, p. 404].

2.3.1 Shock Distance

Although certain insights were given by Euler, Earnshaw and Lagrange [8, pp. 10-11], it was Poisson who found the exact solution for finite amplitude waves (equation (2.1)) by using Boyles law on Eulerian coordinates as well as a velocity potential. However, he interpreted his solution incorrectly [8, p. 6].

atmospheric pressure. When this happens, the linear wave equation for air no longer applies, resulting in a greater number of stronger, higher harmonic components present in the sound. When the sound is actually heard by a listener, the note will have a harsh, and almost unmusical [55].

Let us consider a boundary at a fixed point x_o that has a velocity $u(x_o, t)$ for all time (this is called the source condition). Then, the wave propagation for outgoing waves, that is, in the positive x direction, can be described by the following equation

$$\frac{\partial u}{\partial t} + (c_o + \beta u)\left(\frac{\partial u}{\partial x}\right) = 0, \tag{2.1}$$

where u is the particle velocity, c_o is the sound speed, β is the coefficient of nonlinearity [8, p. 10-11] [18] and t is time. The solution to (2.1), known as Poisson's solution, is

$$u = f\left(t - \frac{x}{c_o + \beta u}\right), \tag{2.2}$$

where f is a function of time. It can be found by using the initial condition [8, p. 11]. The solution (2.2) is known as Poisson's solution. However, it is important to note that in (2.1) energy losses and viscosity are not considered, so strictly speaking, this model fails after the shock forms [8, p. 71].

In order to obtain the shock formation distance x_s, we observe that at the shock the tangent to the wave form is vertical, i.e., $\frac{\partial u}{\partial t} = \infty$. Taking the source condition to be at the origin $x = 0$, this results in

$$u(0, t) = f(t). \tag{2.3}$$

Differentiating (2.2) gives

$$\frac{\partial u}{\partial t} = \left(1 + \frac{\beta x \frac{\partial u}{\partial t}}{(c_o + \beta u)^2}\right) f'. \tag{2.4}$$

Solving for $\frac{\partial u}{\partial t}$, we arrive at

$$\frac{\partial u}{\partial t} = \frac{f'}{1 - \frac{\beta x f'}{(c_o + \beta u)^2}}. \tag{2.5}$$

Note that $\frac{\partial u}{\partial t} = \infty$ when $1 - \frac{\beta x f'}{(c + \beta u)^2} = 0$. Thus

[18] The coefficient of linearity in gas is defined as $\beta = \frac{1}{2}(1 + \gamma)$, where γ is approximately equal to 1.4 in air [8, p. 10]. To see the definition of γ, please refer to section 3.2.

$$x_{vertical} = \frac{(c_o + \beta u)^2}{\beta f'}. \tag{2.6}$$

The smallest $x_{vertical}$ is the distance desired. For acoustic problems $\beta|u| << c_o$, and the u term above is ignored [8, pp. 71-72]. The smallest $x_{vertical}$ corresponds to the maximum positive slope of f' giving

$$x_s = \frac{c_o^2}{\beta \frac{\partial f}{\partial t}_{max}}. \tag{2.7}$$

Finally, since f stands for velocity, [19] $p = u\rho c_o$ is now in the numerator [42]. Thus, the shock formation distance in terms of pressure is

$$x_s = \frac{\rho c_o^3}{\beta \frac{\partial p}{\partial t}_{max}}. \tag{2.8}$$

Thus, to obtain the distance required for a shock to be formed, recall that $c_o^2 = \frac{\gamma p}{\rho}$ and $\beta = \frac{1}{2}(\gamma + 1)$ [8]. Substituting these relations into (2.8), the following expression from [29, p. 1755] is obtained

$$x_s = \frac{2\gamma p c_o}{(1+\gamma)\frac{\partial p}{\partial t}_{max}}. \tag{2.9}$$

Notice that the shock distance is reciprocally dependent on the maximum change of the mouthpiece pressure with time. This is not surprising since, as discussed above, the pressure at the mouthpiece is highly non-sinusoidal (especially for large amplitude waves). It is this behaviour that is partially responsible for the formation of shock waves.

Although this gives a good approximation of the shock distance, it is not completely accurate. Firstly, only the right moving waves are considered. Despite that the harmonic components above a certain frequency range mostly propagate out of the bell, the lower frequencies cannot be neglected since it is these reflections that allow the generation of standing waves. Furthermore, in the case of nonlinear acoustics, neglecting the higher harmonic components is not physical since there are general acoustic consequences. Nonetheless, the derivation of (2.9) will be a good approximation to determine if and where shock waves are produced in brass instruments.

[19] Since this is the type of function being considered and solved for (this is also done is [8, p. 75]).

2.3.2 Further Consequences of Nonlinear Effects inside Brass Instruments

Once the initial research on brass instruments was done, some groups attempted to classify quantitatively the nonlinear behaviour of wave steepening and how it affects an instrument's timbre. In a 2007 paper [15], it was found that nonlinear wave propagation is able to account for the observed differences between the quality of sound in brass and reed instruments. In particular, the brightness of sound formed at high playing levels in brass instruments [20] was strongly correlated to the nonlinear propagation in the bore. This *brassiness parameter* was calculated from the bore geometry of each brass instrument [15, p. 5].

Gilbert, Campbell, Myers and Pyle concluded that conical (or flared) instruments are not as brassy as cylindrical instruments. In conical instruments, the flare of the instrument follows an approximate x^2 curve. As the pressure wave enters this region, the wave amplitude decays faster and the wave steepening is reduced as the waves energy spreads out in the flare [29, p. 1756]. If one were to compare the geometry of the saxhorns with the trumpet, wave steepening is observed to decay faster in regions with less curvature [29, p. 1756]. The hypothesis that the brightness of sound is associated with shock wave formation is therefore supported. The authors of the 2007 paper also came to the same conclusion by taking measurements of the brassiness variable for several brass instruments [15].

Once Hirschberg, Msallam and Wijnands published their experimental results regarding the formation of shock waves in trombones in [29] (in 1995), soon after other groups began studying further consequences of nonlinear wave propagation. In addition, mathematicians and physicists became curious if nonlinear wave propagation affects other musical instruments as it does the trombone.

It was speculated that wave steepening would also be experienced in the trumpet. However, it took several years before this hypothesis was tested. In 2001, Pandya, Settles and Miller published [43], claiming that shock waves were observed in the trumpet rather than just wave steepening by using the schlieren system. Several images were taken with a high speed camera depicting (what they perceived to be) shock waves propagating outside of the bell. They also stated that this particular method used was constructive because if two or more shocks were produced for a particular note, the speed of the shock waves could be calculated [43, p. 3365]. Although the acoustic community accepted their findings and their results have been used in much of the literature on the topic, their experiments were

[20] Which the authors Gilbert, Campbell, Myers and Pyle refers to as the *brassiness* of an instrument.

never repeated. The paper presented two plots illustrating the waveform captured by the microphone (assumed to be at the bell, the paper did not say) that are not in agreement with [29, p. 1756], [3, p. 510], [23, p. 879], as well as this thesis (which will be presented in chapter 4). Therefore, one of the goals of this thesis is to determine if shock waves (not just wave steepening) are actually produced in the trumpet and if so, for which notes and what loudness.

Chapter 3

Mathematical Fundamentals

In the previous chapter, a general explanation of how acoustic waves propagate through brass instruments when nonlinear effects are and are not considered was given. We now desire to translate these concepts into a mathematical framework. Despite the fact that this will not lead to an analytical solution, it is still possible to solve the equations of motion numerically. In this chapter, we will discuss the physics of sound and the relevant gas dynamics to develop a model in order to describe how nonlinear waves travel through brass instruments.

3.1 Sound and Compressible Flow

3.1.1 Introduction

To avoid confusion, it is important to clearly define what field of study this thesis falls under since it is merging many areas within physics and mathematics. As mentioned before, the study of sound is known as acoustics. More precisely, acoustics is the science of sound propagating through fluids and solids. Within this field, convective motion of the fluid is usually neglected. In this thesis, we will be investigating sound production and propagation within brass instruments. Therefore, it is necessary to take the motion of air into account. This type of problem falls under the field of aerodynamics.

Fluid mechanics is a branch of physics that encompasses the study of all fluids and the forces acting on them. If one would like to specifically study fluids in motion and the

forces that act on them, this is a subfield known as fluid dynamics. Depending on the fluid in consideration, the field of fluid dynamics can be further divided into compressible or incompressible. Flow properties such as flow type (laminar or turbulent), viscosity, or time dependence is considered regardless of the sub-discipline. It is important to note however that in reality, all fluids are compressible, viscous and heat conducting [49, pp. 5-6].

In general, compressibility is a measure of the change of volume of a liquid or gas under the action of external forces (from [49, p. 9]). In compressible fluid dynamics, variations in temperature as well as density are fundamental to understanding the state of a fluid. [21] However, for incompressible fluid dynamics, the fluctuations in temperature and density are so tiny that they can be neglected and temperature and density can be thought of as constant. Since the compressibility of liquids is rather small, it can be neglected in many cases. Thus, the motion of most liquids can be classified as incompressible (as in the case of water). However, gases are compressible. For instance, air it is roughly 20,000 times more compressible than water. Thus the incompressible idealization cannot be made [49, p. 10].

A branch of fluid dynamics that studies the motion of gases and its effect on physical systems is called gas dynamics. Normally within this field, the flows considered have speeds comparable to the speed of sound. As a consequence, temperature and pressure fluctuations are not negligible. This implies that thermodynamic effects must also be looked at. A further subfield of gas dynamics is aerodynamics, which studies the motion of air specifically [36, pp. 2, 17].

Therefore, to study sound production and propagation within musical instruments, the theory will be based from a field known as aeroacoustics. This is the study of acoustics where the sound source is a moving gas. In particular, it relies heavily on the principles in gas dynamics, specifically aerodynamics [30, p. 559].

3.1.2 Speed of Sound and Mach Number

In order to describe the motion of air inside a musical instrument, compressible flow equations need to be considered. In gas dynamics there are a couple of parameters that are fundamentally used. The first is the speed of sound, denoted c. This is the speed that a

[21] It is now relevant to consider the pressure changes of the fluid motion because it leads to volume variations. Also, when determining if compressibility is applicable, it is useful to see how the density varies in a system rather than the volume. For instance, if the relative density fluctuations are small, then $\frac{\delta\rho}{\rho_0} << 1$ and we can say the fluid is incompressible [49, p. 10].

small disturbance (or wave) propagates in a compressible medium [36, pp. 50-51]. The speed of sound is related to compressibility in (3.1)

$$c^2 = (\frac{\partial p}{\partial \rho})_s, \tag{3.1}$$

where the subscript s indicates that the constant is entropy [36, p. 51].

When a sound wave travels through a fluid, small disturbances are produced. This forms temperature and velocity gradients (which produce the pressure and density gradients). In many cases, these perturbations are so small that the entropy associated with the fluid particles remains roughly constant [36, pp. 50-51], [49]. This is referred to as an isentropic process. However, if the frequency of a constant amplitude wave increases enough, the gradients become too large for the process to be considered isentropic. Nonetheless, in a perfect gas, if the process is assumed to be isentropic, compressible flow theory states that

$$\rho = Cp^{\frac{1}{\gamma}}, \tag{3.2}$$

where C is proportionality constant [36, p. 51]. This implies that c can be written as

$$c^2 = (\frac{\gamma p}{\rho})_s = \gamma RT, \tag{3.3}$$

where R is the gas constant and T is the absolute temperature [36, p. 51]. The speed of sound is also slightly sensitive (a second-order anharmonic effect [22]) to the sound amplitude. [23] Moreover, in a moving fluid, the speed of sound c, is extremely useful in measuring the influences of compressibility when it is compared to u, the velocity of the fluid. This leads to the second important parameter in compressible flow theory, the nondimensional parameter known as the Mach number [49, 19]. It is defined as

$$M = \frac{|u|}{c}. \tag{3.4}$$

The Mach number is not constant throughout the fluid. The velocity is changing between various points and c depends on the local conditions as seen in (3.2). If $M < 1$ the flow is referred to as subsonic. If $M > 1$ the flow is called supersonic. If $M < 0.3$ throughout

[22] Anharmonic refers to an oscillator that is not oscillating in simple harmonic motion [8].

[23] This means that there are nonlinear propagation effects, such as the production of harmonics and mixed tones not present in the original sound (see parametric array) [8].

a flow, it is classified as incompressible. For this type of flow, the density variations which may arise from pressure changes can be neglected since the velocity variations are more influential [36, pp. 52-53].

3.1.3 The Connection between Physics and Sound

The behavior of a compressible flow is rather similar to an elastic solid: a displaced particle compresses and increases the density of adjacent particles that move and increase the density of the neighboring particles and so on. This disturbance in the form of a pressure or elastic wave, travels through the medium. The speed of propagation is faster if the medium is more rigid. In particular, if the amplitude of the pressure wave is sufficiently small, it is called an acoustic or sound wave [35, p. 717].

In terms of auditory perception, we perceive sound when the tympanum (ear drum) detects the mechanical effect from variations in air pressure. The human ear can identify sound waves of frequencies ranging from 20 Hz to 20 kHz, however, detecting frequencies below 100 Hz or above 10 kHz is difficult [32], [42, 12-13].

So, what exactly is sound? Sound is a sequence of pressure waves that propagate through a compressible medium such as air. However, sound waves cannot travel in a vacuum. Sound can also propagate through incompressible mediums (such as water), as well as solid objects. However, there will be other types of propagation, such as transverse waves [32], [42, pp. 12-13]. Thus, we will ignore these other mediums and focus on air.

A sound wave will propagate through a medium assuming a vibrating object couples to the air to excite the sound waves [24]. Therefore, one can say that the prerequisite for sound is that the medium of propagation, in this case a fluid air, has no elastic resistance to shear. Also, sound waves have viscous resistance. This implies the only waves that are able to propagate are longitudinal (compressive); meaning the direction of motion and wave propagation is the same for a sound wave [24]. While the wave is moving, it is possible for it to be reflected, refracted or attenuated. To formulate all these ideas mathematically, it is vital to be aware of the parameters that affect sound propagation. The behaviour of sound propagation is influenced by the following [32], [55]:

* The interaction between density and pressure which is influenced by the temperature of the fluid (recall that the temperature contributes to determining the speed of sound)

* The motion of the medium itself - if the medium is moving, the sound propagates further (if u and c have the same sign)

* The viscosity of the medium, which establishes the rate at which sound attenuates (however, for fluids such as air or water, attenuation due to viscosity is negligible in most cases)

* If the medium of propagation does not have constant physical properties, sound waves can be internally refracted (in inhomogeneous medium)

Sound pressure is the difference between the average local pressure in the medium and the sound pressure wave. In general, sound pressure is averaged over time or space. It is typical to take the square root of the average squared pressure, $\sqrt{\acute{p^2}}$, to give what is called a root mean square value (RMS). For instance, 1 Pa RMS sound pressure corresponding to 94 dB SPL (sound pressure level) in atmospheric air means that the actual pressure in the sound wave oscillates between $(101325-\sqrt{2})$ Pa and $(101325+\sqrt{2})$ Pa. This difference in air pressure is very small relative to an atmosphere. Nonetheless, in the audible sound range the volume can be so high as to cause hearing damage [52]. We normally measure sound pressure in decibels which is a logarithmic scale. The SPL, denoted L_p is defined as

$$L_p = 20\log_{10}\left(\frac{p}{2\times 10^{-5}}\right) dB, \tag{3.5}$$

where 2×10^{-5} Pa is the minimum RMS pressure detected by the human ear at mid frequencies, and p is the RMS sound pressure. In particular, we defined 0 dB SPL (sound pressure level) as the minimum sound pressure heard by people, i.e. 2×10^{-5} Pa [52]. For instance, a pressure measurement of 40 Pa is about 126 dB, which is extremely loud. In terms of wavelength, sound waves range from 17 mm to 17 m [32], [42, pp. 11-13].

Finally, the set of partial differential equations known as the Navier-Stokes (including viscosity) equations or Euler equations (neglecting viscosity) is used to describe the fluid flow in a medium [12, p. 428]. In particular, since the objective is to understand the airflow through a musical instrument, it is necessary to consider the system of equations specifically for air where the viscosity can be neglected. These equations are known as the compressible Euler equations [49, p. 47].

3.2 Equations of Motion

Before making any simplifying assumptions to the problem, let us first consider the equations of motion for a Newtonian, compressible, viscous fluid. The parameters of the

closed system are the three velocity components of the flow $\vec{u} = (u, v, w)$, the pressure $p = p(x, y, z, t)$, the density $\rho = \rho(x, y, z, t)$ and the temperature $T = T(x, y, z, t)$. In order to solve for any of these quantities, the equations describing of conservation of mass, momentum, and energy as well as an equation of state that comes from thermodynamics, must be considered [49, p. 47].

The equation describing conservation of mass is called the continuity equation and is given by

$$\frac{\partial \rho}{\partial t} + \frac{\partial(\rho u)}{\partial x} + \frac{\partial(\rho v)}{\partial y} + \frac{\partial(\rho w)}{\partial z} = 0, \tag{3.6}$$

or

$$\frac{D\rho}{Dt} + \rho \nabla \cdot \vec{u} = 0, \tag{3.7}$$

where $\frac{D}{Dt}$ is the material derivative [49, p. 65].

The equations describing conservation of momentum is referred to as the Navier-Stokes equations and has three components which are

$$\rho \frac{Du}{Dt} = X - \frac{\partial p}{\partial x} + \frac{\partial}{\partial x}\left[\mu(2\frac{\partial u}{\partial x} - \frac{2}{3}\nabla \cdot \vec{u})\right] + \frac{\partial}{\partial y}\left[\mu(\frac{\partial u}{\partial y} + \frac{\partial v}{\partial x})\right] + \frac{\partial}{\partial z}\left[\mu(\frac{\partial w}{\partial x} + \frac{\partial u}{\partial z})\right], \tag{3.8}$$

$$\rho \frac{Dv}{Dt} = Y - \frac{\partial p}{\partial y} + \frac{\partial}{\partial y}\left[\mu(2\frac{\partial v}{\partial y} - \frac{2}{3}\nabla \cdot \vec{u})\right] + \frac{\partial}{\partial z}\left[\mu(\frac{\partial v}{\partial z} + \frac{\partial w}{\partial y})\right] + \frac{\partial}{\partial x}\left[\mu(\frac{\partial u}{\partial y} + \frac{\partial v}{\partial x})\right], \tag{3.9}$$

$$\rho \frac{Dw}{Dt} = Z - \frac{\partial p}{\partial z} + \frac{\partial}{\partial z}\left[\mu(2\frac{\partial w}{\partial z} - \frac{2}{3}\nabla \cdot \vec{u})\right] + \frac{\partial}{\partial x}\left[\mu(\frac{\partial w}{\partial x} + \frac{\partial u}{\partial z})\right] + \frac{\partial}{\partial y}\left[\mu(\frac{\partial v}{\partial z} + \frac{\partial w}{\partial y})\right], \tag{3.10}$$

where $\vec{F} = (X, Y, Z)$ are the body forces and $\mu = \mu(T)$ is the viscous coefficient. In this case we can just consider gravity, i.e. $\vec{F} = (0, 0, \rho\vec{g})$ [49, p. 65]. To obtain a closed system, the changes in density and pressure as well as how these parameters influence the temperature are needed. The equation of state is

$$P = \rho T R, \tag{3.11}$$

where R is the gas constant and T is the absolute temperature [49, p. 46]. Next, the energy equation in needed. The First Law of Thermodynamics (an expression to balance heat and mechanical energy) will have to be used if we do not have an isothermal process. Assuming that thermal conductivity, k, is constant, the energy equation can be written as

$$\rho c_p \frac{dT}{dt} = \frac{dp}{dt} + k\left(\frac{\partial^2 T}{\partial x^2} + \frac{\partial^2 T}{\partial y^2} + \frac{\partial^2 T}{\partial z^2}\right) + \mu\Phi, \tag{3.12}$$

where c_p is the specific heat of air at constant pressure, Φ is the dissipation function and is denoted $\Phi = 2[(\frac{\partial u}{\partial x})^2 + (\frac{\partial v}{\partial y})^2 + (\frac{\partial w}{\partial z})^2]$ [49, 267].

3.2.1 Small Amplitude Sound Waves

Although in this thesis, we cannot assume that the amplitude of the sound waves is small, it would still be useful to briefly discuss how one is able to describe linear sound waves. To simplify the derivation, it is customary to consider the compressible equations of motion where $\nu = 0$ [24] and $\kappa = 0$ (i.e. we neglect these parameters), so

$$\frac{D\rho}{Dt} + \rho\nabla\cdot\vec{u} = 0, \tag{3.13}$$

$$\rho\frac{D\vec{u}}{Dt} = -\nabla p, \tag{3.14}$$

$$\rho c_p \frac{DT}{Dt} - \alpha T\frac{Dp}{Dt} = 0, \tag{3.15}$$

$$\alpha = -\frac{1}{\rho}(\frac{\partial\rho}{\partial T})_p = \frac{1}{T}, \tag{3.16}$$

$$p = \rho R T. \tag{3.17}$$

We now want to use the above equations to derive one partial differential equation that will describe the propagation of small amplitude sound waves. To begin, we substitute $T = \frac{p}{\rho R}$, $\gamma = \frac{c_p}{c_v}$ into the energy equation (3.5) to obtain

[24] This is the kinematic viscosity and is defined as $\nu = \frac{\mu}{\rho}$.

$$\rho c_p \left[\frac{1}{\rho R} \frac{Dp}{Dt} - \frac{p}{\rho^2 R} \frac{D\rho}{Dt} \right] - \alpha \frac{p}{\rho T} \frac{Dp}{Dt} = 0.$$

This can further be simplified to obtain

$$\rho \frac{Dp}{Dt} - \gamma p \frac{D\rho}{Dt} = 0, \tag{3.18}$$

where the derivation of this can be found in Appendix E. The next step is to linearize the equations by introducing small perturbations of the basic states as follows

$$\begin{aligned} p &= p_o + p' \\ \rho &= \rho_o + \rho' \\ \vec{u} &= \vec{u}' \end{aligned} \tag{3.19}$$

to find the following

$$\frac{d\rho'}{dt} + \rho_0 \nabla \cdot \vec{u'} = 0, \tag{3.20}$$

$$\rho_0 \frac{d\vec{u'}}{dt} = -\nabla \cdot p', \tag{3.21}$$

$$\rho_0 \frac{\partial p'}{\partial t} - \gamma p_0 \frac{\partial \rho'}{\partial t} = 0. \tag{3.22}$$

The next step is to combine the equations (3.20), (3.21) and (3.22) to find one partial differential equation for p'. Taking the partial derivative with respect to time of (3.20) as well as the divergence of (3.21) and then combining these two equations we obtain

$$\frac{\partial^2 \rho'}{dt^2} = -\nabla^2 p'. \tag{3.23}$$

Finally, to eliminate p', one takes the partial derivative with respect to time of the energy equation (3.22) and then substitutes it into (3.23) arriving at

$$\frac{\partial^2 p'}{dt^2} = c^2 \nabla^2 p', \tag{3.24}$$

where c is the speed of sound defined as $c^2 = \frac{\gamma p_0}{\rho_0}$. This is called the wave equation which has a solution for one dimensional waves of the form

$$p'(x,t) = f(x - ct) + g(x + ct), \tag{3.25}$$

where f and g are found from the initial conditions $p' = (x, t = 0)$, $\frac{\partial p'}{\partial t}(x, t = 0) = 0$. Notice that the solution consists of left and right moving waves propagating with speed c, without changing shape. These types of waves are referred to as non-dispersive [53].

3.2.2 Large Amplitude Sound Waves

Since the purpose of this thesis is to better understand nonlinear wave propagation inside of a trumpet (and determine if the nonlinear behaviour is strong enough to steepen into a shock wave), it is important to recognize that the linearization assumption used above in section 3.2.1 fails because the amplitudes of the pressure waves are finite.

In reality, we should be taking the losses due to viscous friction and heat transfer into effect [24, p. 193], [5]. The walls contribute a viscous drag which is associated with the velocity of the air in the pipe. The magnitude of this drag depends on the thickness of the viscous boundary layer r_v, which is proportional to the square root of the viscosity η divided by the angular frequency ω (in relation to the pipe radius a) [24, pp. 193-194]. Thus

$$r_v = \left(\frac{\omega\rho}{\eta}\right)^{\frac{1}{2}} a. \tag{3.26}$$

Also, the thermal transfer from the air to the walls adds resistance to the compressibility of the air which is denoted as r_t. The magnitude in this case depends on the ratio of the pipe radius a to the thermal boundary layer thickness, so

$$r_t = \left(\frac{\omega\rho c_p}{\kappa}\right)^{\frac{1}{2}} a, \tag{3.27}$$

where κ is the thermal conductivity. Taking the ratio of the viscous diffusion rate squared $\left(\frac{r_t}{r_v}\right)^2$, we obtain the dimensionless number called the Prandtl number [24, p. 194]

$$P_r = \frac{c_p \eta}{\kappa}.$$

The Prandtl number is normally used to help classify heat transfer problems since it controls the relative thickness of the momentum and thermal boundary layers. Small P_r implies that the heat diffuses much faster compared to the momentum. In other words, this means the thermal boundary layer is larger than the velocity boundary layer. Whereas high P_r corresponds to the convection transfer being strong [35, p. 294].

Continuing, Bernade was able to simplify the expressions for r_t and r_v near 27^oC (300 K) to be roughly

$$r_v \approx 632.8af^{\frac{1}{2}}(1 - 0.0029\Delta T), \tag{3.28}$$

and

$$r_t \approx 532.8af^{\frac{1}{2}}(1 - 0.0031\Delta T), \tag{3.29}$$

where a is the radius of the tube, f is the frequency and ΔT is the temperature deviation from 300 K [24, pp. 193-194]. This makes the wave number k complex and leads to attenuation of the propagating wave as is passes along the pipe [5].

If one desired to take these wall losses into consideration, it would have to be done in the boundary conditions. Theoretically, the process of deriving boundary conditions with r_t and r_v is not difficult. But practically, it is computationally expensive and the implementation quickly becomes complicated. In general, it would no longer be appropriate to assume that $\nu = 0$ or $\kappa = 0$. Instead, the variables in (3.26) and (3.27) could be isolated and then substituted into the energy equation (3.12). An interesting consequence of this would be that the wall losses are proportional to frequency. Intuitively, this seems reasonable assuming that the following claim is true: if higher frequency notes are played in brass instruments, nonlinear propagation (and thus wave steepening) becomes more prominent. In chapter 6, this hypothesis will be tested. Nonetheless, due to time constraints and complexity, these losses will be neglected.

Therefore, when neglecting walls losses, the formulation for finite amplitude sound waves greatly simplifies. Firstly, due to the axial symmetry of a trumpet, the z-axis will be ignored as well as the body forces. Also, since attenuation due to viscosity in air is

reasonably small, we set $\nu = 0$ and $\kappa = 0$. Notice that these are the same assumptions that were made in the beginning of section 3.2.1. The difference however, is that the equations cannot be linearized.

3.2.3 Conservation Laws for Finite Amplitude Sound Waves

For this thesis, we base our model on the two dimensional compressible inviscid Euler equations. To obtain the equations of motion in conservation form, the above assumptions (at the end of section 3.2.2) must be applied to equations (3.7), (3.8), (3.9), (3.10) and (3.12). After expanding and simplifying these expressions, we find the following:

$$\frac{\partial \rho}{\partial t} + \frac{\partial(\rho u)}{\partial x} + \frac{\partial(\rho v)}{\partial y} = 0, \tag{3.30}$$

$$\frac{\partial(\rho u)}{\partial t} + \frac{\partial(\rho u^2 + p)}{\partial x} + \frac{\partial(\rho uv)}{\partial y} = 0, \tag{3.31}$$

$$\frac{\partial(\rho v)}{\partial t} + \frac{\partial(\rho uv)}{\partial x} + \frac{\partial(\rho v^2 + p)}{\partial y} = 0, \tag{3.32}$$

$$\frac{\partial E}{\partial t} + \frac{\partial(u(E+p))}{\partial x} + \frac{\partial(v(E+p))}{\partial y} = 0, \tag{3.33}$$

where again ρ is the density of air, $(\rho u, \rho v)$ are the momenta in the x and y direction respectively, p is the internal pressure of air, and E is the total energy [54]. The total energy is written as follows

$$E = \frac{p}{\gamma - 1} + \frac{\rho}{2}(u^2 + v^2). \tag{3.34}$$

In other words, as the sum of kinetic energy (due to momentum) and potential energy (due to internal pressure). The paramter γ is a constant which will vary depending on the gas in consideration. For air, γ is approximately equal to 1.4 [54, p. 206]. This parameter comes from the equation of state and is referred to as the specific heat ratio, and is defined as

$$\gamma = \frac{c_p}{c_v}. \tag{3.35}$$

In (3.35), c_v is the specific heat capacity when volume is taken to be constant and c_p is the specific heat capacity when pressure is assumed to be constant. In particular, from thermodynamics, the relation between c_p and c_v can be derived to obtain $c_p = R + c_v$ where, R is the gas constant [41].

Chapter 4

Laboratory Experiments

In order to verify previous reported results and to gather useful data for numerical simulations, several experiments have been carried out for this thesis. The collected data was processed using Fourier analysis to obtain information about the harmonic spectrum of the developing pressure profile inside the trumpet. To reconstruct the observed pressure waveforms measured at the mouthpiece of the trumpet as a sum of the varying harmonic components, Fourier synthesis was then carried out. This mathematical representation of the pressure measurements at the mouthpiece can then be used as part of the boundary condition in the numerical model to reproduce the sound disturbance observed in the lab. Finally, since the pressure waves at the bell of the trumpet were also measured, the mathematical model can be reviewed by comparing experiments with numerical simulations.

4.1 Experimental Setup

The experiments that were carried out took place in Dr. J. Vanderkooy's acoustic lab. More specifically, pressure measurements were taken on a B^b trumpet shown in figure 4.1. As one can see, three separate microphones were attached at various locations along the trumpet. The first microphone was a $\frac{1}{4}$ inch in diameter and was mounted to the cylindrical part of the trumpet mouthpiece. The second $\frac{1}{4}$ inch microphone was attached to the cylindrical tubing of the trumpet before the first bend and the last microphone was placed 16-17 *cm* outside the trumpet bell.

To mount the microphone at the mouthpiece and bend, small holes were cut into the cylindrical part of the mouthpiece and trumpet bore. In a great attempt not to alter

the acoustic properties of the trumpet, the holes made were slightly greater than a $\frac{1}{4}$ inch in diameter and the microphones were placed inside the holes so they would make the boundary of the tube as smooth as possible. A compressible o-ring seal held the microphone securely and prevented any air leakage. The microphones were then connected to 3 inputs of a four channel oscilloscope and the data was saved onto the local computer. The microphone models and calibration details can be found in Appendix A.

Figure 4.1: Placement of microphones on the trumpet.

4.2 Experimental Procedure

Since an actual brass player is more capable of reaching higher notes on a trumpet compared to a loud speaker [5], Philip Rempel from the music department at the University of Waterloo provided all of our desired notes on the trumpet shown in figure 4.1. In addition, several measurements were also taken on a bass trombone. However, we did not own the trombone and thus were not able to manipulate the instrument in any way. Thus, only one pressure measurement was taken 10cm inside of the bell. Nonetheless, the trombone data will still provide insight because the note recorded was played at the same volume in three different octaves. These results will be discussed shortly.

It was decided that in order to make the path of the airflow more direct and to avoid using the valves of the B^b trumpet, Phil played a C_3 and C_4, which correspond to a concert B_3^b and B_4^b respectively. In order to determine how the loudness of the note influences the wave propagation, both of these tones were played at mezzo-forte (mf) and forte (f) i.e. medium-loud and loud. These notes are played with the valves left open which implies

Figure 4.2: Zoom-in of the microphone at the mouthpiece.

the corresponding length of the trumpet is roughly 1.48 m. When the valves are used, the effective length of the trumpet is longer, resulting in lower resonant frequencies.

In the case of the trombone, data was collected for the notes F_2, F_3 and F_4. Since the measured pressure was only recorded at the bell, it was decided that this experiment would be more useful if all notes were played at *mf*. This way, one can observe how the wave profile and frequency spectrum varies for a note played in several octaves.

Continuing, the trumpet data from all three microphones was collected from the oscilloscope simultaneously. The data recorded was obtained once the note of choice was steady and only a couple of periods of the raw data was saved. Later in the thesis, the consequences of this choice will be discussed. The data was then imported into the Matlab code shown in Appendix B. The purpose of this code is to read in the raw experimental data and output the pressure waveform p, measured in Pascals $[Pa]$ versus time, t, measured in seconds $[s]$. By taking the discrete Fourier transform (DFT) [25] of the pressure waveform, (denoted $DFT(p) = P$), the frequency spectrum is also obtained in terms of the frequency, f, measured in hertz $[Hz]$ and the associated sound pressure level, SPL, measured in decibels $[dB]$ [52].

The plots were obtained in the following way: First, the data was imported into Matlab.

[25] In Matlab, the fast Fourier transform (fft) is an algorithm employed to compute a discrete Fourier transform (DFT) containing N points.

However, we only used one period to make the Fourier analysis more straight forward. The number of points, denoted by N, was determined by finding the length of a period [26]. Since the raw data contained a time axis, the parameter time, t, was determined by taking the time difference between each recorded data point. The general form of the sampling frequency, denoted by F_s, was then found by taking $\frac{1}{t}$. Next, the pressure variable, p, was obtained by taking the raw pressure data and multiplying it by the calibration factor (for more details on the calibration factor see Appendix A). The pressure waveform can now be plotted in a physically meaningful way.

In order to find the corresponding plots in the frequency domain, we first found an expression for frequency, f, in terms of F_s and N. However, instead of considering the domain $[0, N]$ (also written $[0, F_s]$) we will consider the domain $[0, \frac{N}{2} + 1]$ (also written as $[0, \frac{F_s}{2}]$) [27]. Consequently, the frequency can be defined as $f = \frac{F_s}{N}[0 : \frac{N}{2} + 1]$ (for more details, see section 5.2.3 or Appendix B) and the DFT of the pressure waveform, P, is determined by the following relation

$$P = \left(\frac{1}{N}\right) \text{fft}(p). \tag{4.1}$$

To convert Pa into $SPL\ dB$ (to find the corresponding amplitude for each frequency component), we use equation (3.5), i.e.

$$L_p = 20 \log_{10} \left(\frac{\sqrt{2}P}{2 \times 10^{-5}}\right) dB.$$

Note that we multiplied by $\sqrt{2}$ to obtain the RMS values (refer to section 3.1.3) [52].

4.3 Experimental Results

Let us first review the resulting plots of the data associated with the B_3^b and B_4^b notes played at mf and f on the trumpet. Figures 4.3 and 4.4 present one period the measured pressure

[26] Which was done by carefully inspecting the saved data. The exact numbers can been found in Appendix B.

[27] The first half of the frequency range (from 0 to $\frac{F_s}{2}$) is sufficient to identify the component frequencies in the data, since the second half is just a reflection of the first half. This is sometimes labeled as aliasing in literature. The frequency $\frac{F_s}{2}$ is called the Nyquist frequency after the engineer Harry Nyquist. It is defined to be half the sampling frequency of a discrete signal. It sometimes also called the folding frequency of a sampling system [37].

waveforms of a B_3^b played at *mf* and *f*, and figures 4.6 and 4.7 show similar measurements for the B_4^b. Since the pressure at the bell is much lower than inside the instrument, we show it in the right plots of these figures, whereas the left plots show the relative shape of the waveforms measured at the mouthpiece, bend and bell. The corresponding plots in the frequency space are depicted in figures 4.5 and 4.8. Finally, tables 4.1 and 4.2 list some important values of the obtained sound pressure levels of these notes at the mouthpiece and bell.

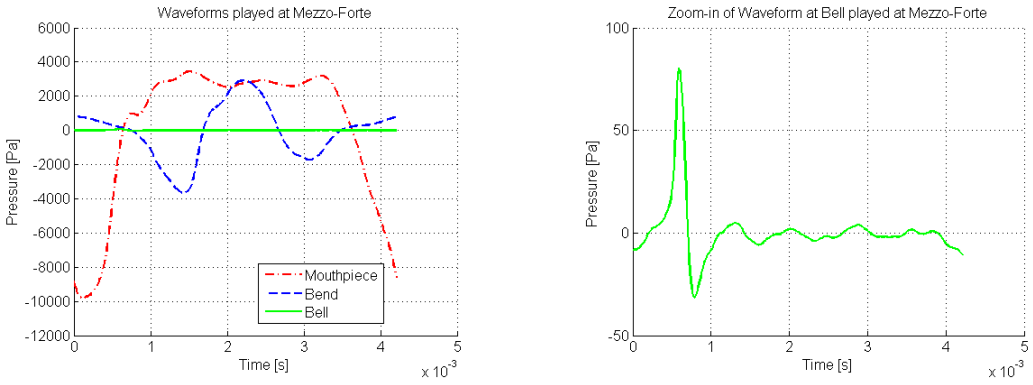

Figure 4.3: Measured pressure waveforms at the (left) mouthpiece, bend and (right) bell of a B_3^b at *mf*.

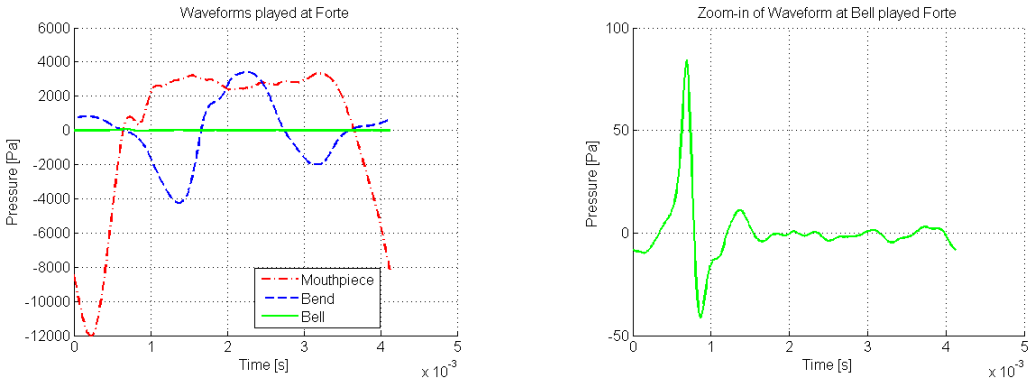

Figure 4.4: Measured pressure waveform at the (left) mouthpiece, bend and (right) bell of a B_3^b at *f*.

We observe that when the trumpet is played at *mf* for both notes, the highest SPL is 250 Hz (the fundamental frequency) at the mouthpiece. The measured values are 164.08

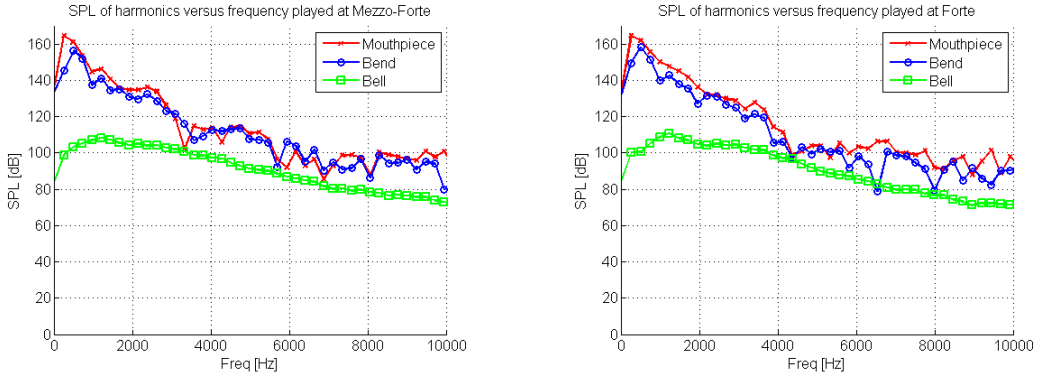

Figure 4.5: Frequency spectra of a B_3^b at the mouthpiece, bend and bell played at *mf* (left) and *f* (right).

dB for the B_3^b and 164.98 dB for the B_4^b. However, when the propagating wave exits the bell, the fundamental frequency has a SPL of 99.82 dB and 105.40 dB for the B_3^b and B_4^b respectively; but the maximum SPL at the bell occurs at the fifth harmonic for the B_3^b (108.88 dB) and the third harmonic for the B_4^b (111.42 dB).

Table 4.1: Maximum sound pressure levels measured in dB at the mouthpiece and bell for all the trumpet notes recorded in the lab.

Trumpet Note	Dynamic Level	Max SPL dB at Mouthpiece	Max SPL dB at Bell
B_3^b	mf	164.080103 (242.130751Hz)	108.884963 (1210.653753Hz)
B_3^b	f	164.599379 (242.130751Hz)	110.737153 (1210.653753Hz)
B_4^b	mf	164.985167 (484.261501Hz)	111.416162 (968.523002Hz)
B_4^b	f	166.953042 (484.261501Hz)	113.870887 (968.523002Hz)

Similarly for the notes at *f*, we see that the SPL's have all increased slightly compared to the corresponding pitches played at *mf* (see Table 4.1). The SPL of the fundamental frequency at mouthpiece (which also happens to be the maximum) was measured at 164.60

dB for the B_3^b and 166.95 dB for the B_4^b, whereas at the bell, the SPL's were 100.20 dB for the B_3^b and 107.35 dB for the B_4^b. The maximum SPL at the bell corresponded the fifth harmonic for the B_3^b (110.74 dB) and the third harmonic for the B_4^b (113.87 dB).

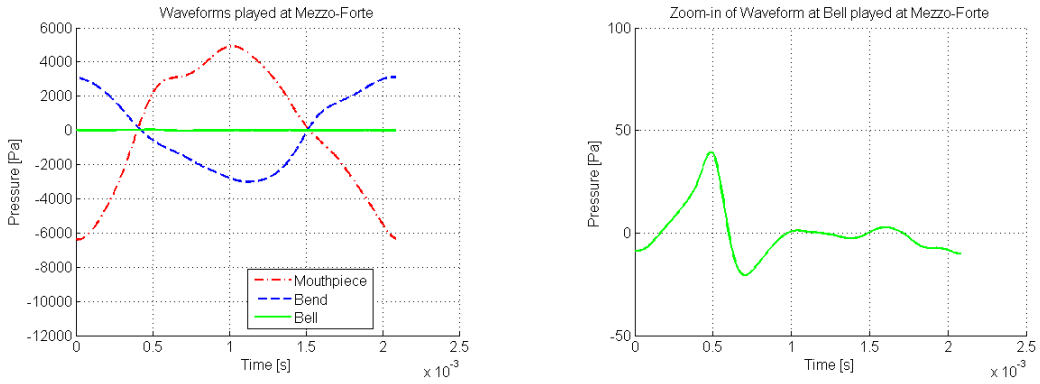

Figure 4.6: Measured pressure waveforms at the (left) mouthpiece, bend and (right) bell of a B_4^b at *mf*.

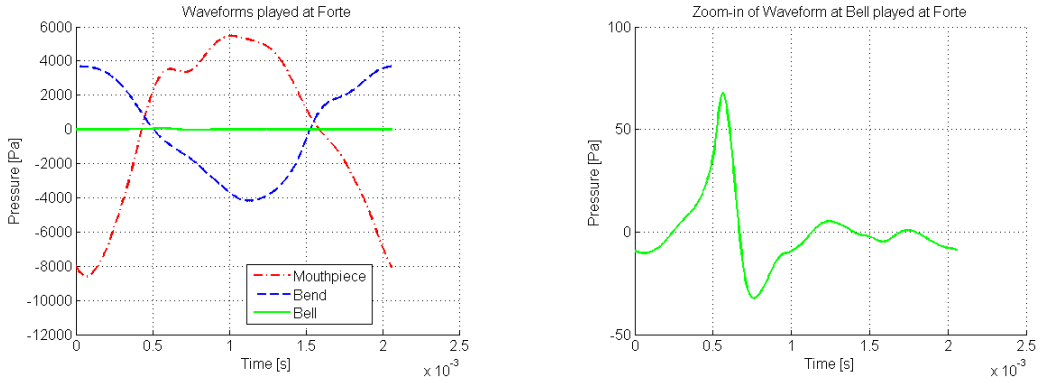

Figure 4.7: Measured pressure waveforms at the (left) mouthpiece, bend and (right) bell of a B_4^b at *f*.

From the values in Table 4.1 we conclude that both loudness and frequency of the note influence the strength of the pitch. Indeed the SPLs of the B_3^b played at f are larger than the values measured at mf but not the values of the B_4^b at mf. Thus, as expected, the SPLs for the B_4^b played at f are the biggest. We also observe in figures 4.5 and 4.8 the nonlinear behaviour of the propagation as the wave travels through the instrument. By

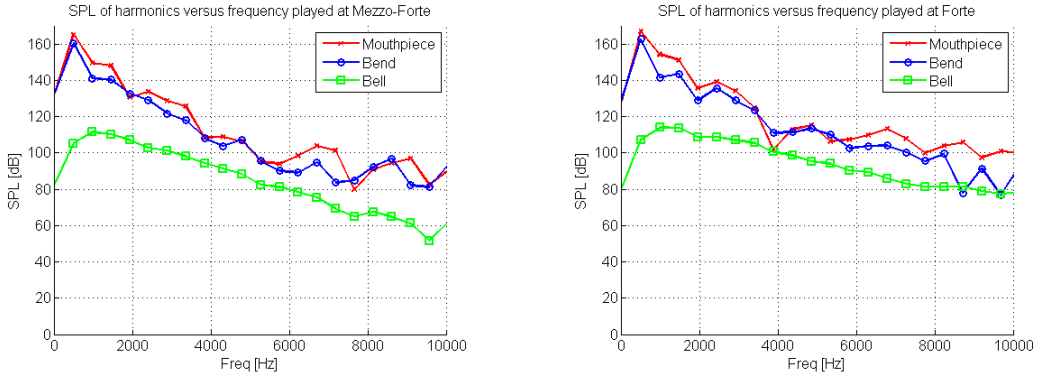

Figure 4.8: Frequency spectra of a B_4^b at the mouthpiece, bend and bell played at *mf* (left) and *f* (right).

Table 4.2: Sound pressure levels of the fundamental frequency at the mouthpiece and bell for each recorded trumpet pitch.

Trumpet Note	Dynamic Level	SPL dB at Mouthpiece of Fund.	SPL dB at Bell of Fund.
B_3^b	mf	164.080103 (242.130751Hz)	99.816358 (242.130751Hz)
B_3^b	f	164.599379 (242.130751Hz)	100.201551 (242.130751Hz)
B_4^b	mf	164.985167 (484.261501Hz)	105.401942 (484.261501Hz)
B_4^b	f	166.953042 (484.261501Hz)	107.354401 (484.261501Hz)

comparing the frequency spectrum at the mouthpiece and bend to the spectrum at the bell, we see that at the bell the spectrum is represented by a flatter curve. We hypothesize that this implies a transfer of energy to the upper harmonics as the propagating wave steepens, especially if a shock wave is produced (recall from section 2.1.1 that shock waves correspond to non-negligible upper harmonics). This will be discussed in more detail in section 4.3.1.

As a final remark in regards to the trumpet data, one may notice that there is little

variation in the sound pressure levels of the B_3^b played at *mf* and *f* (or the B_4^b played at *mf* and *f*). A possible reason for this is that when Phil played the B_3^b at *mf* and *f*, the measured voltage was 7.35 V and 8.21 V respectively. However, when the B_4^b was played at *mf* and *f*, the voltage measured was 6.05 V and 7.45 V respectively [28]. Thus, it is evident that there is a larger difference between the measured voltage values for the B_4^b compared to the B_3^b (and this difference is also seen in the SPL values). This may explain the similar maximum SPL dB in tables 4.1 and 4.2, especially for the mouthpiece data.

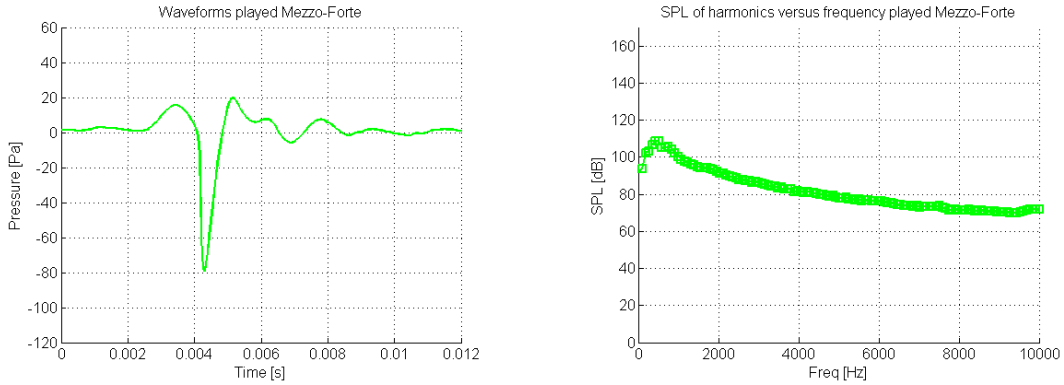

Figure 4.9: Waveform (left) and corresponding frequency spectrum (right) of an F_2 played at *mf* 10 *cm* into a trombone bell.

Next, we will review the findings corresponding to the trombone data measured 10 *cm* inside the bell. The notes that were recorded, an F_2, F_3 and F_4, were all played at *mf*. The measured pressure waveforms are illustrated in the left plots of figures 4.9, 4.10 and 4.11 for the F_2, F_3 and F_4 respectively; and their corresponding DFT plots are shown on the right in figures 4.9, 4.10 and 4.11. It is interesting to note that the pressure measurements inside the bell of the trombone for the F_3 and F_4 have a higher SPL than any of the trumpet waveforms (despite the fact that the F_3 is lower than the B_3^b). The maximum SPL for the F_2, F_3 and F_4 were measured to be 108.76 dB, 119.25 dB, and 123.47 dB respectively. However, these SPLs correspond to the second harmonic for the F_4, the fourth harmonic for the F_3 and the sixth harmonic for the F_2.

Similarly to the played trumpet notes, it is evident that the waveforms measured in the trombone become smoother in the mathematical sense (i.e. it appears that the increase in pitch means that even lower harmonics are now emitted more from the bell) as the fundamental frequency is increased. Although this is consistent with the idea that when

[28] An increase of 3 dB implies an increase in voltage by a factor of approximately $\sqrt{2}$ [52].

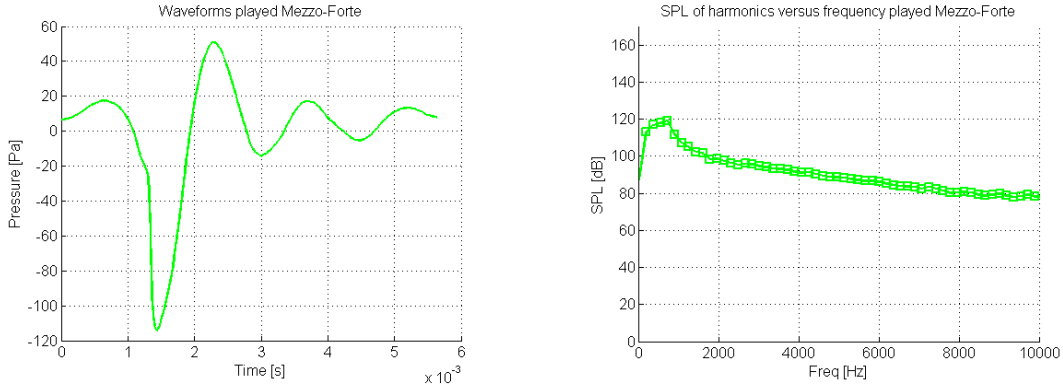

Figure 4.10: Waveform (left) and corresponding frequency spectrum (right) of an F_3 played at *mf* 10 *cm* into a trombone bell.

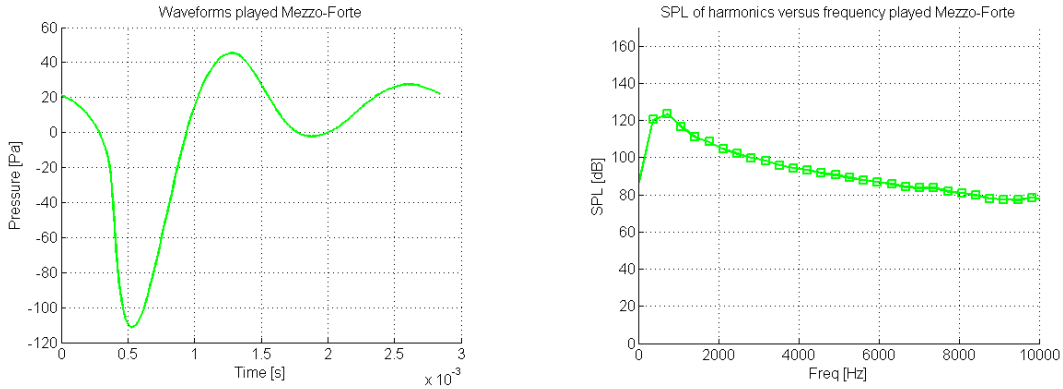

Figure 4.11: Waveform (left) and corresponding frequency spectrum (right) of an F_4 played at *mf* 10 *cm* into a trombone bell.

higher frequency notes are played, more energy is emitted out the bell, this result was not so prominently expected.

4.3.1 Further Discussion of Results

In this section, we will take the time to expand on the observations made above. To begin, upon reviewing the B_3^b and B_4^b pressure waveforms in figures 4.3, 4.4, 4.6 and 4.7, one can see a noticeable difference in the waveform shapes. In particular, the B_4^b's waveforms appear

Table 4.3: Sound pressure levels of the measured trombone notes 10 cm inside the bell. The specified frequencies are the fundamental and most influential harmonic.

Trombone Note	Dynamic Level	SPL dB at Bell of Fund.	Max SPL dB at Bell
F_2	mf	93.721586 (80.645161Hz)	108.760526 (483.870968 Hz)
F_3	mf	112.844014 (176.678445 Hz)	119.251437 (706.713781 Hz)
F_4	mf	120.519429 (350.877193 Hz)	123.466603 (701.754386 Hz)

to be smoother (i.e. less oscillations) relative to the B_3^b's waveforms. The B_4^b's frequency range may provide an explanation for this. For the B_4^b, the standing waves are composed of fewer resonances from the trumpet but overall has more harmonic components greater than 1500 Hz compared to the B_3^b. [29] Therefore, more of the B_4^b's frequency spectrum will be lost. Furthermore, as the fundamental frequency of a tone increases, so do the energy losses [29]. So for the B_4^b, a greater amount of energy will be lost as the wave propagates through the instrument. Fortunately, for a player to successfully higher frequency and louder notes, a higher blowing pressure level is required. This is demonstrated by comparing the values in tables 4.1 and 4.2.

We also noticed that the B_3^b pressure waveforms at the bell have a rather sharp character regardless of the playing volume. One could speculate that a possible reason for this behaviour has to do with the way the lips close to make a rarefaction that is sharp. For the lower frequency notes, this particular lip movement will take place over a smaller portion of a period. In addition, the B_3^b's standing waves will be stronger since more harmonic components are reflected. Nevertheless, the signals at the bell overall seems quite repetitive and stable [52].

It would now be useful to compare these findings to previous results to see if our experiments are in agreement. We will begin by reviewing the sound pressure measurements obtained in [29] by Hirschberg, Gilbert, Msallam and Wijnands. Although their experiments were done with a trombone, the selected notes and set up was relatively similar to ours (also, [29] was one of the first papers publishing such results). In particular, in [29],

[29] Recall from chapter 2 that at the higher frequency range, more energy is emitted out of the bell rather than being reflected.

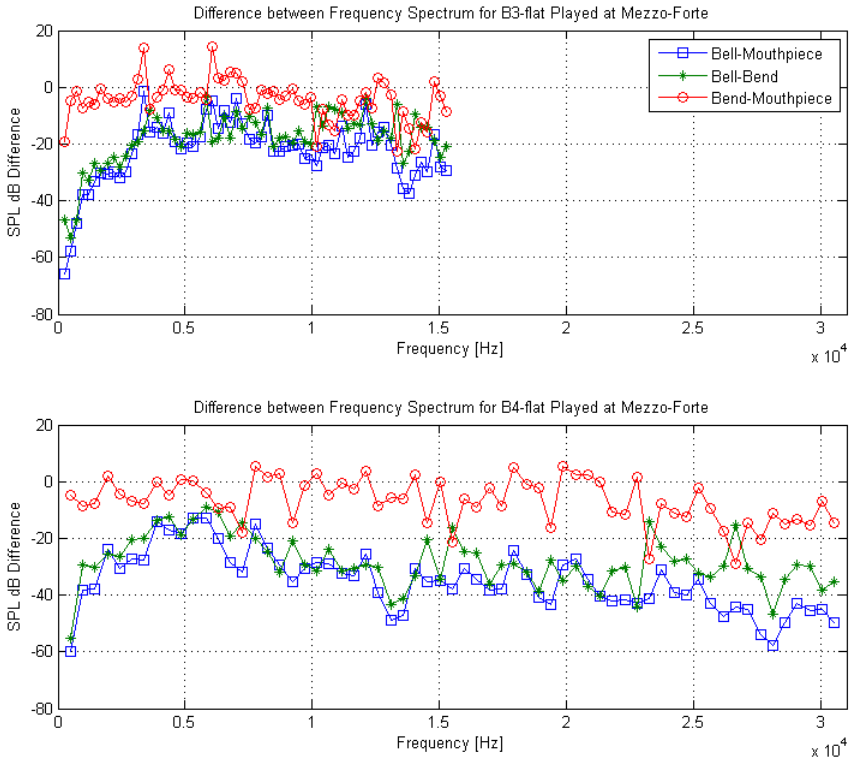

Figure 4.12: Difference between the SPL (in dB) of the bell and mouthpiece (blue line), bell and bend (green line), and bend and mouthpiece (red line) for the B_3^b and B_4^b played at *mf*.

two different notes were considered, each played at *p*, *mf* and *f*. The first note played was approximately 250 Hz while the second was an octave higher (and these are roughly the same notes that we considered in the lab). The authors also attached three microphones to the instrument. The first microphone was placed at the mouthpiece, the second was located before the flare and finally, one was placed 4.5 cm outside the bell [29, p. 1754]. Interestingly, despite that our measurements were done on a trumpet, the shape of the waveforms presented in figures 4.3, 4.4, 4.6 and 4.7 are very similar to the plots depicted in [29, pp. 1756-1757]. Even the SPLs are very close. For instance, the trombone notes played at f at the mouthpiece produced a SPL of roughly 162 dB, whereas playing at p created a wave with a SPL of 154 dB [48, p. 1099]. In addition, in [29], the authors found that the pressure level outside the bell peaked at roughly 300 Pa for the 250 Hz note, and

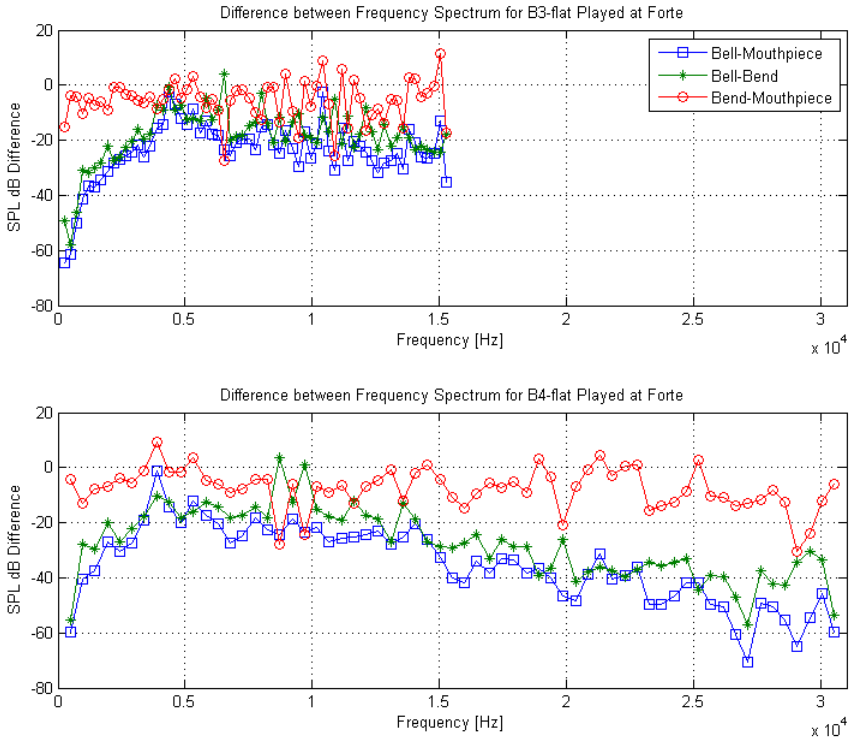

Figure 4.13: Difference between the SPL (in dB) of the bell and mouthpiece (blue line), bell and bend (green line), and bend and mouthpiece (red line) for the B_3^b and B_4^b played at f.

$1000Pa$ for the 500 Hz tone. Again, these values generally agree with our experiments, [30] with the exception that the SPL for the B_4^b measured outside the trombone bell in [29] was slightly higher. Finally, the authors also obtained similar waveform differences between the 250 Hz and 500 Hz note in [29]. The higher frequency pressure plots (in [29]) illustrate that the shape of the 500 Hz waveform is smoother relative to the 250 Hz note [29, p. 1757]. More importantly, the authors claimed that they observed the formation of shock waves for the 500 Hz note instead of only wave steepening [29, p. 1756]. However, the location of the shock distance was not mentioned. Overall, the bell pressure measurements obtained for the 500 Hz note in [29, pp. 1756-1757] do not resemble the trumpet plots

[30] Remembering that the microphone outside the trumpet bell was placed $16cm$ away rather than 4.5 cm.

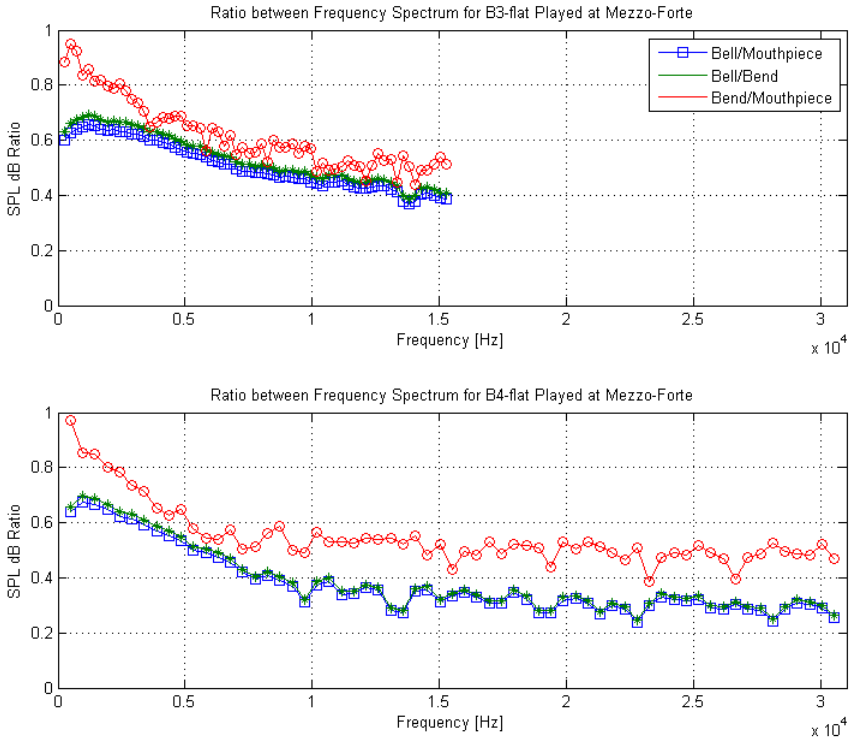

Figure 4.14: Ratio between the SPL (in dB) of the bell and mouthpiece (blue line), bell and bend (green line), and bend and mouthpiece (red line) for the B_3^b and B_4^b played at *mf*.

that we found. Although this in itself is not too surprising because the trombone is longer than the trumpet. What is surprising however, is that the pressure measurement in [29, pp. 1756-1756] are very different from our trombone measurements shown in the left part of figures 4.9, 4.10 and 4.11. Potentially this may be the case because our highest note was only 350 Hz and was played at *mf*; nonetheless, this outcome was not expected.

The key question now is does this data demonstrate nonlinear wave propagation? In general, if a periodic wave is considered, depending on the harmonic components it will either be symmetric or asymmetrical. For example, if the wave is composed of the fundamental and only odd harmonics (f, $3f$, $5f$, $7f$, ...), the summed wave is symmetric (so it can be phase shifted and inverted but remain the same). However, if the wave contains any even harmonics ($0f$, $2f$, $4f$, $6f$, ...), it will be asymmetrical. Conversely, a system

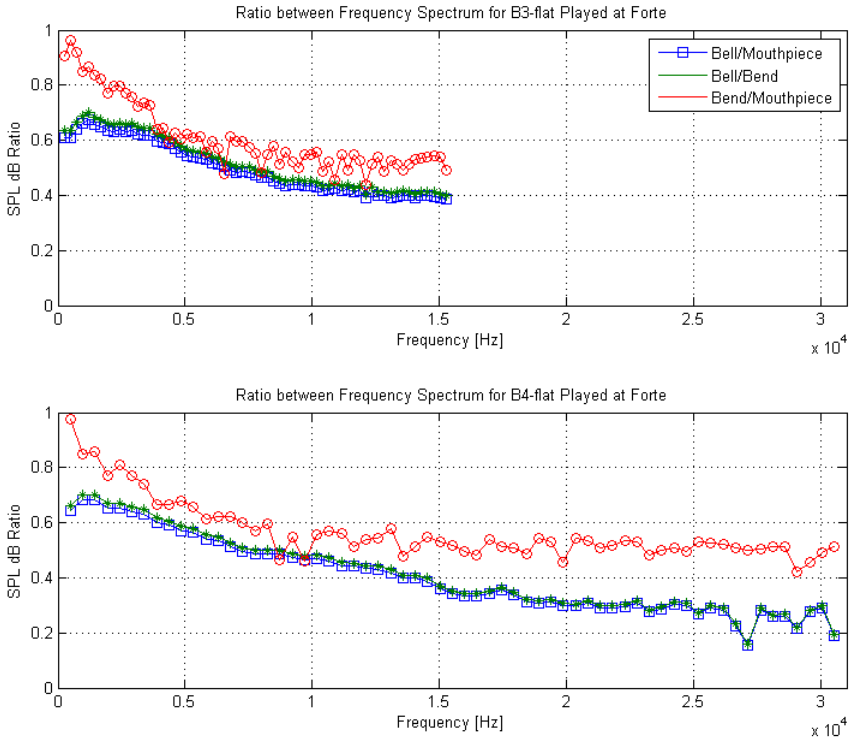

Figure 4.15: Ratio between the SPL (in dB) of the bell and mouthpiece (blue line), bell and bend (green line), and bend and mouthpiece (red line) for the B_3^b and B_4^b played at *f*.

which changes the shape of the wave (beyond simple scaling or shifting) potentially creates harmonic distortion. In other words, there may be a redistribution of energy across the higher frequency spectrum [8, pp. 19, 71-73]. This is called a nonlinear system [48, p. 1096].

According to the literature (for the trombone especially), one should expect to see the effects of nonlinear wave propagation increase as the wave travels further through the instrument [29, p. 1755]. Narezo, Bustamante and Lopez explain in [48] that nonlinear propagation is associated with the large-scale distortion of a sound wave through the cumulative effect over a long distance or time of locally small nonlinear effects (from [48, p. 1096]). In other words, the nonlinear cumulative effects of the sound wave usually can only be identified when considering the evolution of the wave propagation through the instrument [48, p. 1096]. This nonlinear distortion is observed through the steepening of the

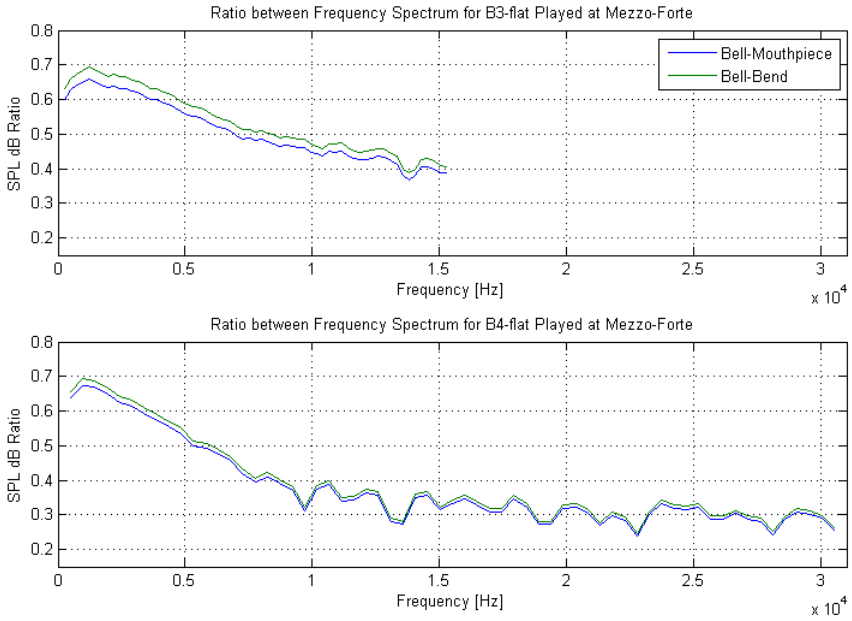

Figure 4.16: Close up of ratio between the SPL (in dB) of the bell and mouthpiece (blue line), bell and bend (green line) for the B_3^b and B_4^b played at *f*.

wave profile. The rate at which the wave steepens depends on the maximum slope of the initial pressure profile produced by the source, as well as the distance the wave travels [48, pp. 1096-1097]. If the nonlinear effects are strong enough, the waveform distortion may generate a thin region where the pressure perturbations become almost discontinuous. The structure of these discontinuities depends on whether nonlinear propagation effects can be balanced by attenuation (from [48, p. 1096]).

It can however be very difficult to determine if the effects due to nonlinear propagation are present solely by considering the shape of the pressure waveform, especially if no shock wave is generated. [31] Nevertheless, another way to detect the nonlinear distortion is by considering the higher frequency spectrum. Recall that when wave steepening occurs in a brass instrument (prior to the formation of a shock wave), the different spectral components that make up the wave interact in such a way that energy is redistributed over the higher frequency spectrum. This is what characterizes nonlinear propagation [48, p. 1097]. Overall, for similar amplitudes, the higher frequencies change faster which means

[31] It is possible although to detect distortions purely by looking at the wave profile if the pressure levels are around 170 dB, but even then it is not always conclusive [48, pp. 1099-1100].

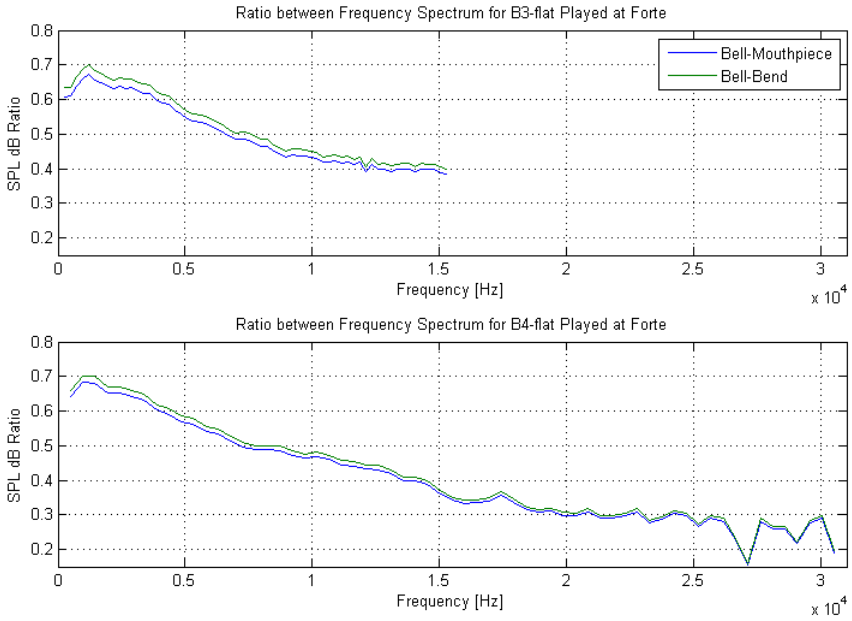

Figure 4.17: Close up of ratio between the $SPL\ dB$ of the bell and mouthpiece (blue line), bell and bend (green line) for the B_3^b and B_4^b played at f.

that they have higher derivatives, and as a consequence the higher frequencies should steepen faster [34].

It is important to note that as a pulse travels further down the instrument (in reality, thermoviscous losses are present), attenuation becomes the main influence (and is more efficient for higher frequencies) on the wave profile. As a result, attenuation outweighs the effects of energy pumping due to nonlinear behaviour [48, p. 1096]. Narezo, Bustamante and Lopez state in [48, p. 1097] that when considering a pulse of greater amplitude, the difference between spectra is less marked and can only be accounted for by nonlinear propagation effects (which will be more prominent precisely for the pulse of greater amplitude [48, p. 1097]). The authors argue that in order to accurately measure the transfer of energy to the upper frequencies (called, energy spectral densities), one must take the difference (and/or ratio) of the SPL's at the bell and mouthpiece between each frequency and the initial amplitude. [32] If the ratio of SPL's between the pulses are plotted, we can then observe the rate of decay of the spectra at high frequencies [48, p. 1099].

[32]Radiated harmonics depend on the amplitude of the initial signal [48, p. 1096].

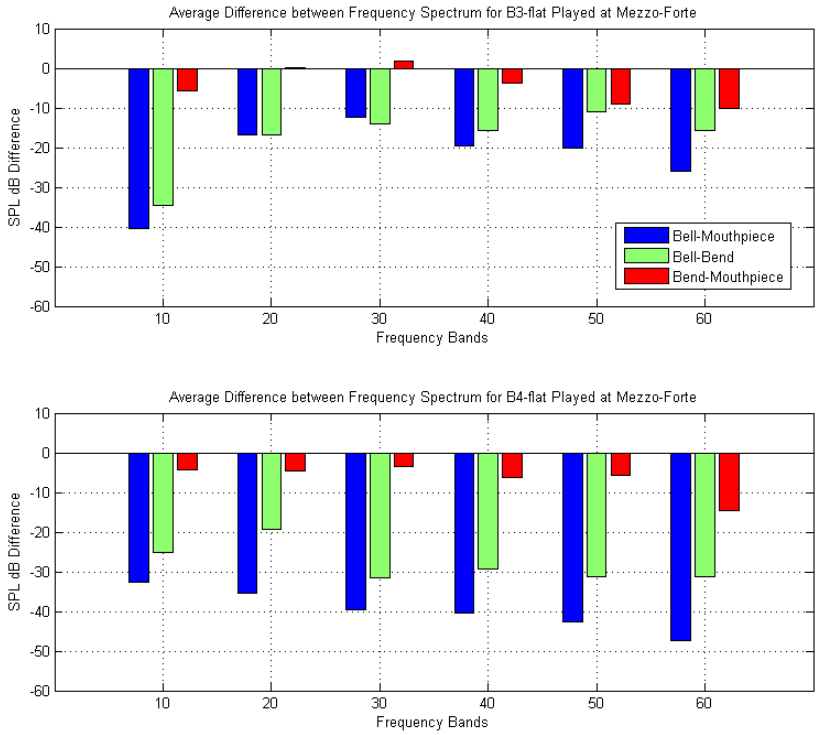

Figure 4.18: Average difference between the SPL (in dB) of the bell and mouthpiece (blue line), bell and bend (green line), and bend and mouthpiece (red line) for the B_3^b and B_4^b played at *mf*.

Therefore, if we want to establish the affects of the nonlinearities associated with a traveling wave or pulse, we need to compare the different pressure levels (of the note being played) at various positions along the instrument. This will allow one to verify if nonlinear effects become more influential at higher SPL's and at higher frequency notes (and thus also confirm the findings in [48]). For this thesis, since the pressure measurements were taken at the mouthpiece, bend and bell, we can determine how the frequency components interact and change as the wave propagates further through the instrument.

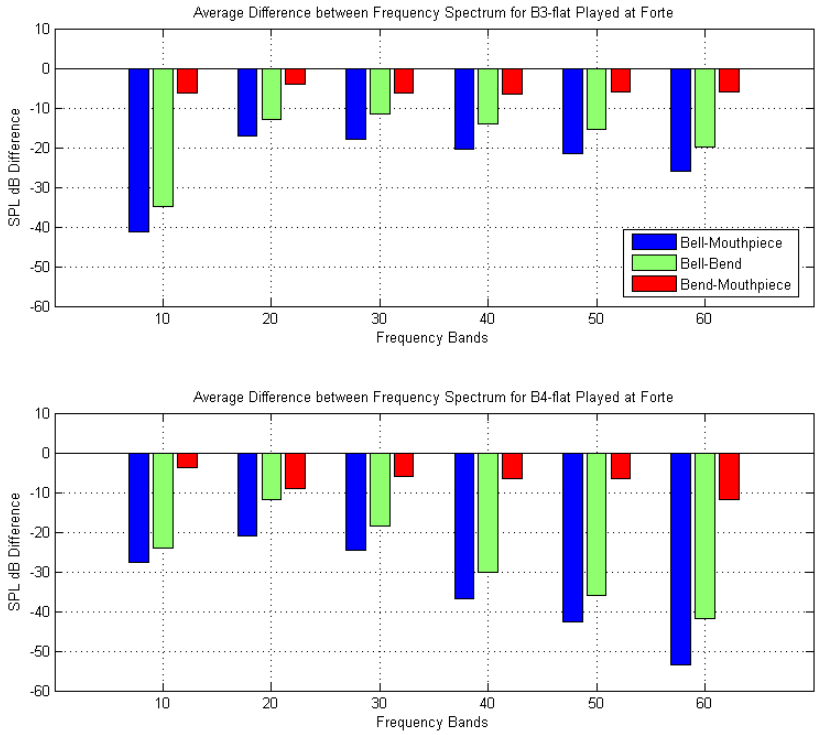

Figure 4.19: Average difference between the SPL (in dB) of the bell and mouthpiece (blue line), bell and bend (green line), and bend and mouthpiece (red line) for the B_3^b and B_4^b Played at *f*.

4.3.2 Analysis of Pressure Measurements

To examine how the energy associated with the pressure waves in figures 4.2, 4.3, 4.6 and 4.7 is distributed amongst the harmonics, we will inspect the first 64 harmonics of the B_3^b and B_4^b. [33] We will first consider the difference in the SPLs between the bell and mouthpiece (blue line), bell and bend (green line), and finally the bend and mouthpiece (red line). Figures 4.12 and 4.13 respectively illustrate these comparisons for the B_3^b and B_4^b played at *mf* and at *f*. While figures 4.18 and 4.19 show the same data, except the components are grouped into frequency bans (each containing ten components) and the

[33] Recall that the relative changes between the SPLs at the mouthpiece, bend and bell of these notes are depicted in figures 4.5 and 4.8.

SPLs are then averaged.

As one would expect, as the pressure wave approaches the first bend, its shape will not change as much as it would further down the instrument. Therefore, the difference in the SPLs between these two positions (red line) in figures 4.12 and 4.13 will be more or less around zero. This is evident for the pitches played at *mf*, especially for the B_3^b in the top plot of figure 4.12. For the B_4^b however, the red line values (seen in the bottom plots of figures 4.12 and 4.13) starts to change more (negatively) for the frequencies greater than 25000 Hz. However, it is important to recognize that it is mainly the bell that disperses the sound. This also appears to be the trend when comparing the blue (bell and mouthpiece) and green (bell and bend) line in the bottom plots of figures 4.12 and 4.13. For harmonic components greater than 25000 Hz, the difference values start to become more negative, especially for the blue line and particularly for the B_4^b played at f seen in the bottom plot in figure 4.13.

Since losses occur as the wave propagates down the tube, the quotient of the amplitudes for each harmonic corresponding to the different positions must also be examined. Then, the obtained plots will depict the relative change in power for the first 64 harmonics between the bell and mouthpiece (blue line), bell and bend (green line), and finally, the bend and mouthpiece (red line). This is precisely what figures 4.14 and 4.15 shows. It is interesting to observe that the blue and green curves are very similar (figures 4.16 and 4.17 depict a close up of these relations).

From these plots, we can see (in the top plots of figures 4.14 and 4.15), that the relative change in power for the B_3^b played at *mf* and f is greatest for the second harmonic; whereas for the B_4^b at these volumes (which can be seen in the bottom plots of figure 4.14 and 4.15), it is the fundamental frequency. In addition, when comparing the B_3^b's results, the ratio of the bend and mouthpiece appears to be more constant (i.e. the line is straighter, there is less variation) at *f*. This is also true for the B_4^b data. There also appears to be a greater difference in the relative power changes between the red line compared to the blue, and green line for the notes played at *f*. So in general, the prominent behaviour that we are seeing is a 20 dB to 30 dB reduction for all frequencies. Although we hypothesis that this is mostly due to the wave spreading in the bell (which does not need losses to explain it since the wave is spreading in three dimensions) [52].

Chapter 5

Numerical Method

5.1 Introduction to the Model

Like for many problems in mathematics, obtaining an analytical solution in the field of nonlinear acoustics is usually not practical or possible. As mentioned in chapter 3, the equations of motion that will be used to model wave propagation within a brass instrument are the inviscid compressible Euler equations. In order to determine if this hyperbolic system of PDEs (presented in section 3.2.3) is accurate, it is necessary to solve the set of the equations numerically. [34]

The numerical method known as the discontinuous Galerkin method (DGM) will be used to solve the Euler equations in conservative form. Since the equations are a system of nonlinear hyperbolic PDEs, it is possible for the solution to form shock waves as a consequence. This is one reason why choosing the DG method is so practical, because our model will potentially have to resolve shock waves and handle nonlinearities. [35] Therefore, the purpose of this chapter is to formulate the DG method and review the necessary theory.

[34] Recall that a system of PDEs is characterized as hyperbolic by a finite speed of information propagating, specifically along the characteristics of the equation. Also, a PDE is hyperbolic if the Jacobian matrix ($f'(u)$) has m real eigenvalues and is diagonalizable)[27, p. 2].

[35] The implementation of the DG method used for this thesis was written by Lilia Krivodonova.

5.2 Overview of Discontinuous Galerkin Method

The DG method was first proposed in the 1970s. It has been used to solve a variety of different types of partial differential equations such as hyperbolic, elliptic as well as parabolic problems from fluid mechanics, gas dynamics, electrodynamics and more. This method uses certain characteristics mostly from finite volume methods and also from finite element methods [54, p. 10].

For instance, just as in finite element methods, the DGM has the flexibility to achieve higher order accurate solutions and is able to handle complex geometries. Additionally, the DGM is able to obtain local conservative statements of the equation through explicit schemes (i.e. the system of equations is solved at each interface, using the previous and current time step, rather than solving the global problem) [54, pp. 6-7], [13]. However, it is important to be aware that a unique solution cannot always be guaranteed at the interface. Fortunately, this is addressed in the DGM (also in finite volume methods) by using a numerical flux. Furthermore, depending on the flux, one can find a strong or weak form of the conservation laws. Nevertheless, if a weak solution is obtained, uniqueness is lost and instead it is necessary to obtain an entropy consistent solution [53]. [36] Overall, this implies the DGM is able to handle complex geometries, higher order accuracy and hp-adaptively [37], explicit semi discrete form as well as conservation laws [54, p. 7].

This is computationally useful for the purposes of this thesis for a couple reasons. The first (which has already been mentioned) is the ability to handle possible shock waves [27, p. 14]. This is why solving the conservation laws locally (i.e. at each interface) is so useful [13], [53]. Another positive feature is that the mesh does not have to be uniform; this implies that the mesh can have regions with better refinement. In addition, the mesh can become even more cost effective by eliminating regions that are not needed. For instance, instead of having a box completely around the trumpet for the computational domain, it is more efficient to have the majority of the domain only around the trumpet bell.

[36] Note that it can be shown that the weak and strong forms of the problem are equivalent. However, if one finds the strong solution, the weak solution will be the same, but the converse does not always hold [54, p. 22], [53].

[37] hp-FEM is a finite element method (FEM), which is a numerical method to solve PDEs based on piecewise polynomial approximations that uses elements of variable size h and polynomial degree p [4, p. 6].

5.2.1 Discontinuous Galerkin Formulation

Consider a general nonlinear hyperbolic system that is written in the following conservative form

$$\frac{\partial \vec{u}(\vec{x},t)}{\partial t} + \nabla \cdot F(\vec{u}(\vec{x},t)) = \vec{0}, \tag{5.1}$$

where $\vec{x} \in R^2$ and $\vec{F}$ is referred to as the flux function [54, pp. 10, 169]. For convenience , we will write (5.1) as follows

$$\vec{u}_t + \nabla \cdot F(\vec{u}) = \vec{0}. \tag{5.2}$$

The derivation of the DGM begins with putting equation (5.1) into integral form since the weak solution is desired. In order to obtain the integral form of the conservation law, the computational domain, denoted by Ω, will be divided into a collection of triangular elements Ω_j whose size and shape can be non-uniform. We write this as

$$\Omega = \bigcup_{j=1}^{N_h} \Omega_j \tag{5.3}$$

where N_h is the total number of elements in the computational domain [54, p. 169]. The next step will be to introduce a test function $v(\vec{x})$ (which is assumed to be square integrable for the first partial derivative), multiply (5.2) by v, and then integrate over an element Ω_j to obtain [54, pp. 20-21]

$$\int_{\Omega_j} v\vec{u}_t dV + \int_{\Omega_j} v\nabla \cdot F(\vec{u}) dV = 0. \tag{5.4}$$

Then we consider the vector identity

$$\int_{\Omega_j} v\nabla \cdot F(\vec{u}) dV = \int_{\Omega_j} \left[\nabla \cdot (vF(\vec{u})) - F(\vec{u}) \cdot \nabla v\right] dV, \tag{5.5}$$

and the Divergence theorem

$$\int_{\Omega_j} \nabla \cdot (vF(\vec{u}))\, dV = \int_{\partial\Omega_j} vF_n ds, \tag{5.6}$$

where $\partial\Omega_j$ is the boundary of Ω_j, $F_n = F(\vec{u}) \cdot \hat{n}$, and $\hat{n}$ is the outward facing normal vector to $\partial\Omega_j$ [53], [54, pp. 8,170]. Upon substituting (5.5) and (5.6) into (5.4), we obtain

$$\int_{\Omega_j} v\vec{u}_t dV + \int_{\partial\Omega_j} vF_n ds - \int_{\Omega_j} F(\vec{u}) \cdot \nabla v dV = 0. \tag{5.7}$$

The next step is to approximate the normal flux F_n across the boundary $\partial\Omega_j$. Denoting the components of $F(\vec{u})$ by $(F_1(\vec{u}), F_2(\vec{u}))$ [18, p. 25], we arrive at

$$\int_{\Omega_j} v\vec{u}_t dV - \int_{\Omega_j} (F_1(\vec{u})v_x + F_2(\vec{u})v_y) dV + \int_{\partial\Omega_j} v(F_1(\vec{u})n_x + F_2(\vec{u})n_y) ds = 0. \tag{5.8}$$

Now on each element Ω_j, we will approximate the global solution $\vec{u}(\vec{x}, t)$, by the approximate solution $\vec{U}_j(\vec{x}, t)$, which is a piecewise (no higher than) p^{th} order polynomial defined as

$$u(\vec{x}, t)|_{\Omega_j} \approx U_j = \sum_{i=1}^{N_p} c_{ij}\psi_i, \tag{5.9}$$

where N_p is the number of basis functions, and $\{\psi_i\}_{i=1}^{N_p}$ is a basis of degree p on Ω_j [53], [54, pp. 20-21]. Note that p is used to depict both the pressure of the flow and the order of approximation but since they are used in different contexts, hopefully there is no confusion. These functions in the DGM do not have to be continuous on the interfaces between elements.

The next step is to choose the test function $v(\vec{x})$

$$v(\vec{x}) \approx \sum_{k=1}^{N_p} l_k \psi_k(\vec{x}). \tag{5.10}$$

However, since each l_k can be arbitrarily chosen, it is convenient to say that $v(\vec{x}) = \psi_m(\vec{x})$ for $m = 1, 2, ..., N_p$. Choosing the space of our test functions where the locally defined spaces are defined as the span$\{\psi_k\}_{k=1}^{N_p}$, is the key to the Galerkin formulation [54, pp. 20-21], [18, p. 25]. In choosing the space of the test functions to be the same finite dimensional

subspace of the solution space we obtain the Galerkin approach as desired. [38] [39] Thus, we can rewrite (5.8) in terms of the approximate solution (5.9) and our test function (5.10) to obtain

$$\sum_{i=1}^{N_p} \frac{dc_{ij}}{dt} \int_{\Omega_j} \psi_k \psi_i dV = \int_{\Omega_j} \left[F_1 \left(\sum_{i=1}^{N_p} c_{ij}\psi_i \right) v_x + F_2 \left(\sum_{i=1}^{N_p} c_{ij}\psi_i \right) v_y \right] dV + \int_{\partial\Omega_j} \psi_k \left[F_1 \left(\sum_{i=1}^{N_p} c_{ij}\psi_i \right) n_x + F_2 \left(\sum_{i=1}^{N_p} c_{ij}\psi_i \right) n_y \right] ds. \tag{5.11}$$

Furthermore, the notation can be simplified by defining the integral on the left hand side as a mass matrix M, and the two integrals on the right hand side as a loading vector $\vec{L}$. Therefore, we can write (5.11) in the form of an ordinary differential equation [18, pp. 24-25]

$$M \frac{d}{dt} \vec{c} = \vec{L}. \tag{5.12}$$

Each component of $\vec{L}$ contains two integrals; one integrates over each element Ω_j and the other over the boundary $\partial\Omega_j$. Now since the basis functions and test functions are polynomials, they can be calculated by numerical quadrature [45, pp. 7-8]. Thus to complete the DGM space discretization, we only have to define the numerical flux [45, p. 187]. We then discretize the resulting ODE system by using the explicit Runge-Kutta scheme. We do this by considering the time interval $(0, T)$, where T is the final time and we partition the interval as $\{t^n\}_{n=0}^{N}$ and set $I = (t^n, t^{n-1})$ where $n = 0,\ 1,\ldots,\ (N-1)$ [13, p. 731], [45, p. 7].

The mass matrix, denoted M, is local due to the fact that the basis functions are only defined on the specified cell. A nice consequence of this is that the mass matrix can be easily inverted making the implementation more cost effective [54, p. 6],[18, pp. 30-31].

[38] Fortunately, as a consequence of the Galerkin approximation, the residual is orthogonal to the test function in $\mathcal{L}^2(\Omega_j)$ since we do not have to have continuous basis functions [54, pp. 5, 20].

[39] In other words, in the DGM, the local basis functions ψ_i are set to be zero for all values other than the current element j that is being considered. However, this is not true for finite element methods because the basis functions must be continuous [54, p. 5].

5.2.2 Discretization of the Conservation Laws

In order to simulate propagating acoustic waves inside of a trumpet, the two-dimensional compressible Euler equations which were presented in section 3.2.3 will be implemented. Moreover, to discretize the nonlinear equations, it is necessary to write them out in vector form [40]

$$\frac{\partial \vec{u}}{\partial t} + \frac{\partial \vec{F}}{\partial x} + \frac{\partial \vec{G}}{\partial y} = \vec{0}, \tag{5.13}$$

where $\vec{F}$ and $\vec{G}$ are the nonlinear fluxes [54, p. 206]. In this case, $\vec{u} = [\rho, \rho v_x, \rho v_y, E]^T$, $\vec{F} = [\rho u, \rho u^2 + p, \rho uv, u(E+p)]^T$ and $\vec{G} = [\rho v, \rho uv, \rho v^2 + p, v(E+p)]^T$. So the system can be written as

$$\begin{pmatrix} \rho \\ \rho u \\ \rho v \\ E \end{pmatrix}_t + \begin{pmatrix} \rho u \\ \rho u^2 + p \\ \rho uv \\ (E+p)u \end{pmatrix}_x + \begin{pmatrix} \rho v \\ \rho uv \\ \rho v^2 + p \\ (E+p)v \end{pmatrix}_y = \vec{0}. \tag{5.14}$$

The vector $\vec{u}$ is usually referred to as the state vector, whereas $\vec{F}$ and $\vec{G}$ are the two nonlinear fluxes. In order to solve these equations, initial as well as boundary conditions are needed [54, pp. 206-207].

5.2.3 Initial and Boundary Conditions

In the DGM code that was used, instead of nondimensionalizing the equations of motion, the variables were scaled. The speed of sound, c, which is around 340 m/s in air, was scaled to be 1; the pressure, p, which in air is approximately 101325 Pa (i.e. 1 atmosphere) was scaled to be 1; and the specific heat ratio γ, in air is approximately equal to 1.4. We also know

$$\text{Ideal gas law: } \begin{cases} c = \sqrt{\frac{\gamma p}{\rho}}, \\ p = (\gamma - 1)(E - \frac{1}{2}\rho u^2), \end{cases}$$

which implies that the initial density ρ_0, can be set to 1.4. In addition, it was assumed that initially the flow was at rest, i.e. the velocity in the horizontal and vertical direction

[40] It is important to note that the hyperbolic system in conservative form do not take into account thermal diffusion as well as viscosity [54].

was set to zero. Again, by the ideal gas law this implies that the initial energy is $E = \frac{p}{\gamma-1} + \frac{\rho}{2}(u^2+v^2) = 2.5$. Thus, in summary

$$\text{Initial Conditions:} \begin{cases} p_0 = 1.0, \\ \rho_0 = 1.4, \\ u_0 = 0.0, \\ v_0 = 0.0, \\ E_0 = 2.5. \end{cases}$$

The walls of the trumpet (excluding the mouthpiece) in figures 5.1 to 5.4, are set to have reflective boundary conditions whereas the boundary of the computational domain around the trumpet has absorbing boundary conditions [54, pp. 206-207].

The input from the mechanical oscillator (measured in the lab) was used as the boundary conditions at the vertical wall of the mouthpiece.[41] This ensures that as long as a note is being played, there will always be a pressure (as well as velocity) input that will flow freely through the trumpet (so energy is always being pumped into the system). We will now examine how the expression for the boundary conditions at the mouthpiece was derived using the information obtained from the experimental data.

When a player blows into a trumpet, the sound which radiates out of the bell has a complex waveform where the amplitude of the harmonics may be as large as or possibly larger than the amplitude of the fundamental frequency [3, p. 509]. According to literature, the pressure that is produced in the mouthpiece (as a consequence of the air that travels to the mechanical oscillator) can be as much as 20%- 30 % above atmospheric pressure. This variation depends on the influence of the harmonics [23, p. 874]. Comparing these reported values to our own measurements seen in figures 4.3 to 4.8; one can see that we observe relatively high amplitudes. This is particularly seen in the pressure waveforms at the mouthpiece of the trumpet for the B_3^b and B_4^b played at f (which were depicted in figures 4.4 and 4.7). However, these plots demonstrate that the maximum pressure measurements that we found were only around 12% of atmospheric pressure. Nonetheless, these are the waveforms that we want to use as boundary conditions for the trumpet mesh at the mouthpiece. Therefore, in order to mathematically reproduce the plots shown in figures 4.4 and 4.7, Fourier analysis will have to be carried out on the sounds recorded by the oscilloscope.

[41] It should be mentioned that the boundary conditions at the bell were left open. Thus, the wave was free to propagate outside the bell.

The oscilloscope used in the lab recorded sound clips that were generated by the brass player Philip Rempel. The oscilloscope recorded three pressure measurements (all consisting of 1000 points) along the trumpet simultaneously. However, instead of using all 1000 points, exactly one period of the data was isolated and used. Thus, suppose that one period contains $N+1$ samples, then the size of the fast Fourier transform (fft) must be N and the frequencies will be proportional to $N-1$. Since exactly one period of data has been considered, the frequencies obtained from the fft are precisely the harmonics of the signal. The direct current (DC) [42] will be in the first entry of the array (also referred to as bin 1); the fundamental will be in bin 2, the second harmonic in bin 3 are so forth. The direct current will be real, and all the other values will have both real (in-phase) and imaginary (quadrature phase) components since these values are the harmonic components of the waveform [52]. Furthermore, the frequency of the n^{th} index will be $\frac{(n-1)F_s}{N}$ where F_s is the sampling frequency. If we take the real and imaginary parts of the Fourier transform, then the phase of each harmonic will be $\arctan(\frac{\text{imaginary coefficient}}{\text{real coefficient}})$, using a 4-quadrant arctangent [52].

Once the Fourier analysis (in other words finding the spectral components of the wave) has been completed, the final step in mathematically reconstructing the pressure waveforms in figures 4.4 and 4.7 is known as Fourier synthesis. Therefore, the periodic pressure waveforms measured at the mouthpiece of the trumpet can be expressed mathematically as the sum of sinusoidal waves which are integer multiples of the fundamental frequency. In other words, by Fourier's Theorem, the trumpet sound B_3^b (which has a fundamental frequency $f = 240\ Hz$) can be described as a sum of sine/cosine waves: f, $2f$, $3f$, each with a corresponding amplitude, A, and phase shift, ϕ.[43] Since the harmonic component in each bin contains a real and imaginary part, the sinusoidal function of a harmonic can be rewritten as a phase-shifted cosine function that is a superposition of the real and imaginary parts with amplitudes α, and β [21, s. 50-2]

$$\alpha_i \cos(\omega_i t) + \beta_i \sin(\omega_i t) = A_i \cos\left(2\pi f_i t + \phi_i\right), \tag{5.15}$$

where i corresponds to the harmonic number that is being considered, t is time, f_i is frequency, $\omega_i = 2\pi f_i$ is the angular frequency and the amplitude A is defined as

[42] When considering a periodic function described in the frequency domain, the direct current (DC) is the mean value of the waveform. Feynman describes it as representing the shift of the average value (that is, the "zero" level) of the sound pressure [21, s. 50-2].

[43] In other words, if the sinusoidal waves were played together at the same time with the specified loudness defined by the Fourier coefficient, they would reproduce the sound heard in the lab [50]. Thus, by taking the inverse fast Fourier transform ($ifft$), one can verify that the resulting graphs in the time domain are the same as the oscilloscope plots (and sure enough the plots matched!).

$$A_i = \sqrt{(\alpha_i^2 + \beta_i^2)}, \tag{5.16}$$

and finally, the corresponding phase angle ϕ_i is defined as

$$\phi_i = \arctan\left(\frac{\beta_i}{\alpha_i}\right). \tag{5.17}$$

Therefore, one period of the entire pressure waveform of a desired note is expressed as

$$p = A_0 + \sum_i A_i \cos\left(2\pi f_i t + \phi_i\right). \tag{5.18}$$

The A_i's are the amplitudes of the harmonic components (called Fourier coefficients), where A_0 is the DC term, and t is time [21, s. 50-2]. One may notice that the discrete Fourier transform does not show separated lines on the plots in figures 4.5 and 4.8. The curve may appear like mush, but this is fine since in fact it represents the harmonic spectrum. Instead, if many oscillations were taken, a more traditional line spectrum would be present [52]. In addition, it is only necessary to consider a certain number of harmonics in order to reconstruct the waveform for the B_3^b or B_4^b played at f. This will be further examined in section 6.3.1.

Now that the boundary condition for the pressure at the mouthpiece is obtained, the corresponding density at the mouthpiece was chosen such that it would represent isentropic flow. Thus,

$$\rho = C p^{\frac{1}{\gamma}}, \tag{5.19}$$

where C is the proportionality constant and $\gamma \approx 1.4$ in air at roughly 300 K. In this case, $C = \gamma$ [24]. Finally, an expression relating the mouthpiece pressure, p, and flow velocity, u, is needed. In linear acoustics, this relationship is defined as follows

$$p - p_o = \rho_o c u, \tag{5.20}$$

where p_o is atmospheric pressure (which is scaled to 1) [42, p. 22]. We use (5.20) to set the boundary condition for velocity using the recorded pressure values of p. We write,

$$u = \frac{p - p_o}{\rho_o c}. \tag{5.21}$$

However, it is important to understand the physics of this relationship. When we physically consider a player blowing into a musical instrument, pressure is generated as a consequence of the flow velocity, not the other way around. Therefore, if (5.21) was used in the simulations to obtain a closed system, it would have to be physically justified [52]. If in fact the relationship between u and p was correct, as a consequence, the pressure waveform measured in the laboratory should be accurately reproduced. To precisely determine an expression for u as a function of p, more experiments would have to be carried out. In theory, one could attempt to find such an expression with our current knowledge. Unfortunately, to obtain such a result analytically requires the convolution theorem which assumes linearity. Although this idea will not be fully explored in this thesis due to time constraints, this proposal is currently being studied. For a more detailed discussion on the set up of this problem, see Appendix D.

It should also be mentioned, Rossing presents an alternative expression for the relationship between u and p (at the mouthpiece for a brass instrument). In particular, the volume flow at the mouthpiece was defined as

$$U \approx \gamma x p^{\frac{1}{2}} \tag{5.22}$$

where x is the lip opening ratio to the diameter of the mouthpiece. This expression was taken from [24, p. 446] under the assumption that one has large amplitude nonlinearities such that the lip opening x is small and the blowing pressure at the mouthpiece is large [24, p. 445].

We applied both (5.21) and (5.22) to (5.11). In reviewing the numerical results, we found that (5.21) did reproduce the pressure waveforms illustrated in figures 4.4 and 4.7. So for our purposes, it is an acceptable approximation. When (5.22) was considered, the waveforms generated had the correct shape; however, there was a large shift in the amplitude (it was shifted downward by approximately 6000 Pa, and the difference between the maximum and minimum pressure was too small). Therefore, in summary, the system of PDEs used in the DGM was constructed as follows

$$\text{Boundary Conditions: } \begin{cases} p = A_0 + \sum_i A_i \cos\left(2\pi f_i t + \phi_i\right), \\ \rho = \gamma p^{\frac{1}{\gamma}}, \\ u = \frac{p - p_o}{\rho_o c}, \\ v = 0.0, \\ E = \frac{p}{\gamma - 1} + \frac{\rho}{2}(u^2 + v^2). \end{cases}$$

5.2.4 Mesh

We performed the computations on unstructured triangular meshes. The mesh for any problem is important because the refinement determines not only how accurate a simulation is, but also how computationally burdensome it is. As the number of cells increases, so does the accuracy and run time. The stable time step Δt is determined by the Courant-Friedrichs-Lewy (CFL) condition. [44] In particular, the CFL condition states

$$\Delta t \leq \frac{\Delta x}{\lambda_{max}(2p+1)} \tag{5.23}$$

where Δx is the element size, p is the order of the polynomial basis, and λ_{max} is maximum wave speed of propagation. This constraint has to be satisfied for the DGM, assuming the time scheme is a Runge-Kutta method of order $(p+1)$ [53], [18, pp. 22-23]. [45]

For the numerical experiments that will be discussed in the next chapter, several unstructured triangular meshes have been used. They are shown in figures 5.1, 5.2, and 5.3. Tables 5.1, 5.2 and 5.3 summarize the number of nodes, cells and edges for each mesh respectively. As one can see in the figures, the top plots depict a trumpet mesh with one bend, whereas the middle plots show a trumpet mesh with no bend, and the bottom plots show a straight tube (the details explaining why these meshes were designed this way can be found in chapter 6). The trumpet meshes were constructed such that one unit on the axis represents 1 cm. The total length of the duct in each mesh is equivalent to 1.48 m. The dimensions of the box around the trumpet in each mesh shown in figure 5.4, is equivalent to 1.60 m by 0.72 m. Figures 5.1 and 5.3 however are constructed such that the box in each mesh is around the trumpet bell (there is only a small boundary around the actual tubing) rather than the entire trumpet. We did this to make the computation less expensive. Thus, these were the main meshes used for the numerical simulations that will be presented in chapter 6. The dimensions of the box around the bell in each plot is equivalent to 2.5 $1m$ by 0.72 m.

[44] The requirement of this condition is that the time step, denoted Δt, must be less than a certain time in an explicit scheme, otherwise stability will not be achieved [53].

[45] It should also be noted that the size of the elements for a mesh influences the numerical dispersion and diffusion which for DGM have order h^{2p+2} and h^{2p+1} respectfully [18, p. 23].

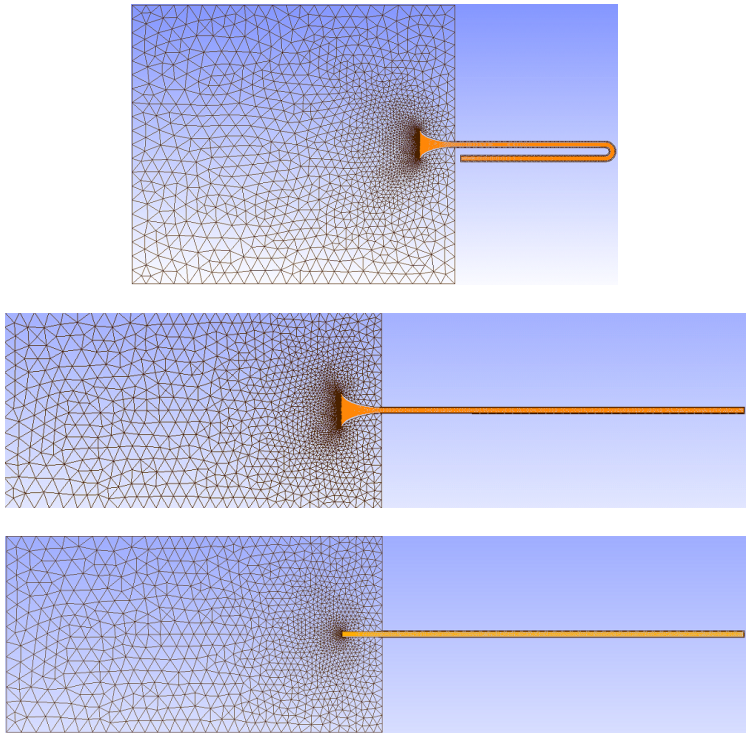

Figure 5.1: Trumpet meshes with the box around the end of the duct. Mesh with a flare and bend (top), only a flare (middle) and, no bend or flare (bottom).

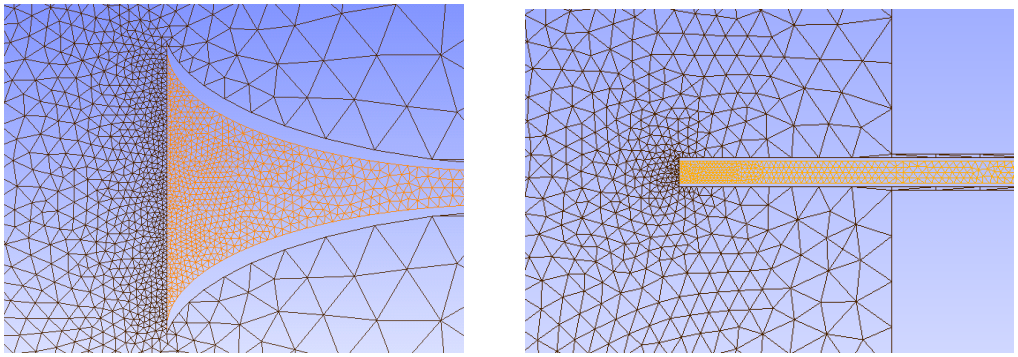

Figure 5.2: Close up of the mesh refinement at the mouthpiece. Note that the refinement in the cylindrical part of the tube is the same in the straight tube mesh.

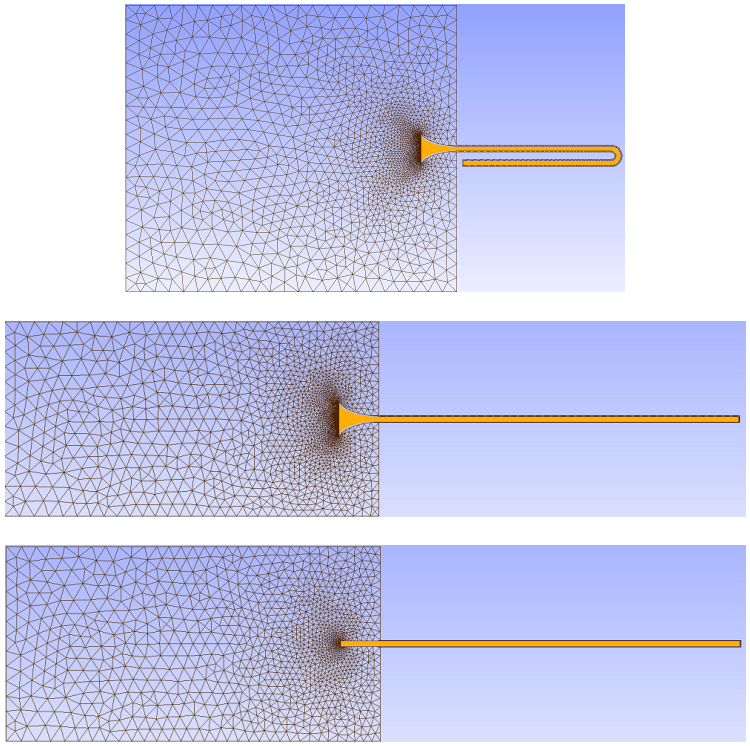

Figure 5.3: Meshes shown in figure 5.1 with more refinement. Mesh with a flare and bend (top), only a flare (middle) and, no bend or flare (bottom).

Table 5.1: Number of node, cells and boundaries for each of the meshes shown in figure 5.1.

-	Mesh with Bend	Mesh with no Bend	Mesh with no Bend/Flare
Number of nodes	9449	4096	3033
Number of cells	17216	6981	5113
Number of edges	26665	11417	8116

5.2.5 Dimension Considerations: Estimated Difference of Trumpet Output between two and three Dimensions

For this thesis, an important factor that should be considered is the symmetry and dimensionality of our problem. As indirectly indicated in the previous section, all of the

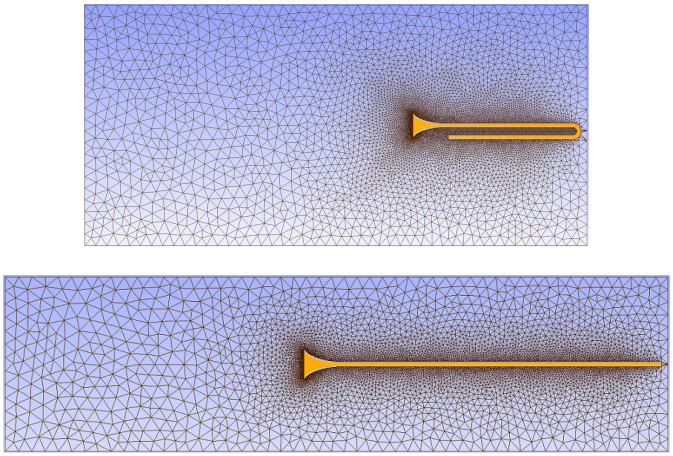

Figure 5.4: Original trumpet meshes with box around entire trumpet. The plots depict a mesh with a flare and bend (top), and only a flare (middle).

Table 5.2: Number of node, cells and boundaries for each of the meshes shown in figure 5.3.

-	Mesh with Bend	Mesh with no Bend	Mesh with no Bend/Flare
Number of nodes	17787	9898	8149
Number of cells	33039	17894	14484
Number of edges	50836	27882	22624

Table 5.3: Number of node, cells and boundaries for each of the meshes shown in figure 5.4.

-	Mesh with Bend	Mesh with no Bend
Number of nodes	10391	10119
Number of cells	19217	18703
Number of edges	29608	28822

simulations that will be discussed in chapter 6 were done in two dimensions (in order to make the problem more manageable). The next step of course would be to extend the

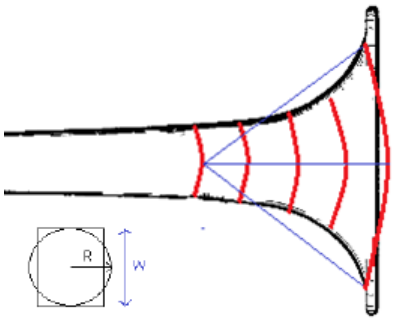

Figure 5.5: Trumpet bell in two dimensions. Notice that in order to approximate the bore with radius R, we would have to use a square with height W.

model to the third dimension since we are missing a degree of freedom.

If we assume that the bends can be neglected (which will be justified in chapter 6), the trumpet mesh has axially symmetry. In addition, if we assume that sound propagates symmetrically outward as it exits the bell, neglecting the third dimension would be a reasonable approximation. A depiction of this can be seen in figure 5.5. It is important to note that in reality the amplitude of the wave across the bell will not be uniform, it will be lower at the "edges of the trumpet bell. Nonetheless, we are going to assume that this variation is negligible.

However, by considering the problem in two dimensions, the pressure waves will not be able spread in the third dimension as they travel out of the bell. As a consequence, we expect that there will be some discrepancies, particularly in the amplitude values, between the experimental and numerical data. More precisely, by estimating the area of the curved wave front (that is propagating out of the bell) between the second and third dimension, we speculate that neglecting the third dimension in our simulations could produce amplitude values that are 3.1 times larger than they should be. This number was determined by looking at the pressure ratio between the second and third dimension and using the fact that energy is proportional to p^2. A detailed derivation can be found in Appendix F.

Chapter 6

Numerical Simulations

6.1 Overview of Numerical Experiments

This chapter will review two major sets of simulations (numerical experiments) that were carried out for this thesis. The first set will be referred to as the *pulse experiments* and the second will be called the *waveform experiments*. For both types of experiments, all the simulations were done in two dimensions. However, we postulated that neglecting the third dimension will affect the results. For the pulse experiments, two groups of pulses will be examined. A group of low amplitude pulses all having the same amplitude but varying durations; and a group of high amplitude pulses which will have the same duration but varying amplitudes. In regards to the waveform experiments, several things will be examined. The first task will be to reproduce the mouthpiece pressure waveforms depicted in figures 4.3, 4.4, 4.6 and 4.7 using Fourier series composition. We will then determine how many harmonic components are needed to construct the waveforms accurately. Once this is completed, the B_3^b and B_4^b note will be simulated.

6.2 Pulse Experiments

Before attempting to reproduce the measured sound pressure waves (of the B_3^b and B_4^b notes shown in chapter 4), we first need to test the numerical model. In particular, through these pulse experiments we want to acoustically validate the DGM implementation. This will

establish confidence in the numerical outputs when reviewing the other results. To perform such an experiment, an acoustic pulse will be sent down the trumpet meshes depicted in chapter 5. However, besides verifying the code and the setup, there are several acoustic reasons for performing these pulse tests:

* The behaviour of the bell can be examined by simulating a low amplitude pulse of say 2% of an atmosphere (2026.5 Pa). From such a trial, we expect to see the fundamental frequency and lower harmonics traveling back up the trumpet toward the mouthpiece; whereas the higher frequencies would propagate out of the bell. This experiment will be especially useful to determine the breakpoint frequency; below which waves are principally reflected by the bell, and above which waves are precisely transmitted out of the bell. From this we also hope to further understand the behaviour of the reflections at the bell.

* By taking increasingly high amplitude pulses of say $2\% - 20\%$ of an atmosphere (2026.5 Pa-20,265 Pa), one can verify that wave steepening becomes more influential for stronger pulses. If shock waves are obtained, the shock distance expression (2.9) for a finite amplitude pulse can also be verified. In addition, by continuously simulating shorter duration pulses with the same amplitude; we can also test the hypothesis that higher frequencies steepen moreso than lower frequencies (remembering of course that steepening is proportional to $\frac{\partial p}{\partial t}_{max}$).

* The importance of the trumpet geometry can also be examined by simulating an acoustic pulse down the instrument. In particular, three meshes will be used to determine (and verify) the significance (and claims) of the flare and bend. These meshes are illustrated in figures 5.1 and 5.3. However, if it is found that the presence of one bend greatly influences the results (compared to the mesh with just the flare); the bend will have to be included in the mesh for all other simulations. It is possible that a mesh with two bends would have to be used to accurately describe the wave propagation through a trumpet.

* Both pressure, p, and velocity, u can be specified at the mouthpiece boundary condition using the relation $p - p_o = \rho_0 c u$, where $p_o = 1.0$ atmosphere, and c is the speed of sound. Moreover, one can justify to themselves that the velocity expression (5.21) is an acceptable relationship to consider.

* Finally, in theory, if a short amplitude pressure pulse was sent down the trumpet, one could convolve this pulse with the pressure waveform measured in the lab (depicted in figures 4.3-4.8) to determine the exact form of the velocity expression (more precise

details can be found in Appendix D). If this obtained velocity was then considered in (5.20), the resulting pressure distribution should be the same as the waveforms shown in figures 4.3, 4.3, 4.6 and 4.7. This would allow one to numerically validate the expression Rossing derives in (5.22). [46]

6.2.1 Low Amplitude Pulse Set Up

The first numerical experiment will be sending a small amplitude pulse down the trumpet at varying durations. From this, it can be determined if wave steepening is more prominent for short duration pulses compared to long duration pulses. Five durations will be considered for this particular experiment, all of which will have an amplitude of $2027Pa$. We will define Pulse 1 as follows

$$p = \left\{ \begin{array}{ll} 1.0 + (0.01 - 0.01\cos(\alpha_i \mathrm{t})) & \text{if t} < \frac{2\pi}{\alpha_i} \\ 1.0 & \text{else} \end{array} \right\}$$

$$\alpha_i = \left\{ \begin{array}{l} \text{where } i = 1 \text{ corresponds to } 0.001595\ s \\ \text{where } i = 2 \text{ corresponds to } 0.0007976\ s \\ \text{where } i = 3 \text{ corresponds to } 0.0003988\ s \\ \text{where } i = 4 \text{ corresponds to } 0.0001994\ s \\ \text{where } i = 5 \text{ corresponds to } 0.0000996\ s \end{array} \right.$$

These pulses are shown in the left plot of figure 6.1. The corresponding frequency spectrum for each pulse is depicted in the right plot of figure 6.1. The other motivation for these simulations is to establish how the geometry of the trumpet effects the propagation of the pulses depicted in figure 6.1. Thus, these pulses will be simulated in three separate trumpet meshes. The first mesh does not have a bend or a flare, the second has a flare but no bend, and finally, the third has one bend and a flare. For α_i, where $i = 1$, 2, 3 and 4, the meshes from figure 5.1 will be used, whereas for $i = 5$, the meshes in figure 5.3 will be used.

6.2.2 Low Amplitude Pulse Results

The low amplitude pulses of varying duration exiting the end of the tube or flare are shown in figure 6.4. The pulses near the mouthpiece (22cm into the mesh) after they have been

[46] The impedance of the trumpet could also be calculated. However, for the purposes of this thesis, these experiments will not be carried out. Nonetheless, a further description of such a procedure can be found in Appendix D.

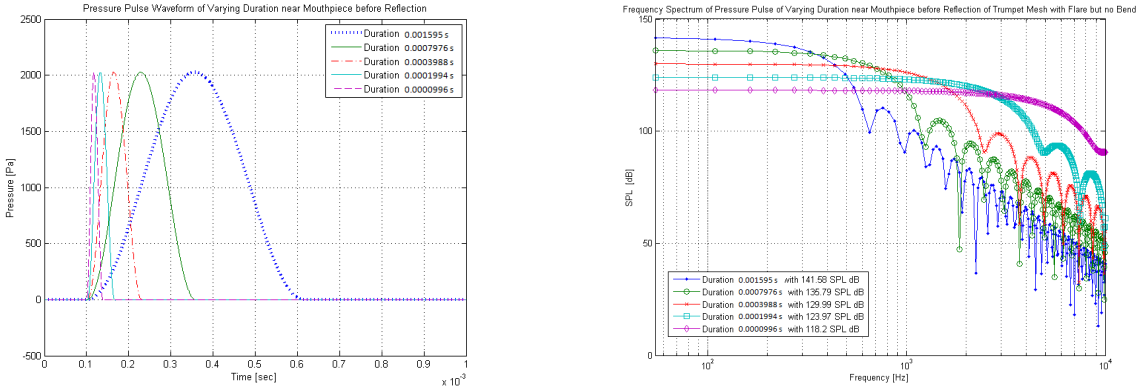

Figure 6.1: Waveforms of the low amplitude pulses $22cm$ into the mouthpiece (before the reflection at the bell) for all trumpet meshes. The durations of the pulses are 0.001595 s (blue), 0.0007976 s (green), 0.0003988 s (red), 0.0001994 s (light blue) and 0.0000996 s (purple).

reflected from the end of the tube are shown in figure 6.2. The corresponding frequency spectra at the bell, and near the mouthpiece after reflection, are shown in figures 6.5 and 6.3 respectively. In each figure, the first plot shows the pulses that were simulated in the mesh with no bend or flare, the second plot shows the results for the mesh without a bend but with a flare, and the third plot depicts the results for the mesh with the bend and flare.

6.2.3 Further Discussion for Low Amplitude Pulse Simulations

Although the results mentioned above are interesting, interpreting the physical significance of the data is difficult. Nonetheless, several observations can be made:

* The shape of the pressure pulses near the mouthpiece (after the reflection has occurred) have a different profile depending on which mesh the pulses were simulated in. The straight tube mesh depicted in the third plot of figure 5.1, produces reflected waveforms (shown in figure 6.2) that are almost an exact mirror image of the initial pulses shown in the left plot figure 6.1. However, the profiles of the reflected pulses that were simulated in the trumpet mesh with a bell and bend (first plot of figure 5.1) and only a bell (second plot of figure 5.1) are distorted. The shape of the distorted reflected pulses in the second and third pulse plots of figure 6.2 are very similar.

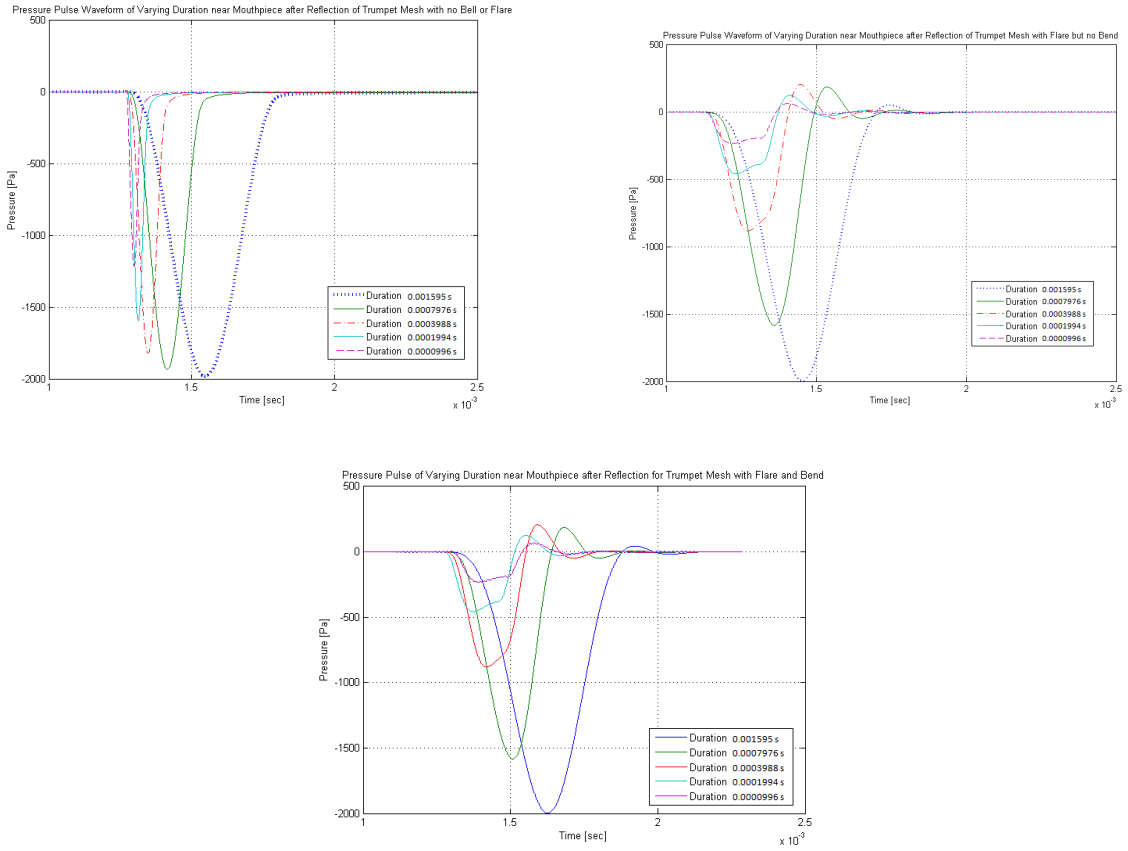

Figure 6.2: Waveforms near the mouthpiece (after the reflection at the bell) where the trumpet mesh in (first plot) does not have a flare or bend, (second plot) has a flare but no bend, and (third plot) has a flare and bend. The durations of the pulses are 0.001595 s (blue), 0.0007976 s (green), 0.0003988 s (red), 0.0001994 s (light blue) and 0.0000996 s (purple).

This suggests that the bend does not greatly influence the propagation (at least for low amplitude pulses), but the flare does. For instance, unlike the first pulse plot in figure 6.2, the second and third pulse plots depict a positive overshoot. This implies one will observe a variation in the harmonic spectrum.

* Upon examining the frequency spectra in figure 6.3 (the reflection pulses of figure 6.2), one can observe that the harmonic spectra in the first pulse plot differs from the second and third pulse plots. The DFT data corresponding to the straight tube mesh

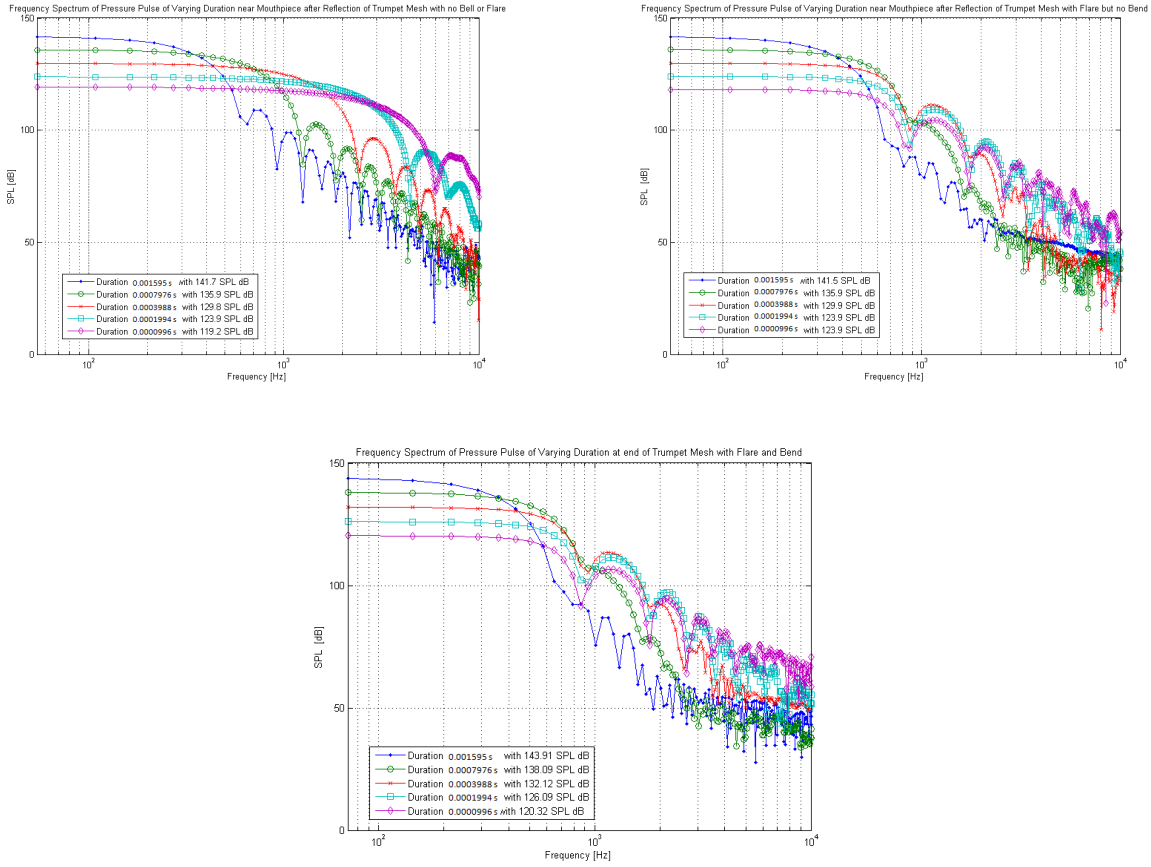

Figure 6.3: Frequency spectra for the low amplitude pulses near the mouthpiece (after the reflection at the bell) where the trumpet mesh in (first plot) does not have a flare or bend, (second plot) has a flare but no bend, and (third plot) has a flare and bend. The durations of the pulses are 0.001595 s (blue), 0.0007976 s (green), 0.0003988 s (red), 0.0001994 s (light blue) and 0.0000996 s (purple).

(figure 6.3) look almost identical to the initial pulse frequency spectra (figure 6.1). In the second and third pulse plots of figure 6.3, the consequences of the flare are quite prominent. In particular, nulls (slinky like jumps) [47] appear periodically every 875 Hz. The exact reasoning for this is not clear, and this type of result was not expected. The only conclusion that we are able to draw from this is that the reflec-

[47] The term nulls will be used to describe the dips in the bounce-type behaviour in the frequency spectra.

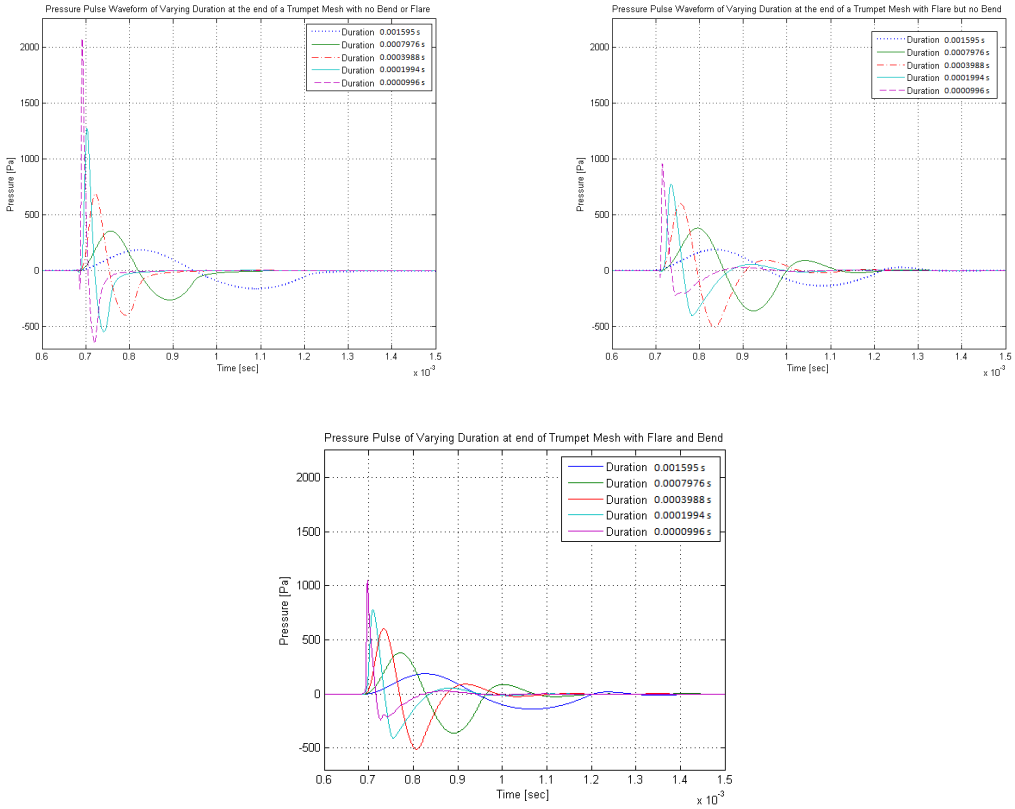

Figure 6.4: Waveforms of the low amplitude pulses at the bell where the trumpet mesh in (first plot) does not have a flare or bend, (second plot) has a flare but no bend, and (third plot) has a flare and bend. The durations of the pulses are 0.001595 s (blue), 0.0007976 s (green), 0.0003988 s (red), 0.0001994 s (light blue) and 0.0000996 s (purple).

tions distribute the harmonic spectra in a particular way independent the frequency considered. Thus, it appears that the flare is a high frequency (transmission) filter for low amplitude pulses. In [48, p. 1102], the authors also suggest from their pulse experiments that the bell acts in some sense as a high pass filter. [48] We speculated that the two dimensional flare would produce rather fat returning pulses, which will consequently have nulls in the falling response like the ones depicted in figure 6.3.

* From reviewing the shapes of the low-amplitude pulses at the junction of the room

[48] In order to make this a more global statement (so to say the flare is a high frequency filter), we would have to see if the same result is obtained for pulses with varying amplitude.

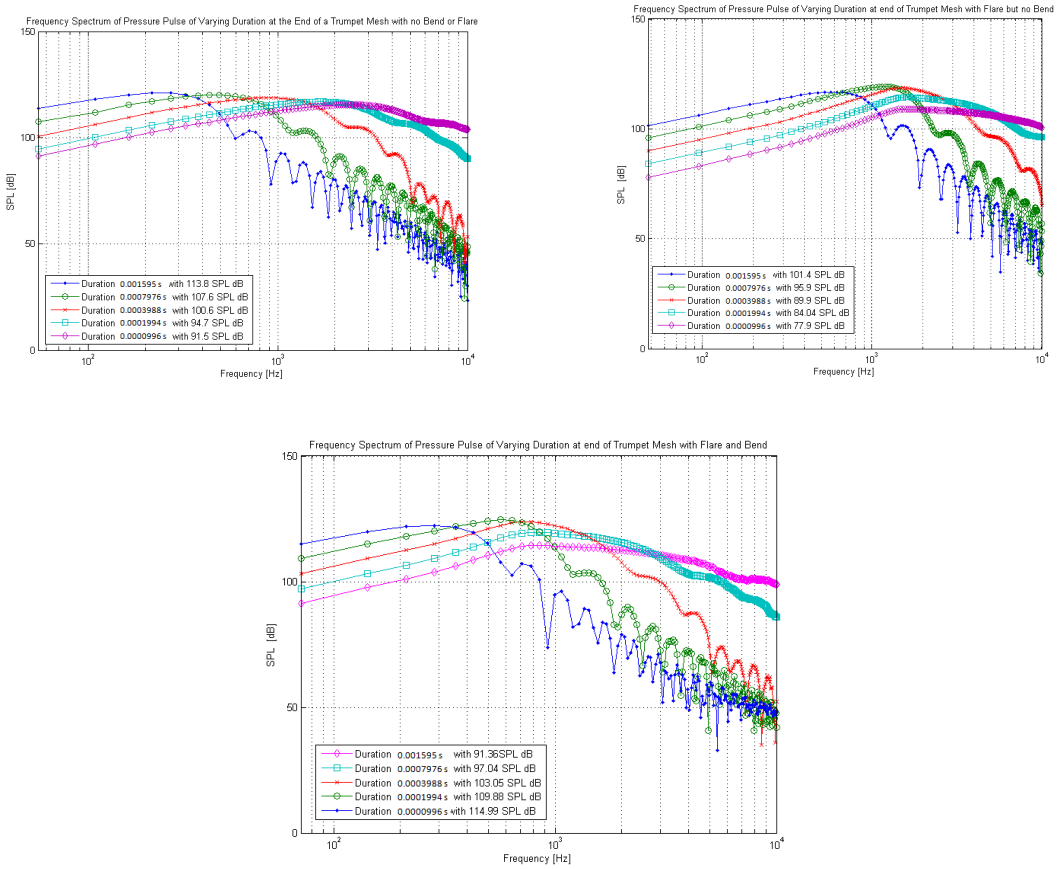

Figure 6.5: Frequency spectra for the low amplitude pulses at the bell where the trumpet mesh in (first plot) does not have a flare or bend, (second plot) has a flare but no bend, and (third plot) has a flare and bend. The durations of the pulses are 0.001595 s (blue), 0.0007976 s (green), 0.0003988 s (red), 0.0001994 s (light blue) and 0.0000996 s (purple).

and bell (figure 6.4), one can see that the profiles leaving the meshes with a flare (second and third pulse plots of figure 6.4) are comparable. More specifically, it appears that as the duration of the pulses decrease, wave distortion becomes more evident. The pulses not only become sharper, but also more deformed. There is a larger (and sharper) negative component to the wave profile. In addition, the amplitude of any one of these pulses leaving the bell is (at least) half the amplitude of the initial pulse. However, the pulses in the first pulse plot of figure 6.4 illustrate that the amplitudes are about twice as large as the other pulses shown in the second

and third pulse plots of figure 6.4. Finally, the global minimum for the pulses becomes larger (i.e. more negative) as the duration decreases.

* The corresponding frequency spectra shown in figure 6.5 illustrates that the propagating behaviour is similar for the pulses simulated in all three meshes. All three plots depict that the loudest pulse becomes the quietest in the highest frequency range; the second loudest becomes the second quietest and so on. The only noticeable differences are the volume variations and slopes. The sound pressure levels shown in the first pulse plot of figure 6.5 are the loudest, but the third pulseplot in figure 6.5 has comparable measurements. However, the sound pressure levels in the second pulse plot of figure 6.5 are around 10 dB lower.

6.2.4 High Amplitude Pulse Set Up

The next numerical experiment will examine if the amplitude of a short duration pulse influences wave steepening. Four separate 0.001277 s duration pulses will be sent down the trumpet tube with varying amplitude. Pulse 2 will be defined as follows

$$p = \left\{ \begin{array}{ll} 1.0 + (\beta_i - \beta_i \cos(\alpha \text{time})) & \text{if t} < \frac{2\pi}{\alpha}\text{, where } \alpha \text{ corresponds to 783.46 } Hz \\ 1.0 & \text{else} \end{array} \right\}$$

$$\beta_i = \left\{ \begin{array}{l} 0.01 \text{ if } i = 1 \text{ which corresponds to 2026.5 } Pa \\ 0.03 \text{ if } i = 2 \text{ which corresponds to 6079.5 } Pa \\ 0.06 \text{ if } i = 3 \text{ which corresponds to 12159 } Pa \\ 0.1 \text{ if } i = 4 \text{ which corresponds to 20265 } Pa \end{array} \right.$$

The pulses which enter the mouthpiece of the trumpet meshes, and their corresponding frequency spectra are depicted in figure 6.6. Again, the high amplitude pulses will also be simulated in the three different trumpet meshes. For β_i, where $i = 1$, 2, and 3, the meshes from figure 5.1 will be used, whereas for $i = 4$, the meshes in figure 5.3 will be used.

6.2.5 High Amplitude Pulse Results

The high amplitude pulses of varying amplitude exiting the end of the instrument are shown in figure 6.10. Figure 6.7 shows the profiles of the reflected pulses 22cm into the trumpet mouthpiece. The frequency spectra of the pulses propagating out the instrument

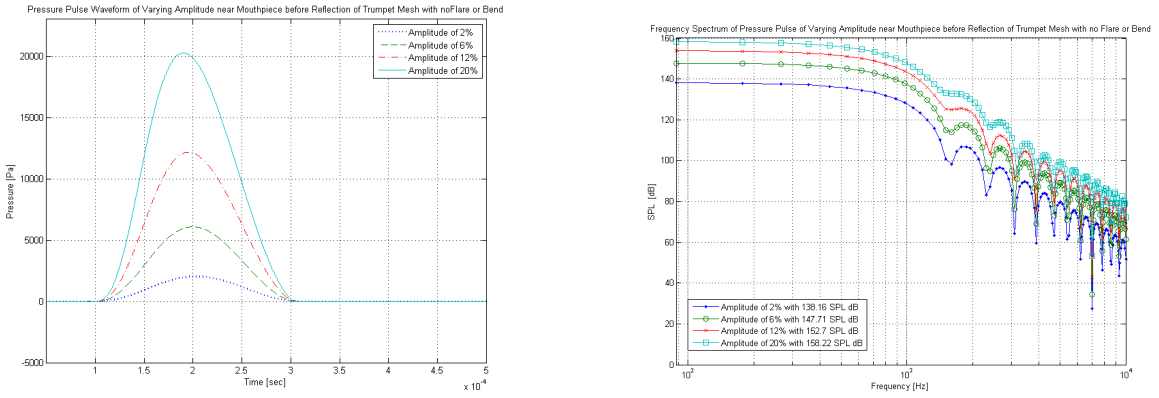

Figure 6.6: Waveforms (left) and frequency spectra (right) of the high-amplitude pulses 22cm into the mouthpiece (before the reflection at the bell) for all trumpet meshes. The amplitudes of the pulses are 2% of an atmosphere (blue), 6% of an atmosphere (green), 12% of an atmosphere (red), and 20% of an atmosphere (light blue).

and the reflected pulses near the mouthpiece are shown in figures 6.11 and 6.8 respectively. Unlike the low amplitude pulses, the high amplitude pulses that propagated through the trumpet mesh depicted in the first plot of figure 5.1 had a small portion of the initial profiles reflect off the bend while they were traveling towards the bell. These waveforms and the corresponding frequency spectra can be seen in figure 6.9.

6.2.6 Further Discussion for High Amplitude Pulse Simulations

From reviewing the results, one can see that as the amplitude of a pulse increases, wave steepening becomes more pronounced. The consequences of such distortion can be observed in numerous ways:

* To begin, from comparing the initial pulses in figure 6.6 (specifically the frequency spectra in the second pulse plot) to the low amplitude pulses in figure 6.1, the plots differ in several ways. For example, the spectra of the high amplitude pulses (in the second pulse plots of figures 6.6 and 6.8) do not intersect at all like in the second pulse plots in figures 6.1 or 6.2. Rather, the harmonic spectrum for each high amplitude pulse is distinct. [49] Moreover, it appears that these triangular-like pulses suppress the nulls that would appear in the frequency spectra.

[49] This potentially means that there was a transfer of energy to the higher harmonic components.

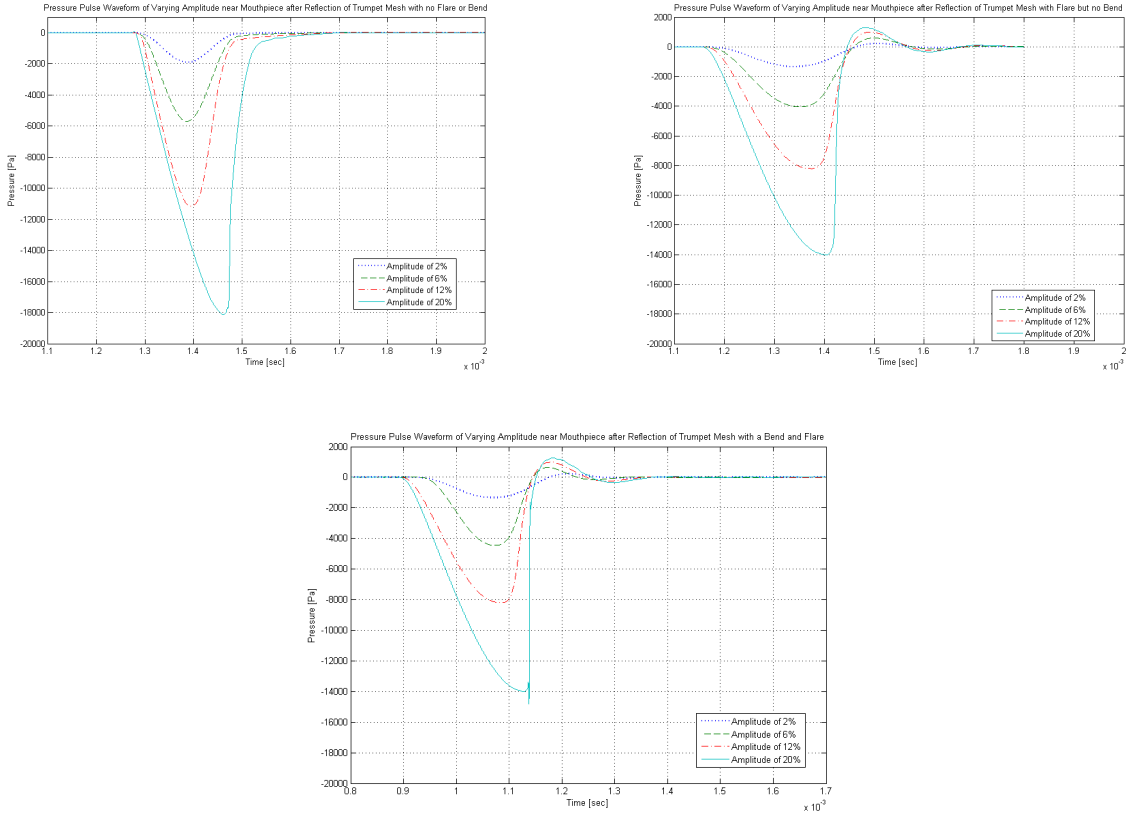

Figure 6.7: Waveforms of the high amplitude pulses near the mouthpiece (after the reflection at the bell) where the trumpet mesh in (first plot) does not have a flare or bend, (second plot) has a flare but no bend, and (third plot) has a flare and bend. The amplitudes of the pulses are 2% of an atmosphere (blue), 6% of an atmosphere (green), 12% of an atmosphere (red), and 20% of an atmosphere (light blue).

* By looking at the high amplitude pulses returning to the mouthpiece after reflection (figure 6.7), one can see that the shape of the pulses has been altered in a fashion similar to the low amplitude pulses in figure 6.2. The key difference is, for the high amplitude pulses, as the amplitude increases, one can clearly observe wave steepening. Especially in the second and third pulse plots when the flare or bend is considered. In the third pulse plot in figure 6.7 (trumpet mesh with bend and flare), it appears that a weak shock wave has been generated for the tallest pulse (baby blue line). Recall that this pulse's amplitude is 20% of an atmosphere. Although the second and third

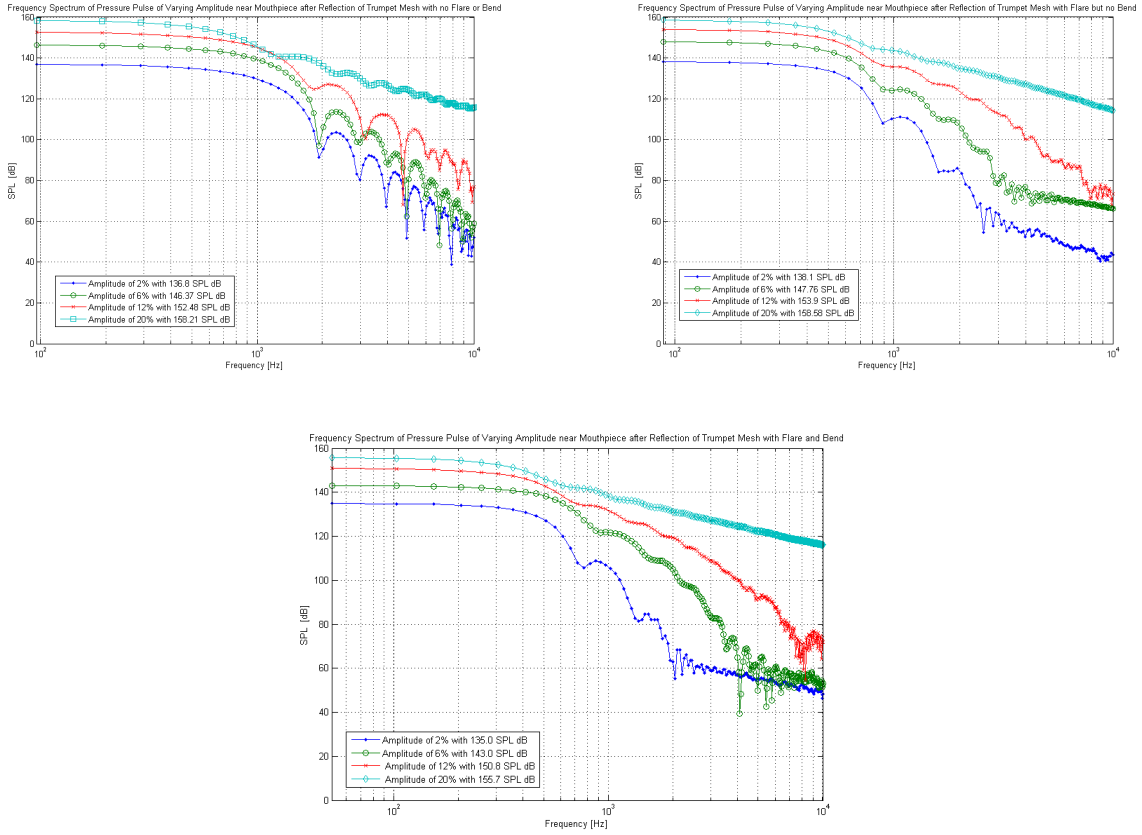

Figure 6.8: Frequency spectra for the high amplitude pulses near the mouthpiece (after the reflection at the bell) where the trumpet mesh in (first plot) does not have a flare or bend, (second plot) has a flare but no bend, and (third plot) has a flare and bend. The amplitudes of the pulses are 2% of an atmosphere (blue), 6% of an atmosphere (green), 12% of an atmosphere (red), and 20% of an atmosphere (light blue).

pulse plots in figure 6.7 are similar, this seems to be the major difference between them (a weak shock is not produced for the mesh only consisting of the flare). In addition (just as in the case for the low amplitude pulses in the first pulse plot of figure 6.2), the straight tube mesh in the first pulse plot of figure 6.7, illustrates that the returning pulse has no positive overshoots. We also see a clear indication of wave steepening in the first pulse plot of figure 6.7.

* From looking at the corresponding harmonic spectra (figure 6.8), additional insight

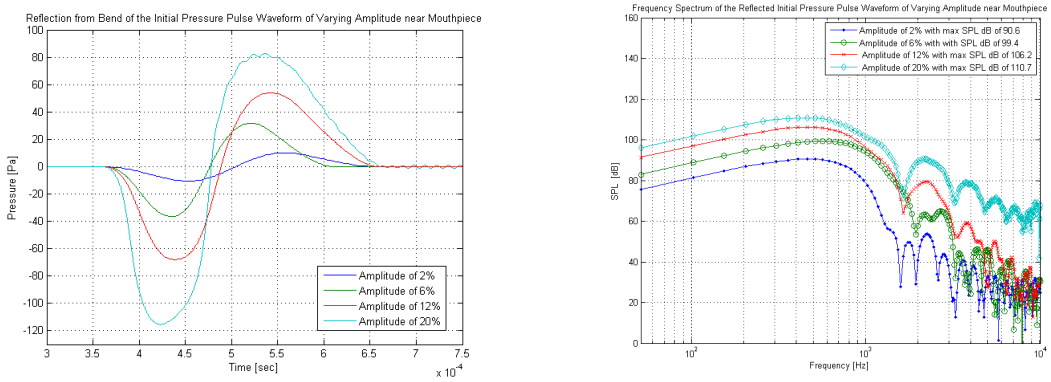

Figure 6.9: Initial waveforms (left) and corresponding frequency spectra (right) of the high amplitude pulses near the mouthpiece after it is reflected at the bend. The amplitudes of the pulses are 2% of an atmosphere (blue), 6% of an atmosphere (green), 12% of an atmosphere (red), and 20% of an atmosphere (light blue).

can be extracted. Firstly, the behaviour of the spectra for the lower amplitude pulses in figure 6.8 is comparable to pulses shown in figure 6.3. In particular, the lowest pulses (blue lines) in figure 6.8 still depict nulls in 875 Hz intervals. However, as the amplitude of the high amplitude pulse gets larger and more steepening is experienced, the waveform and the corresponding frequency spectrum becomes more distorted. For instance, nulls can still be observed in the 2% pulse, but these nulls become less and less visible as the amplitude increases, especially for the second and third pulse plots of figure 6.8. So, if in fact the flare acts as a high frequency filter for the transmission waves, this would imply that as wave steepening becomes more prominent, the higher frequency components become more influential. Therefore, from what we are observing, it would appear that there is a transfer of energy to the higher harmonics when wave steepening occurs.

* As mentioned above, the high amplitude pulses that propagated through the trumpet mesh depicted in the first pulse plot of figure 5.1 had a small portion of the initial profiles reflect from the bend while they were traveling towards the bell. This can be seen in the first pulse plot of figure 6.9. Although the amplitudes of these little pulse reflections are small (the maximum amplitude is only around 120 Pa), it is interesting to note which frequency components compose the reflections. As one can see in the second pulse plot of figure 6.9, the slope of the lines is approximately $+8$ $dB/octave$. Furthermore, it is the upper frequency components that compose

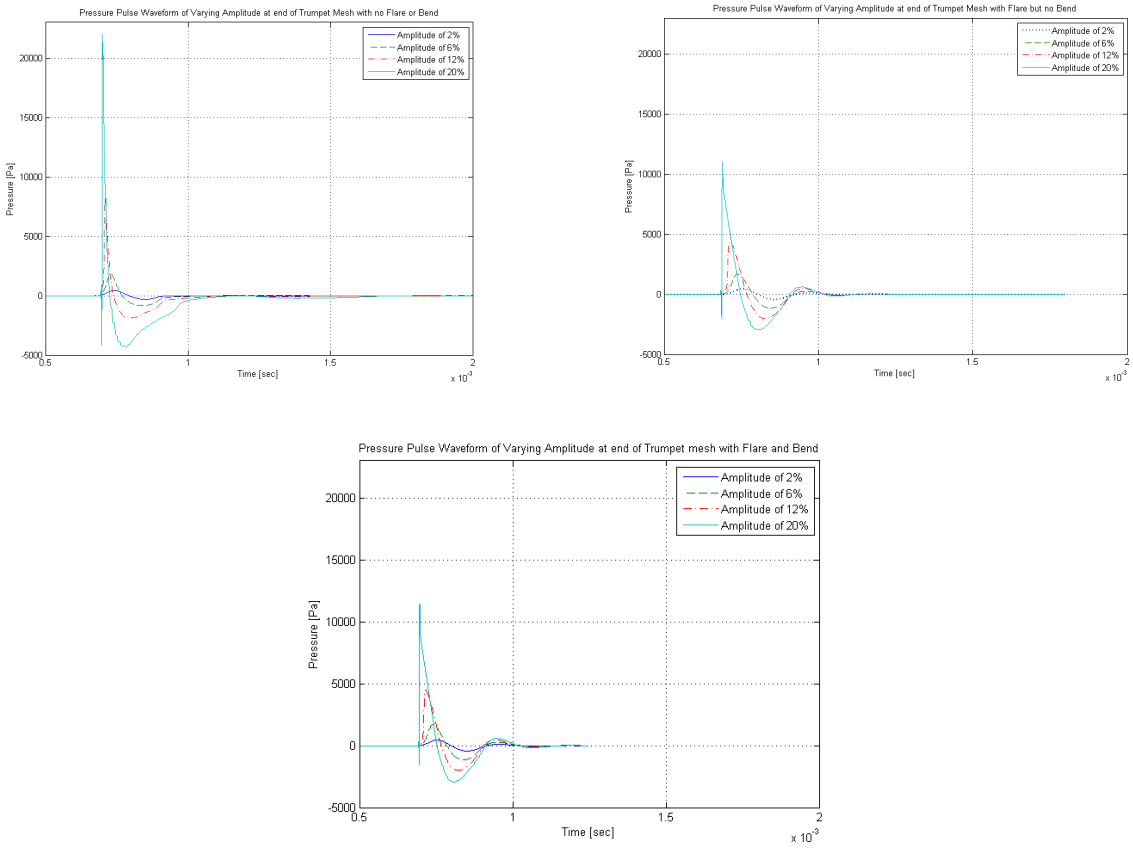

Figure 6.10: Waveforms of the high amplitude pulses at the bell where the trumpet mesh in (first plot) does not have a flare or bend, (second plot) has a flare but no bend, and (third plot) has a flare and bend. The amplitudes of the pulses are 2% of an atmosphere (blue), 6% of an atmosphere (green), 12% of an atmosphere (red), and 20% of an atmosphere (light blue).

the pulses depicted in the first pulse plot of figure 6.9. This may explain why the pulses in the third pulse plot of figure 6.7 seem steeper than in the second pulse plot; because a slightly larger portion of the higher spectra stayed within the confines of the trumpet. This is like adding energy to the higher frequency components, which is like mimicking the consequences of wave steepening.

* The high amplitude pulses exiting the bell can be seen in figure 6.10 and all three plots illustrate weak shock waves for the highest pulse (baby blue). However, the

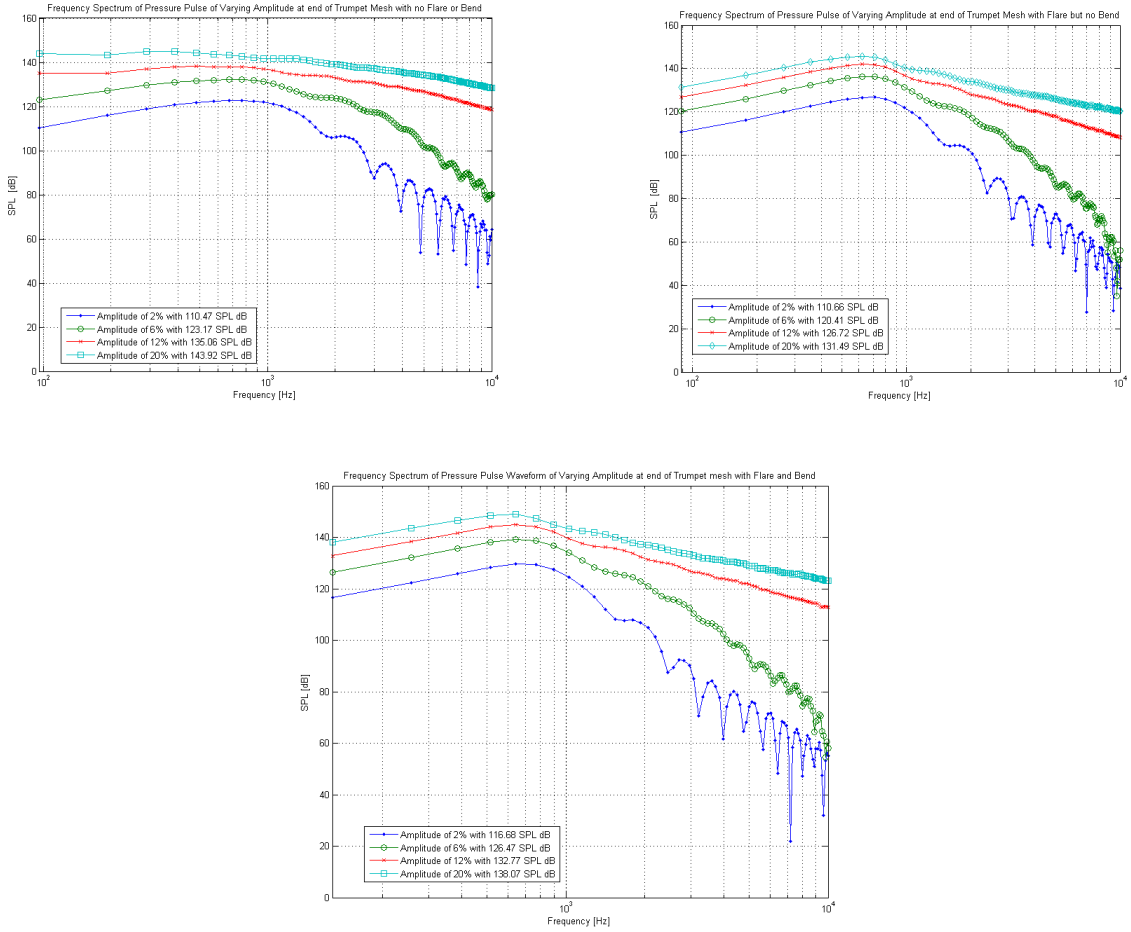

Figure 6.11: Frequency spectra for the high-amplitude pulses at the bell where the trumpet mesh in (first plot) does not have a flare or bend, (second plot) has a flare but no bend, and (third plot) has a flare and bend. The amplitudes of the pulses are 2% of an atmosphere (blue), 6% of an atmosphere (green), 12% of an atmosphere (red), and 20% of an atmosphere (light blue).

shock wave shown in the first pulse plot seems to be the strongest, which is what one would expect given the geometry. In particular, due to the absence of the bell, the cross sectional area remains constant. Furthermore, it appears that the shock wave in the second pulse plot is slightly stronger than in the third pulse plot, which also makes senses from the remarks above.

* Upon examining the frequency spectra of the pulses at the bell in figure 6.11, one can see that the harmonic spectrum for each high-amplitude pulse is distinct. In other words, the spectra in each figure do not intersect as they did for the low amplitude pulses. Furthermore, as the amplitudes of the pulses become larger, the nulls again become less distinct. Once the amplitudes of the pulses start approaching 12% - 20% of an atmosphere, the nulls cannot be seen at all. Thus, it again appears that there has been a transfer of energy to the higher harmonics, which would make sense since weak shocks were generated. The major difference in figure 6.11 is the slope of each plot. The slope is approximately $+3.5 dB/octave$, $+5.5\ dB/octave$ and $+6.5\ dB/octave$ for the first, second and third pulse plots respectively.

6.2.7 Measure of Nonlinearity

From examining the pulse results in the previous section, we now have a better understanding how the geometry of the trumpet effects wave propagation. In particular, these simulations reveal that the trumpet bell is more influential than the bend. The trumpet flare acts as a high pass filter for the higher frequency components, and this causes waves to be reflected at different locations inside the flare. The positions at which the waves are reflected depend on the duration of the pulses. The next numerical experiment will further verify (for musical notes instead of pulses) that the reflection location in the bell depends on the frequency spectra of the waves. These findings support the claim that frequency components greater than about 1500 Hz mostly propagate out of the bell. These results are in agreement with [48].)

According to our results, we also found that the bend does not greatly influence the wave propagation inside the duct. We found that as the pulses traveled toward the bell (if a bend was included), a small port of the wave bounced off the bend and then continued to travel towards the mouthpiece. However, since the reflections were small, we assumed they could be neglected. [50]

From these simulations we can also confirm that wave steepening takes place for high amplitude waves and short duration waves (i.e. high frequency pulses). However, to gain more intuition on nonlinear wave propagation, we require some way to distinguish the importance of the nonlinear effects for these pulses. Therefore, the nondimensional

[50] We performed further numerical experiments to support this claim but they will not be discussed in this thesis.

quantity denoted by ℵ, will calculate the quotient of the shock distance and trumpet length (where wave steepening occurs), i.e.

$$\aleph = \frac{\text{length of trumpet}}{\text{shock distance}} = \frac{l_t}{x_s}, \tag{6.1}$$

where l_t does not include the flare of the trumpet (so, $l_t = 1.33m$). We are introducing this convenient parameter to have a way to classify waves as being in the linear or nonlinear acoustic regime. If $\aleph << 1$, we say the propagating wave is in the linear regime. [51] If $\aleph >> 1$ ($\aleph = O(1)$), this means the propagating wave is in the nonlinear regime, and specifically a shock wave has been produced inside the tube. If $\aleph = 1$, this corresponds to the situation where a shock wave has been produced right before entering the flare, where it will then be diffused and thus weakened very quickly.

We know from [29], that to find ℵ, the shock distance x_s needs to be calculated. This value depends on the maximum change of the mouthpiece pressure with respect to time (denoted by $(\frac{\partial p}{\partial t})_{max}$). For each pulse, these values are summarized in table 6.1 (for the low amplitude pulses) and table 6.2 (for the high amplitude pulses). [52]

Table 6.1: Values for the maximum change of mouthpiece pressure with respect to time, the shock distance, and the measure of nonlinearity for each low amplitude pulse.

Pulse Duration	$(\frac{\partial p}{\partial t})_{max}$	x_s	ℵ
0.001595 s	1,270,266.916 Pa/s	31.64 m	0.0420
0.0007976 s	2,540,532.578 Pa/s	15.82 m	0.0840
0.0003988 s	5,088,504.49 Pa/s	7.91 m	0.1681
0.0001994 s	10,162,135.33 Pa/s	3.95 m	0.3362
0.0000996 s	20,324,270.66 Pa/s	1.98 m	0.6726

From these tables we see that ℵ will increase as either:

* the duration of the pulse decreases, or,

* the amplitude of the pulse increases.

[51] In other words, wave steepening is not prominent and a shock wave would not be generated.

[52] It is important to note that the x_s used was calculated according to theory, i.e. expression (2.9). One must be aware that this expression only considers the forward moving waves and losses are completely neglected. Thus, in reality the x_s values would be larger.

Table 6.2: Values for the maximum change of mouthpiece pressure with respect to time, the shock distance, and the measure of nonlinearity for each high-amplitude pulse.

Pulse Amplitude	$(\frac{\partial p}{\partial t})_{max}$	x_s	$\aleph$
2026.5 Pa	3,234,479.82 Pa/s	12.43 m	0.1070
6079.5 Pa	9,703,445.96 Pa/s	4.14 m	0.3211
12159 Pa	19,406,891.93 Pa/s	2.07 m	0.6422
20265 Pa	32,344,819.88 Pa/s	1.24 m	1.0704

Therefore, the hypothesis that shock waves are produced (and strengthen) for loud, higher frequency waves is supported. Next, we want to find the corresponding position in the trumpet where $\aleph = 1$ for sound waves rather than just pulses. According to previous literature, one should expect to observe the formation of shock waves for the notes presented in chapter 4. Although, it is still not clear that the length of the trumpet is sufficient for such nonlinear effects to develop. This is what will be explored in the remainder of chapter 6.

6.3 Waveform Experiments

We will now present the second set of numerical simulations that were performed for this thesis. These simulations will examine the accuracy of the mathematical model. To do this, we will first reproduce the sound waves shown in chapter 4 (which were recorded in the lab) by using the model from chapter 5. In particular, by using the experimental data collected at the mouthpiece of the trumpet (for the B_3^b and B_4^b notes played at mf and f) as the boundary conditions, we can attempt to simulate the waveforms as they propagate through the trumpet. By then inspecting the resulting waves outside the trumpet bell, the simulated output can be compared to the experimental data. The objectives for performing these numerical simulations are:

* To establish if the sound pressure waves can be reproduced numerically according to the mathematical model. If it is found that the numerical solution differs from the experimental data, one would still be able to determine what important factors were neglected. For instance, if the sound waves exiting the trumpet are too high, perhaps neglecting the third dimension or losses is an approximation that cannot be made.

So, even if the sound waves propagating out the trumpet are not correct, gaining intuition on how to create a better model will be useful.

* From calculating the shock distance for the B_3^b and B_4^b notes, one can examine if shock waves are produced at the shock distance x_s. If a shock wave cannot be produced within the length of the trumpet, the note can then be simulated in a longer trumpet mesh corresponding to the measure shock distance. This way, we will still be able to verify the production shock waves at x_s.

* By reviewing the frequency spectra of the simulated waveforms, we can observe (and thus verify) if there was a transfer of energy to the higher components when wave steepening occurred.

* Finally, although wall losses were be neglected in these simulations, the amplitude of the truncated (simulated) waveforms can be compared to the measured waveforms. This will allow one to determine how much energy should have been lost in order to have agreement between the numerical results the experimental data. From this comparison, we can verify if the factor calculated in section 5.2.5 is correct (which predicts that neglecting the third dimension will affect the amplitudes of waves by a factor of 3.1). In addition, if there are further discrepancies, we can check if the needed amount of energy lost coincides to the percentages reported in literature.

6.3.1 Number of Harmonics

First, the importance of the harmonic spectrum for a given note will be discussed. We need to determine how many harmonics are required in order to reconstruct and accurately describe a pressure waveform for a given note. In the majority of the literature, it is typical for only six to eight harmonics (at maximum) to be considered in describing a note [48], [29], [3]. However, one could speculate that the number of harmonics needed is dependent on the note being played (i.e. the range of the harmonic spectrum). For instance, for lower notes being played on a trumpet, it seems reasonable to assume that more harmonics will be required to describe the waveform (since more components of the wave will be reflected near the bell). Yet at the higher octaves, more of the harmonic components will leak out of the bell, they are not contributing to the production of standing waves.

The measured pressure waveforms at the mouthpiece for the B_3^b and B_4^b notes played at *mf* and *f*, will be reconstructed using 5, 10, 15, 20, 25 and 30 harmonics. Tables 6.3 and 6.4 will summarize the error associated with each waveform. The plots illustrating the shapes

of the original and reconstructed waveform with 5, 10 and 15 harmonics only can be seen in figures 6.12 and 6.13. Generally speaking, these results will help provide intuition on how nonlinear wave propagation is influenced by the upper harmonic spectrum of a given pitch. From chapter 5, we saw that the mathematical representation of the pressure waves are expressed as

$$p = 1.0 + \sum_{i=1}^{m} A_i \cos\left(2\pi f_i t + \phi_i\right),$$

where $m = 5,\ 10,\ 15,\ 20,\ 25,\ 30$. Tables 6.5 and 6.6 list the values for the amplitude, A_i, frequency, f_i, and phase, ϕ_i components. [53] As hypothesized, figures 6.12 and 6.13 reveal that the more complex waveforms seen for the B_3^b note needed a minimum of 15 harmonics in order to precisely reconstruct the waveform. However, for the B_4^b note, the pressure waveform measured at the mouthpiece has a rather good approximation when only considering the first five harmonics.

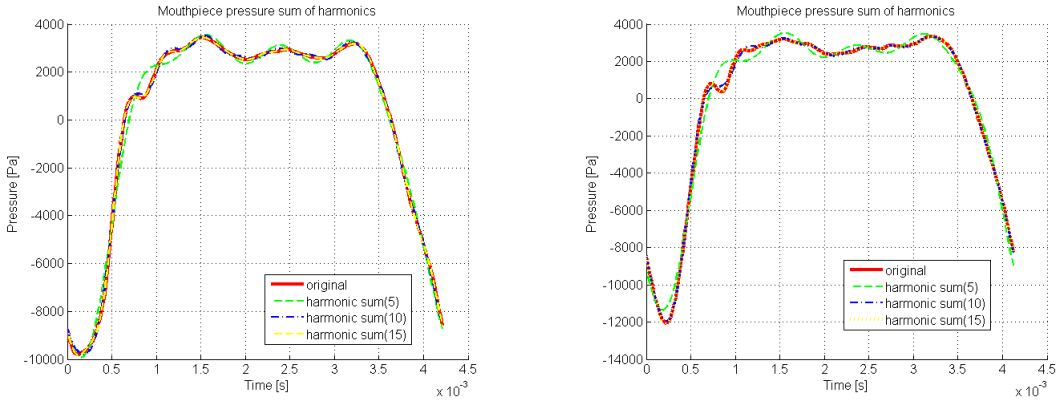

Figure 6.12: Original and simulated pressure waveforms for the B_3^b note played at mf (left) and f (right) considering various harmonics. The total SPL was 166.43 dB and 166.97 dB for the left and right plot respectively.

To determine how good these approximations are, the numerical error between the approximate solution (i.e. the truncated Fourier series) and the experimental data must be examined. One way to analyze the numerical error is to compute the L_2 norm, which

[53] However, only the first 15 components will be given.

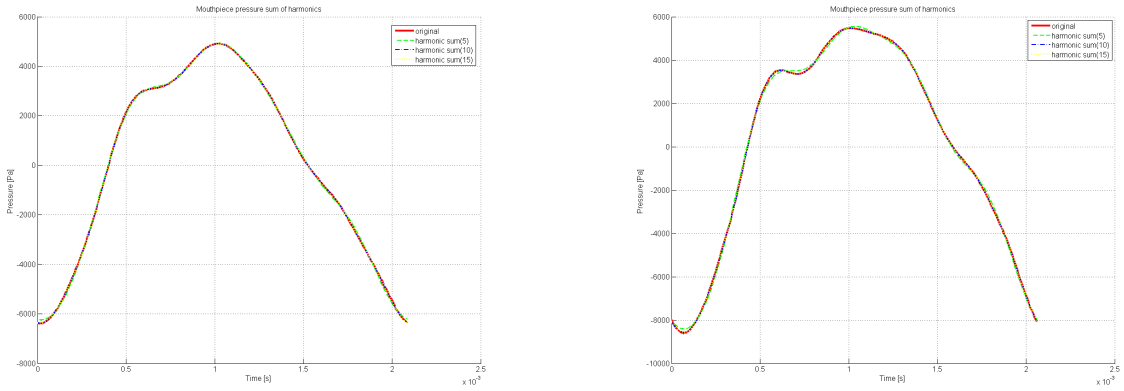

Figure 6.13: Original and simulated pressure waveforms for the B_4^b note played at mf (left) and f (right) considering various harmonics. The total SPL was 165.31 dB and 167.29 dB for the left and right plot respectively.

represents the distance between the two solutions. Determining how quickly the L_2 error goes to zero gives an indication of the accuracy of the solution and is defined as

$$L_2 = \left\| p^{(i)}_{Experimental} - p^{(i)}_{Truncated} \right\| = \left[\int_{\Omega}^{i} \sum_{i=1}^{N_i} \left(p^{(i)}_{Experimental} - p^{(i)}_{Truncated} \right)^2 \mathrm{d}x \right]^{\frac{1}{2}} \tag{6.2}$$

where i is the harmonic number. Another way to compute the numerical error between the truncated series and experimental data is to look at the area between each solution curve. This can be calculated as a percent using the L_2 norm in Matlab as follows

$$error(\%) = \frac{|p^{(i)}_{Experimental} - p^{(i)}_{Truncated}|_2}{|p^{(i)}_{Experimental} - |_2} * 100\%. \tag{6.3}$$

Upon reviewing tables 6.3 and 6.4, several observations can be made. To begin, independent of the notes volume, one can see that the B_3^b's harmonic composition is more complicated than the B_4^b's. In particular, a larger portion of the higher frequencies are needed to accurately reconstruct the B_3^b's waveforms (especially for the B_3^b note played at mf). For the B_4^b note however, it appears that not as many harmonics are needed (although at f, more of the upper frequency components are relevant as indicated by the

Table 6.3: Error associated with the number of harmonics used to reconstruct the measured pressure waveform of a B_3^b note at the bell.

Number of Harmonics	Error for B_3^b at mf	Error for B_3^b at f
5	7.98 %	10.78 %
10	2.66 %	2.44 %
15	0.59 %	0.44 %
20	0.36 %	0.33 %
25	0.24 %	0.29 %
30	0.23 %	0.25 %

Table 6.4: Error associated with the number of harmonics used to reconstruct the measured pressure waveform of a B_4^b note at the bell.

Number of Harmonics	Error for B_4^b at mf	Error for B_4^b at f
5	1.82 %	2.41 %
10	0.24 %	0.40 %
15	0.20 %	0.27 %
20	0.20 %	0.24 %
25	0.19 %	0.22 %
30	0.18 %	0.22 %

slight difference in error). These outcomes support the idea that more of the B_4^b's spectra propagates out of the bell, rather than being reflected at the bell (and then influencing the behaviour of the standing waves in the tube). However, due to the frequency range of the B_3^b note, more reflections occur at the bell, which influence the standing waves. Thus, this pitch is in a range where the high frequency spectra cannot be ignored.

In general, these observations support the claims that the higher harmonic components influence sound production and propagation. Although more of the B_4^b's spectra propagated out the bell, this does not imply these frequency components are not important. In fact, this gives the note the perception of being more brassy. In other words, the timbre of higher, louder notes are described as having more brassiness because the majority of the frequency spectra are emitted out of the bell. Conversely, for a loudly played B_3^b note, these important frequencies are still present, but in addition to several other lower frequencies.

Therefore, given the frequency range, the higher components influence the propagation inside the trumpet compared to outside where the listener can hear it. This is why these notes do not sound as brassy, but more mellow.

6.3.2 Summary of Model Characteristic

Before discussing the final simulations, we will first summarize the important factors that will be used.

* The waveforms considered for the simulations with be the B_3^b and B_4^b notes played at f since there is not a large difference between the playing volumes.
* Upon reviewing the error between the original and simulated (i.e. truncated Fourier series) sound pressure waves at the mouthpiece of the instrument, both notes will be composed with the first 15 harmonics to be consistent (although, it would be acceptable to only consider 5-10 harmonics for the B_4^b note played at f).
* From the pulse results above, it was deemed acceptable to consider a trumpet mesh with a flare, but without a bend.
* Finally, since the linear relationship between the mouthpiece pressure and velocity reproduced the B_3^b and B_4^b waveforms at the mouthpiece boundary, this will be the relationship used for the boundary condition. [54] However, recall that this relationship is an approximation; it is not a physically accurate description (see section 5.2.3).

Recall that in section 5.2.3, the initial and boundary conditions were stated. The mouthpiece pressure will be expressed as a sum of cosine waves, defined as

$$p = 1.0 + \sum_{i=1}^{15} A_i \cos\left(2\pi f_i t + \phi_i\right).$$

The corresponding density at the mouthpiece representing isentropic flow is

$$\rho = \gamma p^{\frac{1}{\gamma}}.$$

Finally, the velocity flow at the mouthpiece will be defined as

$$u = \frac{p - p_o}{\rho_o c} \text{ and } v = 0.$$

[54] We also justified that this approximation was acceptable because when the pulse experiments were being carried out, the pressure and velocity expressions at the mouthpiece were interchanged. The resulting simulated pulses were the same.

6.3.3 B_3^b and B_4^b Waveform Set Up

We will be simulating the B_3^b and B_4^b notes played at *f*. The initial wave profiles that were obtained from the numerical model are illustrated in the right plots of figures 6.12 and 6.13. A summary of the amplitude, frequency and phase components are given in tables 6.5 and 6.6. In this section, three separate simulations will be presented:

* The first simulation will send one period of the B_3^b 's (and B_4^b 's) waveform down the trumpet mesh depicted in the second plot of figure 5.1. The intention of this experiment is to observe how much of the sound pressure wave propagates out the bell and how much is reflected near the bell.

* In the second simulation, instead of only generating one period of the waveforms at the mouthpiece, the initial profiles (illustrated in the right plots of figures 6.12 and 6.13) will be continuously generated at the boundary. In other words, this boundary condition will be applied for the entire duration of each simulation. From this, we can establish if the harmonic components build up within the trumpet. Furthermore, since this situation is more physically accurate, one could examine the waveforms outside the bell to see if the resulting waveforms look like the right plots of figures 4.4 and 4.7.

* The final simulation will also have the boundary condition continually being applied, however the length of the trumpet will correspond to the calculated shock distance. For the B_3^b and B_4^b notes played at *f*, $x_s = 3.61m$ and $x_s = 2.63m$ respectively. By simulating these notes in a longer trumpet mesh, one can verify the x_s values. [55]

6.3.4 B_3^b and B_4^b Waveform Results

The resulting B_3^b waveforms played at *f* are shown in figure 6.14. The bottom plot illustrates the experimental pressure waveform which was measured 17cm outside the trumpet bell. The top and middle waveform plots however show the simulated truncated waveforms measured 26cm outside the bell. Due to the refinement of the mesh immediately in front of the bell, it was not possible to put a sensor in the exact same position. This explains the discrepancy, but nonetheless, the data is still useful. The top waveform plot of figure

[55] In fact, the length of the extended trumpet mesh that will be used for in this final simulations, is equivalent to 4m.

Table 6.5: Variables used in the boundary conditions for B_3^b note played at f according to expression (5.18).

Index i	Coefficient A_i	Frequency F_i in Hz	Phase ϕ_i in rad
1	0.023701036999396	242	2.898463346879768
2	0.017237082406774	484	2.662183331967894
3	0.008300668982163	726	2.452413249448175
4	0.004482236856025	968	2.057385473498371
5	0.003311382322657	1210	1.219714007491466
6	0.002531122812812	1452	0.890743941183490
7	0.001685926978243	1694	0.240201883059213
8	9.088803168254435e-004	1937	-0.717475518236521
9	5.659618472030428e-004	2179	1.855159119719778
10	5.494177809414996e-004	2421	2.637517594877961
11	4.356187563389860e-004	2663	1.441949789307918
12	3.864912657738934e-004	2905	-0.132712665873380
13	2.290099642365016e-004	3147	0.843246249215604
14	3.436222645950906e-004	3389	-2.404146049948991
15	2.166675231553773e-004	3631	2.375657382173665

6.14 shows the resulting sound pressure wave when only one period was simulated at the mouthpiece; whereas the middle waveform plot was obtained by continuously applying the boundary condition.

Although the middle waveform plot is more physically accurate (since in reality, a player must be continuously blowing into the trumpet for a note to be heard), the amplitude is roughly an order of magnitude too high. The maximum amplitude is approximately 1500 Pa, but in the lab, it was measured to be around 100 Pa. However, these higher amplitude values were expected because these simulations were only done in two dimensions. This difference may also be related to the velocity expression at the mouthpiece boundary. Recall, it was not precisely constructed in terms of the measured pressure waveform. Nonetheless, in order to gain more information, the simulation was redone. This time however, only one period of the pressure waveform was simulated at the mouthpiece. The resulting pressure waveform is precisely what is depicted in the top waveform plot of figure 6.14. This numerical experiment was done to determine if the shape of the waveform or amplitude changes.

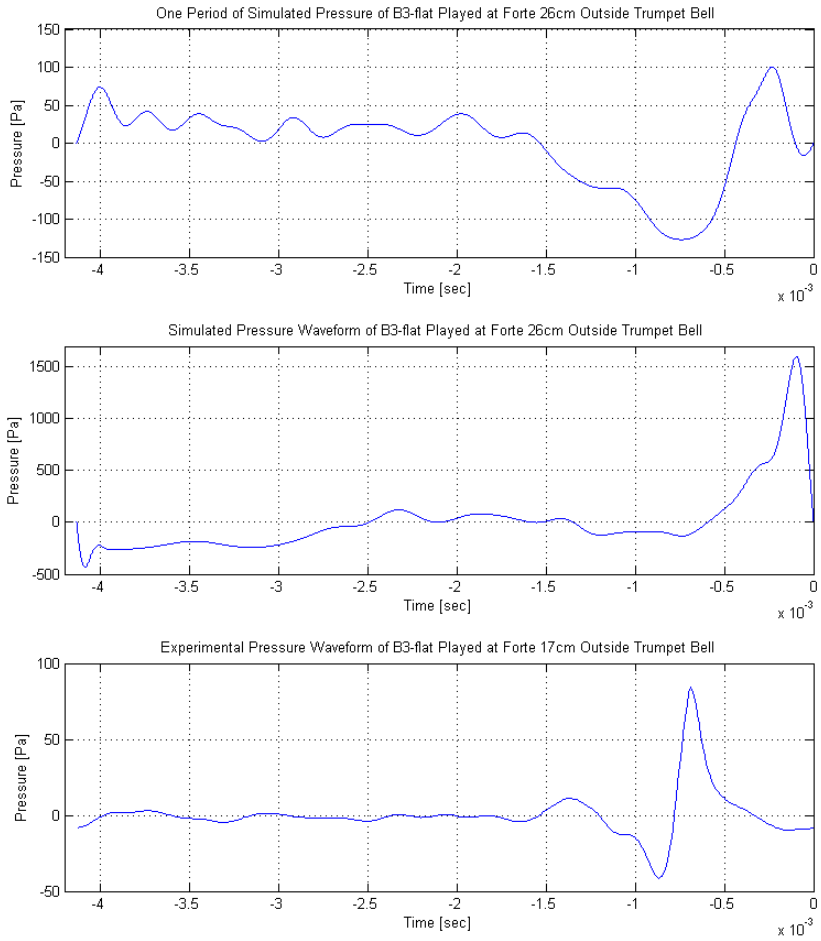

Figure 6.14: Original (bottom), and simulated (top and middle) waveforms exiting the bell. The top plot represents the output for the waveform when one period is simulated, and the middle depicts the waveform when the boundary condition is continuously being applied.

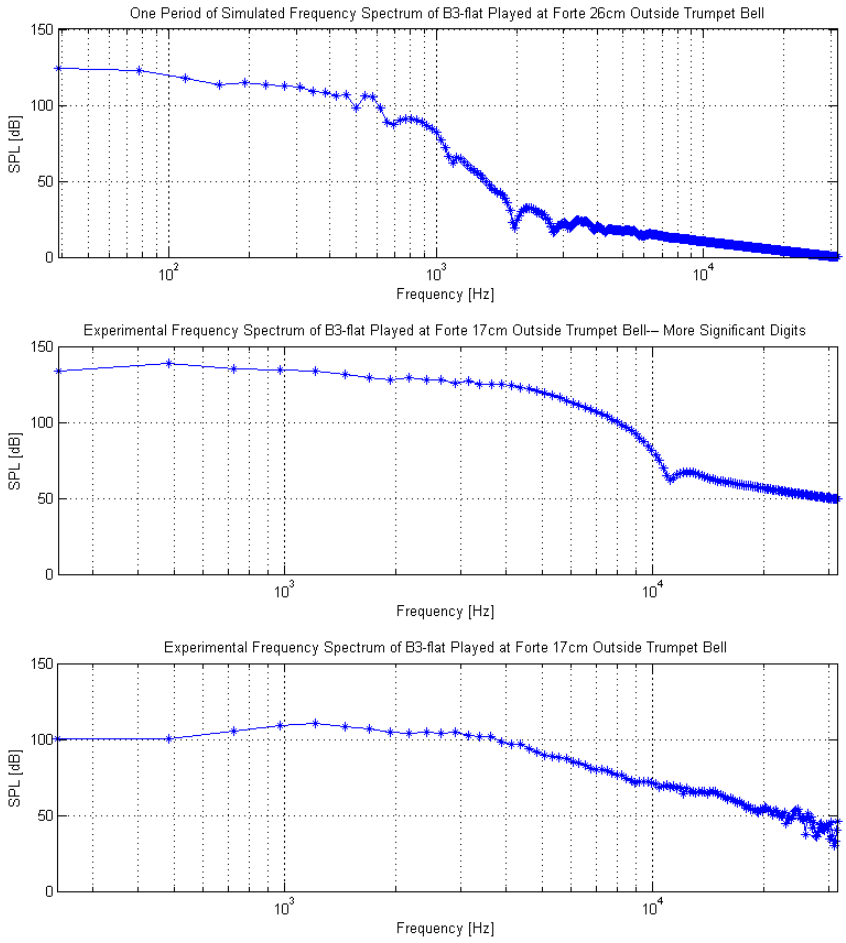

Figure 6.15: Frequency spectra of the original (bottom), and simulated (top and middle) waveforms exiting the bell and shown. The top plot represents the output for the waveform when one period is simulated, and the middle depicts the waveform when the boundary condition is continuously being applied.

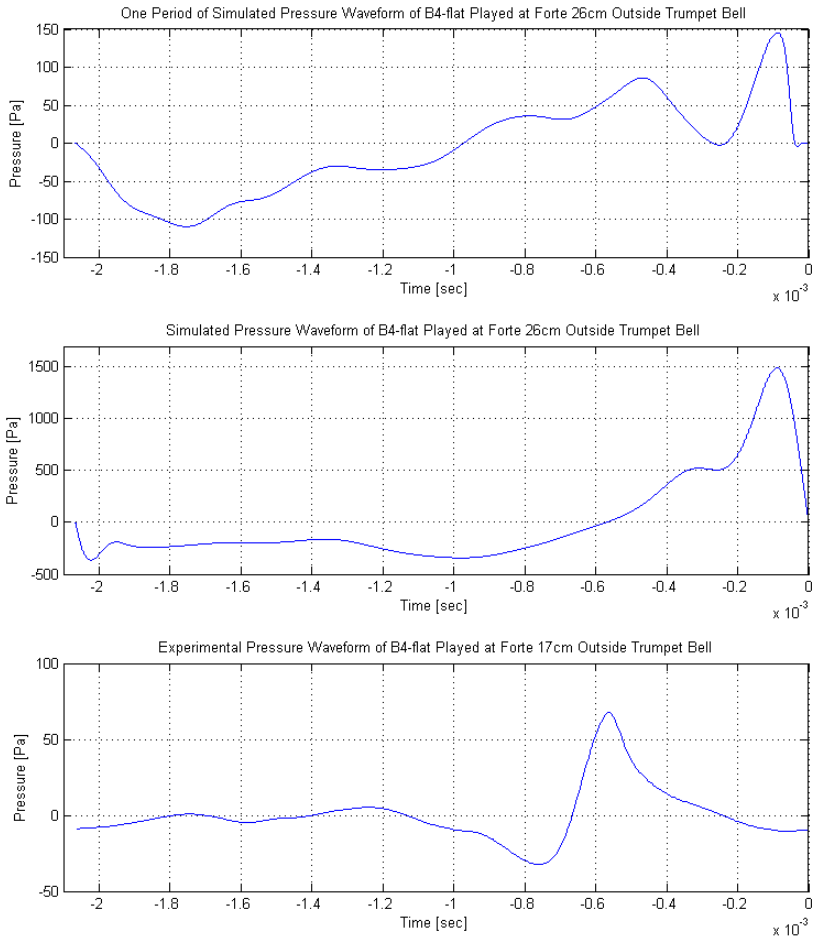

Figure 6.16: Original (bottom), and simulated (top and middle) waveforms exiting the bell. The top plot represents the output for the waveform when 1 period is considered, and the middle depicts the waveform when the boundary condition is always being applied. The original waveform was measured 17cm outside the trumpet bell, whereas the simulated pressure waveforms are illustrated 26cm out of the bell.

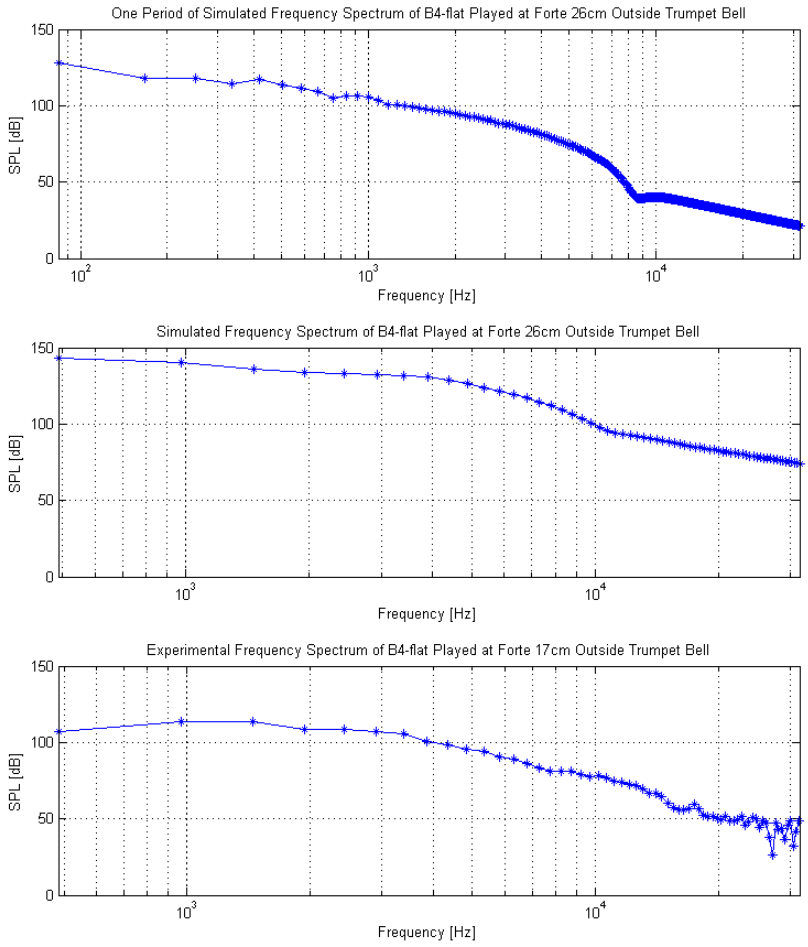

Figure 6.17: Frequency spectra of the original (bottom), and simulated (top and middle) waveforms exiting the bell and shown. The top plot represents the output for the waveform when one period is simulated, and the middle depicts the waveform when the boundary condition is continuously being applied.

Table 6.6: Variables used in the boundary conditions for B_4^b note played at f according to expression (5.18).

Index i	Coefficient A_i	Frequency F_i in Hz	Phase ϕ_i in rad
1	0.031077815979925	484	3.110723035193913
2	0.007208522823608	1452	2.726789974408401
3	0.005030014144019	1937	1.948740778936415
4	0.001291607079264	2421	1.169783046331247
5	8.479753019188015e-004	2950	-2.022175024994273
6	7.206257151014519e-004	3389	2.195188825219146
7	2.421436986048069e-004	3874	1.390345051904985
8	1.723004721656683e-005	4358	2.819032629669553
9	6.169764270096878e-005	4842	-1.708219695341424
10	7.948510342077938e-005	5326	1.577089190334855
11	2.842077974613037e-005	5811	-1.594013344240890
12	3.261901385461865e-005	6295	0.797450048923199
13	4.337582923183830e-005	6779	0.733162946820076
14	6.364657916196645e-005	7263	0.374574375216891
15	3.470049317908877e-005	7748	-0.500430641757610

From carefully comparing these results, we see that when one period is considered, the shape of the waveform does in fact change as does the amplitude. The maximum amplitude is now around 100 Pa which is in better agreement with the experimental data. Also, the shape of the wave is clearly different. The increasing/decreasing behaviour observed in the main peak of the waveform (which is portrayed in the top waveform plot of figure 6.14), is similar to the experimental plot. However, the middle waveform plot portrays the sharpness of the peak more accurately. Generally speaking, one is tempted to say that if a linear combination of the simulated results was taken, the final outcome would be relatively close to experimental data. Although taking a superposition of these two waves, depends on linearity. Therefore, within this thesis, this idea will not be explored.

In speculating why these results were obtained, the following can be suggested. First, let us consider the discrepancy in the shape of the top and middle waveform plots of figure 6.14. The phase shift provides a possible explanation for the profile difference. In particular, the simulation only considering one period of the waveform has no other forward moving waves being generated. This will affect the wave reflections (and thus phase shifts),

especially in regards to the formation of the standing waves. Also, since the energy is not being sustained in the first waveform plot, this could explain the lack of wave steepening (compared to the middle waveform plot). Now examining the increased amplitude values; in chapter 5 we predicted that the dimension (in particular, neglected the third dimension) of the problem may explain these outcomes. Even though there is axial symmetry (when no bends are considered), the equations of motion were not derived to be axisymmetrical. It may be the case that the amplitude is an order of magnitude too high because the wave is not able to spread in the third dimension. Another possible contributing factor may be that the wall losses were not considered. This hypothesis will be further examined in section 6.3.6.

The analogous plot results for the B_4^b note played at *f*, shown in figure 6.16, also illustrates similar consequences. Again, the top waveform plot shows the resulting waveform when only one period of the mouthpiece pressure was simulated. The middle waveform plot depicts the resulting waveform when the boundary condition is continuously applied at the mouthpiece. We see that the shape of the top waveform plot is more deformed compared to the experimental plot on the bottom of figure 6.16. The amplitude however, is on the same order of magnitude as the experimental result. The middle plot shows comparable behaviour to the experimental data; however, the amplitude measurement is again an order of magnitude too high.

The corresponding frequency spectra for the B_3^b and B_4^b notes are shown in figures 6.15 and 6.17 respectively. One can see that the shape of the middle waves are a closer representation to the experimental data. With the exception of course being that the amplitude is too high. The top frequency spectra plots for both notes, displays a difference in the wave behaviour. For both notes, the top waveform plots of figures 6.15 and 6.17 depict nulls; whereas the experimental data does not show such characteristics. The reason for this is unknown. However, one can hypothesize that these nulls may smooth out if the third dimension is considered [52].

6.3.5 Discussion - Importance of Losses

We will now take the time to further discuss and explore the importance of losses within the trumpet. Although the losses were neglected in our model, we can now examine if this was a reasonable simplification. Above, it was hypothesized that the amplitude difference in the simulations could be due to:

* The third dimension being neglected.

* The velocity input for the boundary condition has not been precisely determined from the measured pressure waveforms (recall this procedure is further discussed in Appendix D). Thus, after reflections occur, it is very possible that our approximation breaks down.

* Wall losses not being considered.

In section 5.2.5, we looked at how neglecting the third dimension could influence the amplitude of the sound pressure waves by a factor of 3.1. Nonetheless, the first two points cannot be fully examined within this thesis. They are currently being studied (and the results will be available in future papers). Again, the third possibility cannot fully be explored; but, the amplitude values of the different frequency components of the numerical (i.e. truncated series) and experimental data can be compared. Although literature has conflicting information regarding the importance of energy losses (and moreover how influential they are); by considering the discrepancies in the amplitude values, one can observe if the variation corresponds to the energy losses predicted in literature. This however would be assuming that there are small discrepancies between the B_3^b and B_4^b data. If however we find that that the differences are not small, this suggests it is likely that the amplitude variation is due to numerical error. In examining the difference of the experimental amplitude values (denote by p_E), to the simulated amplitude values (i.e. truncated Fourier series) (denoted by p_T) of a given note, the percent difference can be obtained. In particular, we calculate this percentage difference as follows

$$\text{Losses}(\%) = \left(\frac{p_E}{p_E - p_T} \right) * 100\%. \tag{6.4}$$

The losses needed to be in agreement with measured amplitude values for the B_3^b and B_4^b notes are illustrated in the top and middle plots of figure 6.18. For frequency components less than 9,000 Hz, the top and middle plots illustrate the differences between numerical and experimental data as a percentage of the experimental data. The top plot examines the simulations for a single period of the B_3^b and B_4^b waveform. The bottom plot considers the waveform to be continuously simulated.

As one can see the plot of the single period simulation with the mouthpiece pressure shows that almost all frequency components less than 4000 Hz require losses around 10% for both notes to be in agreement with values measured in the lab. However, the fundamental frequency in particular has roughly 20% excess energy. For the frequency components between 4000 Hz $-10,000$ Hz, the losses required are around $10 - 20\%$. Comparing these

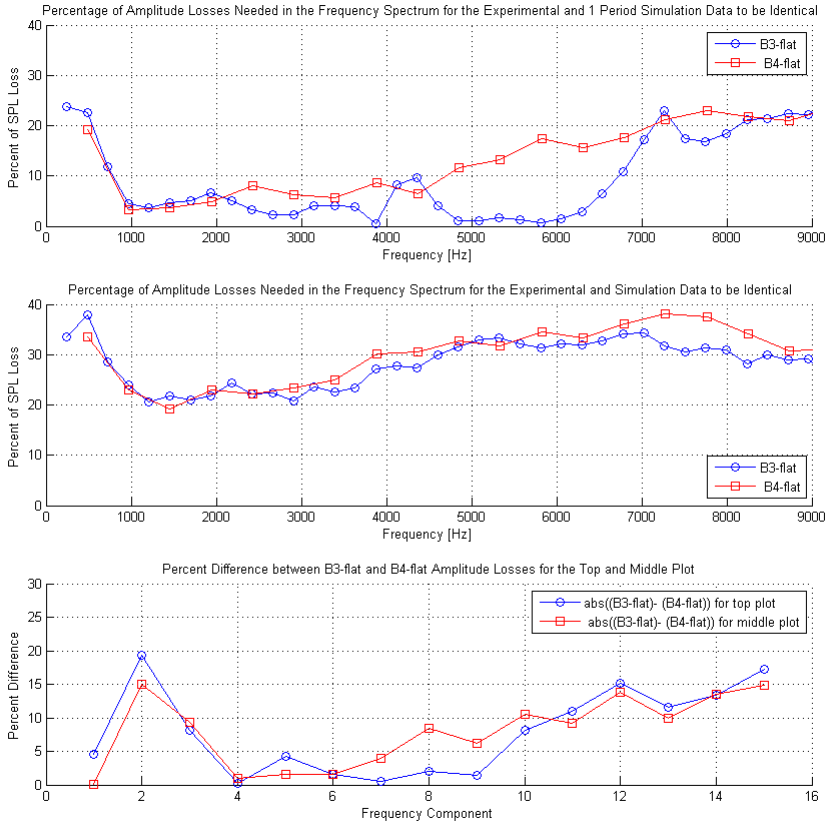

Figure 6.18: Frequency spectra amplitude differences as a percentage between the original and simulated waveforms played at *f*. (Top) simulation for single period of the waveform at mouthpiece; (middle) simulation for waveform continuously being applied at the mouthpiece; (bottom) difference between the B_3^b and B_4^b data for each plot.

experimental verses simulated values of the B_3^b to the B_4^b, we see there is a relatively similar pattern present for the losses. These is especially noticeable for the frequencies less than 4000 Hz. In regards to the middle plot, it is apparent that a higher percentage of losses are needed for the experimental and simulated data to be in agreement for the continuous simulations. In particular, the losses calculated are between 20% and 40%.

The bottom plot of figure 6.18 shows a strongly correlated pattern of error, independent of the note played. This pattern signifies the difference of continuous simulation to single period simulation. In addition, if one calculates the average of these losses, the top plot give 7.1% (B_3^b) and 10.8% (B_4^b). The middle plot gives an average of 24.6% (B_3^b), and 29.1% (B_4^b). It is tempting to say that a portion of the amplitude losses are due to the absence of corrections needed for energy losses. Nonetheless, these are all speculative ideas. Overall, not a lot can be said until it is determined (i.e. verified numerically) whether the dimension of the mesh could be is responsible for these amplitude differences.

In section 5.2.5 however, it was also shown that neglecting to model three spatial dimensions could produce amplitude values approximately 3.1 times larger than the expected values. This amplification factor results from considering conservation of energy with deducing the spatial degree of freedom (by going from three dimensions to two dimensions). Interestingly, the factor is approximately equal to the inverse of the experimental losses, that is, the mean measured energy loss (as a percent) over the frequency components (independent of the pitch); particularly for the B_4^b note.

The measured percent energy losses for the B_3^b are lower, around 10%. Although, in [33], the authors hypothesize that frequencies 1500 Hz and below are mostly reflected at the end of the instrument, retraining 90% of the energy. For frequency components higher than 1500 Hz, 90% of the energy propagates out of the bell as sound. So, for the B_3^b note played at *f*, we are getting similar results.

6.3.6 Shock Distance Remarks

The final numerical experiment in this thesis will be examining if shock waves are generated for the B_3^b and B_4^b notes played at f within a certain distance. For this numerical experiment and all others discussed in this chapter, the DGM was able to resolve all of the simulations (i.e. the code did not crash and it was not necessary to consider a flux limiter) [34]. Therefore, if shock waves did form, they would have been very weak. The resulting waveform shapes seen in figures 6.14 and 6.16 do not suggest that shock waves were produced.

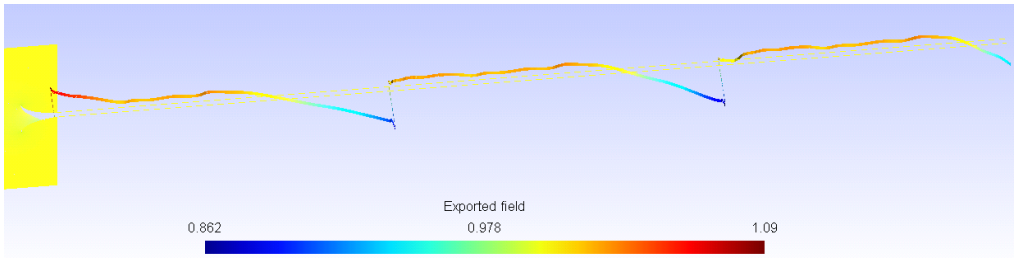

Figure 6.19: Position where shock wave formed for B_3^b , 3.85 m into the trumpet.

As mentioned in section 2.3.1, according to the literature, the shock distance is defined to be

$$x_s = \frac{2\gamma pc}{(1+\gamma)\frac{\partial p}{\partial t}_{max}}.$$

Assuming this expression is accurate, a shock wave should be produced for a B_3^b and B_4^b played at f at 3.61 m and 2.63 m respectively.[56] In order to test this expression, a 4 m trumpet mesh with only a flare was constructed. The simulated waveform for the B_3^b and B_4^b notes played at f was used to verify if a shock wave would be generated at this theoretical location.

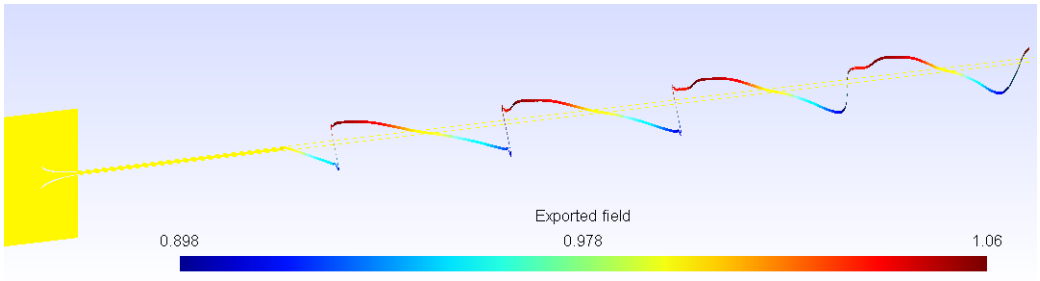

Figure 6.20: Position where shock wave formed for B_3^b , 2.83 m into the trumpet.

The resulting waveforms that were generated in the 4 m trumpet can be seen in figures 6.19 and 6.20. Upon reviewing the results, a shock wave was produced as hypothesized, but at a distance greater than x_s (for both notes). Figures 6.19 and 6.20 show the position where the shock waves were produced. These pictures have been raised in the z-axis and

[56]These values were calculated using the expression for x_s. In particular, $\frac{\partial p}{\partial t}_{max}$ was calculated directly in Matlab from the experimental data.

slanted to make it easier to observe the deformation of the initial pressure waveforms as they propagate through the trumpet.

One may notice that the second period of the initial waveform that was generated also depicts slight overshoots. However, only the first period (in these images) steepens fully into a shock wave [57]. The overshoots observed in the second period are only illustrating wave steepening. Nonetheless, it appears the expression for the shock distance is a rather good approximation. The variation in shock wave length for the B_3^b and B_4^b was equivalent to 0.24 m and 0.20 m respectively. If a small amount of losses were considered, this could potentially explain the observed difference [52]. [58]

Upon reviewing these results, it appears that a weak shock wave cannot form within the calculated shock distance. Due to the fact that the numerical model and its expression for x_s neglect wall losses, we can say with confidence that a shock wave will not and is not produced within an actual trumpet. Nevertheless, wave steepening does still occur as visible in the spectrum for the single period to continuous period simulations in the extended (and regular) trumpet mesh. In addition, as mentioned in [29, p. 1756], the profiles obtained from the experiments and simulations outside the bell illustrate that the radiated sound is dominated by the high frequencies (as indicated by their sharp shape). As a final remark, we have calculated the importance of the nonlinearities using expression (6.1), finding that $\aleph = 0.3454$ for the B_3^b and $\aleph = 0.4699$ for the B_4^b. Since $\aleph$ is not approximately 1, it should be no surprise that the generation of shock waves was therefore not observed.

[57] This was verified by considering the Rankine-Hugoniot relations as discussed in [10, s. 7.2.4]. Furthermore, these shock waves are very weak, barely satisfying the necessary conditions.

[58] It may seem unintuitive that the discrepancy in x_s is slightly different for each note, but remember that x_s proportional to $\frac{\partial p}{\partial t}_{max}$.

Chapter 7

Conclusion

As mentioned in the overview of the thesis, the purpose of this research is to further understand the nonlinear wave propagation within the trumpet but also to lay out a framework for mathematicians and physicists to do additional work. With the information collected from the experimental data as well as the simulations, we have taken another step forward in describing this physical phenomenon.

7.1 Comparison Between Theory and Experiment

In figure 7.1 and 7.2, one can compare the numerical results with the experimental in order to determine the accuracy of the model presented within this thesis.

The top plot in each figure illustrates the resulting harmonic spectrum for each simulation along with the numerical data. In addition, the middle plot calculates the difference in the SPL's; whereas the bottom plot determines the ratio of the SPL's between the experimental and numerical data.

If we consider the B_3^b results first, it is evident from examining the ratio/difference plots, that the different simulations match each other quite well for the frequency components greater than 12,000Hz. One can see that this is also true for the B_4^b, except for frequencies greater than 25,000 Hz. However, recall that these high frequency components mostly propagate out of the bell rather than contributing to the generation of standing waves. Nonetheless, as mentioned in chapter 6, although the shape of the resulting waves are relatively similar to the ones measured in the lab, the variation in amplitude is appreciable.

However, as briefly mentioned at the end of chapter 6, one can hypothesize that neglecting wall losses as well as approximating the velocity relation at the mouthpiece, is partly responsible for these inconsistency. Moreover, it is our thought that neglecting the third dimension is probably the largest factor for these discrepancies. Another result that gives more credibility to this proposition is the linear and nonlinear numerical pulse experiments. Recall that the simulations which had reasonably small amplitudes displayed distinct nulls in the frequency spectrum. In particular, these nulls were seen in roughly 875Hz intervals. One potential idea to why this was observed may be because the bell can be considered as a high frequency filter. Conversely, another hypothesis is that these nulls are present because the third dimension is neglected. Nonetheless, these claims will only be confirmed or denied when a simulation in the third dimension is attempted (which is currently being set up) [52], [34].

Therefore, on the contrary to previous claims regarding these musical notes, we conclude that only wave steepening took place within the trumpet. Shock waves were not observed from numerical simulations presented in chapter 6, nor in the experimental data discussed in chapter 4. This proposition is also supported by the numerical simulations outlined in section 6.3.8. For the B_3^b and B_4^b, a weak shock wave was generated at a distance equivalent to 3.85 m and 2.83 m respectfully. Both of these distances are somewhat larger than x_s. As a final remark, the results we obtained for the B_3^b played at f are very similar to [29, p. 1756]. The pressure measurements outside the bell illustrate sharp wave profiles and as stated in [29], these waveforms demonstrate that the radiate sound is dominated by the higher frequency components. Our results for the B_4^b played at f are different, but this is not surprising since in [29, p. 1757], their note was produced at *ff*.

7.2 Future Work and Further Discussion

An unfortunate detail, regarding the starting time for the pressure measurements, was discovered after the experimental data was collected. For this thesis, all the measurements made in the lab were done only once the pitch of interest achieved (and remained) steady. In other words, all data was collected once the note was played and heard. However, this does not provide an accurate description for the initial pressure wave before steady state behaviour was achieved. Since we only had access to pressure measurements once standing waves were created, the majority of the initial harmonics above 1500 Hz traveled outside of the bell and are thus missing in the experimental data. The saving grace of this is, once a note is actually heard, these upper harmonics can be neglected. This still makes our above simulations useful for watching the development of the nonlinear acoustic wave

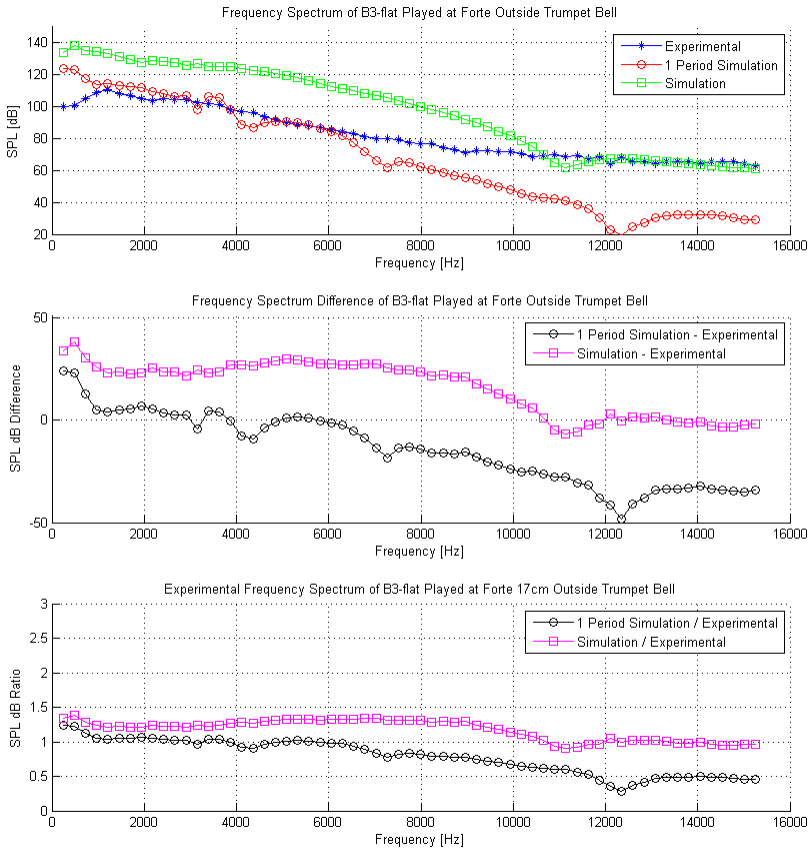

Figure 7.1: The top figure illustrates the SPLs of the first 64 harmonics in the frequency spectra of the original (blue) and simulated waveforms (red is 1 period, green is continuous periods). The middle plot depicts the difference between in the experimental and two numerical outputs. Finally, the bottom figure looks at the quotient between the simulated and experimental results.

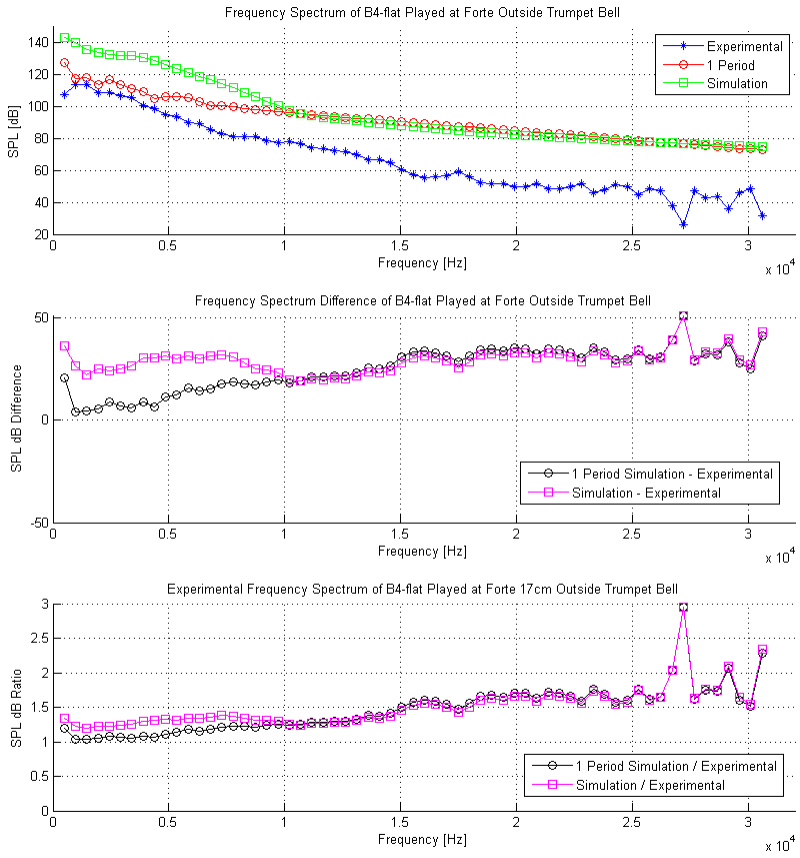

Figure 7.2: The top figure illustrates the SPLs of the first 64 harmonics in the frequency spectra of the original (blue) and simulated waveforms (red is 1 period, green is continuous periods). The middle plot depicts the difference between in the experimental and two numerical outputs. Finally, the bottom figure looks at the quotient between the simulated and experimental results.

propagation. In order to be more accurate with our physical model of sound production, future experiments must involve recording before the pitch is actually played.

In addition to this, it would have also been useful to have pressure waveform data for higher notes, such as a B_5^b and F_5 or lower pitches like a B_2^b. Being able to study the waveforms for the highest and lowest octave would provide more of a complete picture. But, as any brass player would know, hitting a solid tone for either one of these notes is very difficult; a professional player would be necessary for such an experiment.

For the purposes of this thesis, the energy losses were neglected in the mathematical model. A model taking into account not only the viscous friction but also the wall losses from heat and vibration would be very useful. Some literature claims that the majority of the initial energy put into the system is lost (roughly 90% -95 %) [22, p. 727], whereas others propose it is close to 10% for lower frequency notes [33, p. 25]. Therefore, in the simulations presented in chapter 6, it should be no surprise that the values obtained will be lower in reality. In the case of the trumpet, overlooking such losses could result in either observing a shock wave or not. In the case of a B_3^b, a shock could be developed but it depends on the dynamic the note being played. Remember, these are weak shocks that are produced in brass instruments only when the maximum pressure change is great enough. This affects the distance a wave must propagate before steepening into a shock wave. Recall that in the high amplitude pulse simulations, a small amount of the initial pulse was reflected at the bend, which did contribute to the behaviour of the reflected pulse.

In addition, an improvement in the simulation would involve a more accurate mesh of the instrument. In our simulations, we did not consider a bend. However, an actual trumpet consists of two bends, plus the coiled valves. However, we found that the simulations with a bend and without a bend were relatively similar. It is possible however that with the addition of extra bends and coils, the wave propagation could be altered. For notes in a special range, this may or may not lead to the development of shock waves.

Work is also being done to determine a more accurate approximation for the velocity expression, specifically at the mouthpiece. Simulations are planned to run in a three dimensional mesh of the trumpet. This will enable us to verify the claim that the third dimension contributes to the observed nulls and amplitude variations in the pulse and waveform experiments. If the third dimension proves not to be of great influence to the pressure waveform results, this will provide further evidence on the important of losses, which was briefly discussed in section 6.3.6.

There is one more important point that should be mentioned, although examining it in detail would be extremely difficult. Recall that when shock waves form, the Mach number

is around one. For these types of flow, it is difficult to consider the inviscid and viscous parts separately. In reality, boundary layers and boundary separation at the bends as well as the bell most likely occur for very loud, high frequency notes (and this has important flow consequences) [9]. However, these properties are beyond the scope of this masters thesis, but they will be considered in future research findings and simulations.

Appendix A

Microphone Calibration

A.1 Microphone Calibration for Experimental Data from Chapter 4

This calibration applies to the measurement of the trumpet on January 9, 2012, and the microphones were connected to an oscilloscope that took in 3 concurrent microphone measurements. The calibration was carried out by an 114 dB signal at 1 kHz. This signal is 10.0 $Pa\ RMS$.

* Microphone 1: This was at the mouthpiece. GRAS 40BH on preamp number 1 with special gain switch set to 0 dB. 114 dB produces 5.277 $mV\ RMS$. Microphone 1 calibration: 1,895 Pa/V.

* Microphone 2: This was at the first bend. B & K 4135 on B & K 2610 preamp set to 0 dB input gain, 0 dB output gain, and set to 28 V polarization. 114 dB produces 5.632 $mV\ RMS$. This microphone signal is inverted, so it needs to be multiplied by -1 to agree with microphone 1 and microphone 3. The polarity of all three signals will then be correct, and positive numbers represent positive acoustic pressure. Microphone 2 calibration: 1,776 Pa/V.

* Microphone 3: This was mounted about 16cm from bell. B & K 4133 facing bell, with preamp number 2 set to 10 dB gain. 114 dB produces 375.3 $mV\ RMS$. Microphone 3 calibration: 26.65 Pa/V.

Appendix B

Matlab Code

B.1 Matlab Code for Experimental Data Presented in Chapter 4

```
%John and my code to read in experimental data as of Feb 9, 2012
%The purpose is to read in the experimental data and plot the waveform as
%well as the fft

%%%%%%%%%%%%%%%%%%%%%%%%%%%%%%%%%%%%%%%%%%%%%%%%%%%%%%%%%%%%%%%%%%%%%%%%%%%%%%%
%This is a code that John Vanderkooy and I wrote to read in
%experimental data as of Feb 9, 2012
%The purpose is to read in the experimental data and plot the waveform as
%well as the fft

%optimised by JV june 6, 2012

%%%%%%%%%%%%%%%%%%%%%%%%%%%%%%%%%%%%%%%%%%%%%%%%%%%%%%%%%%%%%%%%%%%%%%%%%%%%%%%
%clear everything
clear all;close all
set(0,'DefaultLineLineWidth',1.5);
set(0,'DefaultAxesFontSize',12);

%Load data
load('scope_21.prn')  % 1000 points; Need to read in scope10,16,18,21
```

```
data=scope_21;
ntotal=length(data(:,1));
nperiod=413; % 413 from inspection of the scope_10 data (B3_f)
             % 418 from inspection of the scope_16 data (B4_mf)
             % 422 from inspection of the scope_18 data  (B3_mf)
             % 413 from inspection of the scope_21 data (B4_f)
figure(10)
plot(data(:,1),data(:,2))
grid on
title('Raw Data')
ylabel('raw mic voltage')
xlabel('raw time')

time=data(1:nperiod,1)-data(1,1); % make time positive starting at zero
mouthpiece1period=data(1:nperiod,2);
bend1period=data(1:nperiod,3);
bell1period=data(1:nperiod,4);

%Find number of points in data of 1 period
N=length(mouthpiece1period);
%Write general expression for sampling frequency
fs=1/(data(2,1)-data(1,1));

cal_factor1=1895;  % Pa/V for mouthpiece mic
%cal_factor1=2500; % if we accept GRAS calibration, which is only 1 digit
cal_factor2=-1776; % Pa/V for bend mic
cal_factor3=26.65; % Pa/V for bell mic

%Define pressures
pressure1=cal_factor1*mouthpiece1period;
pressure2=cal_factor2*bend1period;
pressure3=cal_factor3*bell1period;

figure(20);
hold on
plot(time,pressure1,'r');
plot(time,pressure2,'b');
plot(time,pressure3,'g');
```

```
grid on;
legend('Mouthpiece','Bend','Bell');
title('Waveforms played Mezzo-Forte')
ylabel('Pressure [Pa]')
xlabel('Time [s]')

%Define freq
nnyquist=floor(N/2+1);
freq=([1:floor(N/2)+1]-1)*(fs/N);

%Find fft and ifft
% these are complex amplitudes - need to double them for real cosines
y1f=(1/N)*(fft(pressure1)); %mouthpiece
y1i= N*ifft(y1f);

y2f=(1/N)*(fft(pressure2)); %bend
y2i=N*ifft(y2f);

y3f=(1/N)*(fft(pressure3)); %bell
y3i=N*ifft(y3f);

figure(30);
hold on
% to get rms values we need to multiply by 2/sqrt(2)=sqrt(2)
semilogx(freq,20*log10(sqrt(2)*abs(y1f(1:nnyquist))/abs(2*10^-5)),'r');
semilogx(freq,20*log10(sqrt(2)*abs(y2f(1:nnyquist))/abs(2*10^-5)),'b');
semilogx(freq,20*log10(sqrt(2)*abs(y3f(1:nnyquist))/abs(2*10^-5)),'g');
grid on;
axis([0 10000 50 170])
legend('Mouthpiece', 'Bend', 'Bell');
title('SPL of harmonics versus frequency played Mezzo-Forte')%
ylabel('SPL [dB]')
xlabel('Freq [Hz]')

figure(40)
hold on
plot(time,pressure3,'g');
grid on;
```

```
%axis([0 4*10^(-3) -50 100])
title('Zoom-in of Waveform at Bell played Mezzo-Forte')
ylabel('Pressure [Pa] ')
xlabel('Time [s]')

%%%%%%%%%%%%%%%%%%%%%%%%%%%%%%%%%%%%%%%%%%%%%%%%%%%%%%%%%%%%%%%%%%%%%%%%%%%%

%Now we write the pressure as a sum of harmonics
amplitude=abs(y1f(1:nnyquist));
amplitudePercent = amplitude/101325;
phi=angle(y1f(1:nnyquist));

timesum=zeros(N,1);        %initialize time array
timesum(1:N)=amplitude(1); %DC into array
for k=2:6                  %harmonics excluding DC
   timesum = timesum + 2*amplitude(k)*cos(2*pi*freq(k)*time + phi(k));
end

timesum2=zeros(N,1);        %initialize time array
timesum2(1:N)=amplitude(1); %DC into array
for k=2:11                  %harmonics excluding DC
   timesum2 = timesum2 + 2*amplitude(k)*cos(2*pi*freq(k)*time + phi(k));
end

timesum3=zeros(N,1);        %initialize time array
timesum3(1:N)=amplitude(1); %DC into array
for k=2:16                  %harmonics excluding DC
   timesum3 = timesum3 + 2*amplitude(k)*cos(2*pi*freq(k)*time + phi(k));
   amplitude(k);
   freq(k);
   phi(k)

end

figure(50)
hold on
grid on
plot(time,pressure1,'b')
```

```
plot(time,timesum,'r')
plot(time,timesum2,'g')
plot(time,timesum3,'y')
%legend('original','harmonic sum')
legend('original','harmonic sum(5)','harmonic sum(10)', 'harmonic sum(15)')
title('Mouthpiece pressure sum of harmonics')
ylabel('Pressure [Pa] ')
xlabel('Time [s]')

% calculate total SPL
DC_power_correction=-3*amplitude(1)^2; % removes overcalculation in sum()
harmonic_power=sum(2*amplitude.^2);
total_SPL=10*log10((DC_power_correction+harmonic_power)/4E-10)

%%%%%%%%%%%%%%%%%%%%%%%%%%%%%%%%%%%%%%%%%%%%%%%%%%%%%%%%%%%%%%%%%%%%%%%%%%%
```

B.2 Matlab Code for Ploting the Simulation Resulting in Chapter 6-7

Here is code for making plots from simulation data.

```
 figure(1)
gamma=1.4;
rho=data(:,2);
u_rho=data(:,3);
v_rho=data(:,4);
E=data(:,5);
u=u_rho./rho;
v=v_rho./rho;
p=(gamma-1).*E-0.5*rho.*((u.*u)+(v.*v));
plot(data(:,1)*0.00002457,(p*101325-101325))
title('Mouthpiece Pressure Waveform for B4 flat at mf')
ylabel('Pressure [Pa]')
xlabel('Time [s]')

figure(2)
```

```
p=(gamma-1).*E-0.5*rho.*((u.*u)+(v.*v));
plot(data(:,1)*factor,(p*101325-101325)*factor)
title('Mouthpiece SPL Waveform for B4 flat at mf')
ylabel('SPL[dB]')
xlabel('Time [s]')

p1=floor(length(time)/time(length(time))*a);
p2=floor(length(time)/time(length(time))*b);

diff=p2-p1;
nnyquist=floor((diff/2)+1);
fs=340*floor(length(data (:,1))/data (length(data (:,1)),1));
freq=([1:nnyquist]-1)*(fs/diff);
myFFT=(1/diff3)*fft(mPressure);

figure(3)
p=(gamma-1).*E-0.5*rho.*((u.*u)+(v.*v));
semilogx(freq1,20*log10(sqrt(2)*abs(myFFT1(1:nnyquist1))/abs(2*10^-5)))
title('Mouthpiece SPL Frequency Spectrum for B4 flat at mf')
ylabel('SPL[dB]')
xlabel('Time [s]')
```

Appendix C

C++ Code

C.1 C++ Code to Input Reconstructed Mouthpiece Boundary Condition from Chapter 6

```
// This is a code to write out the pressure waveform at the mouthpiece
//  of the experimental data
// I've taken the values from the matlab code JohnMeCode3.m put them into
// an array to make it easier

#include <iostream>
#include <conio.h>
#include <iomanip>
#include <string>

using namespace std;

 main(){
float coefficent[50] = {0.023701036999396, 0.017237082406774,
0.008300668982163, 0.004482236856025, 0.003311382322657,
0.002531122812812, 0.001685926978243, 9.088803168254435e-004,
5.659618472030428e-004, 5.494177809414996e-004, 4.356187563389860e-004,
3.864912657738934e-004, 2.290099642365016e-004, 3.436222645950906e-004,
2.166675231553773e-004, 7.119513320107869e-005, 5.093910656986453e-005,
```

```
1.212566488912154e-005, 1.548652992037413e-005, 2.189145347061770e-005,
2.217119657876090e-005, 1.014290357463376e-005, 2.564488859931175e-005,
1.393314365295915e-005, 2.056249344572483e-005, 1.846686255662965e-005,
2.831151749505964e-005, 2.954972147832571e-005, 1.474355882741878e-005,
1.352289575624484e-005, 1.249991290607368e-005, 1.590722629041115e-005,
5.514769256190667e-006, 5.034511718079430e-006, 8.821286189942737e-006,
1.103534150091225e-005, 3.418026012241362e-006, 8.187517456924470e-006,
1.656416956779105e-005, 3.787485994328437e-006, 1.106657329678109e-005,
5.669970052482019e-006, 5.189485824612297e-007, 6.313447080780688e-006,
1.549052930580531e-005, 2.332320975418004e-006, 9.345120790733753e-006,
3.613608336555739e-006, 4.894481061531706e-006, 3.801792985704920e-006};

  float phase[50] = {2.898463346879768, 2.662183331967894,
2.452413249448175, 2.057385473498371, 1.219714007491466,
0.890743941183490, 0.240201883059213, -0.717475518236521,
1.855159119719778, 2.637517594877961, 1.441949789307918,
-0.132712665873380, -0.843246249215604, -2.404146049948991,
2.375657382173665, 1.520082035191552, -0.919570401102168,
1.765829604620504, 1.789290743598263, -0.941857233109691,
-0.877565297894654, -0.450527174301916, -1.025133359121165,
-0.360797983088995, 1.056704447406744, 0.342856486606525,
-0.156075054989580, -1.893213093810168, -0.704506540384503,
0.970625461642409, 3.029056364281610, -0.230005360566396,
1.403120194211433, 0.120193066122006, 1.258755830145004,
1.633868464632038, 1.896686042885291, -2.781672467151764,
-1.719577450804601, -3.128526516466232, 3.077356708065948,
2.982164253289429, .157108874265959, 2.859259633143191,
2.039096956031849, 1.776270940504459, 2.041721506225746,
3.121718268986838, -3.080682632703772};

      float frequency[50]= {0.675675675675676, 1.013513513513514,
1.351351351351351, 1.689189189189189, 2.027027027027027,
2.364864864864865, 2.702702702702703, 3.040540540540541,
3.378378378378379, 3.716216216216216, 4.054054054054054,
4.391891891891892, 4.729729729729730, 5.067567567567568,
5.405405405405405, 5.743243243243243, 6.081081081081082,
6.418918918918919, 6.756756756756757,  7.094594594594595,
7.432432432432433, 7.770270270270270, 8.108108108108109,
```

```
8.445945945945946, 8.783783783783784, 9.121621621621621,
9.459459459459460, 9.797297297297298, 10.135135135135135,
10.472972972972974, 10.810810810810811, 11.148648648648649,
11.486486486486486, 11.824324324324325, 12.162162162162163,
12.500000000000000, 12.837837837837839, 13.175675675675675,
13.513513513513514, 13.851351351351351, 14.189189189189189,
14.527027027027028, 14.864864864864865, 15.202702702702704,
15.540540540540540, 15.878378378378379, 16.216216216216218,
16.554054054054053, 16.891891891891891, 17.229729729729730};

     float frequency2[50] ={0.6993, 1.0490, 1.3986, 1.7483, 2.0979,
2.4476, 2.7972, 3.1469, 3.4965, 3.8462, 4.1958, 4.5455, 4.8951,
5.2448, 5.5944, 5.9441, 6.2937, 6.6434, 6.9930, 7.3427, 7.6923,
8.0420, 8.3916, 8.7413, 9.0909, 9.4406, 9.7902, 10.1399, 10.4895,
10.8392, 11.1888, 11.5385, 11.8881, 12.2378, 12.5874, 12.9371,
13.2867, 13.6364, 13.9860, 14.3357, 14.6853, 15.0350, 15.3846,
15.7343, 16.0839, 16.4336, 16.7832, 17.1329, 17.4825, 17.8322};

      float freq[50] = {2.421307506053263e+002, 4.842615012106525e+002,
7.263922518159787e+002, 9.685230024213050e+002, 1.210653753026631e+003,
1.452784503631958e+003, 1.694915254237284e+003, 1.937046004842610e+003,
2.179176755447936e+003, 2.421307506053262e+003, 2.663438256658589e+003,
2.905569007263915e+003, 3.147699757869241e+003, 3.389830508474568e+003,
3.631961259079894e+003, 3.874092009685220e+003, 4.116222760290546e+003,
0.358353510895872e+003, 4.600484261501199e+003, 4.842615012106525e+003,
5.084745762711851e+003,5.326876513317177e+003, 5.569007263922504e+003,
5.811138014527830e+003, 6.053268765133156e+003, 6.295399515738483e+003,
6.537530266343809e+003, 6.779661016949135e+003, 7.021791767554461e+003,
7.263922518159788e+003, 7.506053268765114e+003, 7.748184019370440e+003,
7.990314769975767e+003, 8.232445520581092e+003, 8.474576271186419e+003,
8.716707021791744e+003,8.958837772397072e+003, 9.200968523002397e+003,
9.443099273607724e+003, 9.685230024213050e+003, 9.927360774818377e+003,
1.016949152542370e+004, 1.041162227602903e+004, 1.065375302663436e+004,
1.089588377723968e+004, 1.113801452784501e+004, 1.138014527845033e+004};

 int numHarmonics=15;
   string waveInterim(" ");
```

```
   for(int i=0;i<numHarmonics; i++)
    {
     cout << setprecision (15) << "((" << "2*" << coefficent[i] << ")*"
    << "cos(2*pi*" << (freq[i]/680) << "*time" << "+" << phase[i] << "))"
    << "+";
     waveInterim=" ";
   }
      getch();
  }
```

C.2 C++ Code to Make Data Files Smaller

```
#include <iostream>
#include <fstream>

using namespace std;

int main()
{
    ifstream  stream1("Point_sensor_Aug1_nearmouthpiece2.dat");
    string line ;
    ofstream stream2("Point_sensor_Aug1_nearmouthpiece2_small.dat");

    int lineNumber = 0;

while( std::getline( stream1, line ) )
{
    if (lineNumber == 50)
    {
         stream2 << line << endl;
         cout << line << endl;
         lineNumber = 0;
    }
    lineNumber++;
```

```
}
       stream1.close();
    stream2.close();    return 0;
}
```

Appendix D

Procedure to Determine Volume Velocity

In this appendix, a procedure is outlined to determine an approximate functional form of the volume velocity required to generate a measured mouthpiece pressure. This assumes linearity, and that the simulation is close to being correct. The practicality of such a method is still being reviewed.

Variables are lower case for time domain, and uppercase for frequency domain.

* $p_m(t) <> P_m(\omega)$ measured acoustic pressure at the mouthpiece
* $q_m(t) <> Q_m(\omega)$ required volume velocity at the mouthpiece
* $h_{pq}(t) <> H_{pq}(\omega)$ pressure impulse response at mouthpiece when short (dirac) pulse of volume velocity is put into mouthpiece

If the pulse is quite short, say 10^{-5} seconds, then it will have a flat frequency response to about 100 kHz, for example. We can apply a pulse of low amplitude to keep things linear, and scale the measured response so that the pulse has unit area, for proper normalization. The idea is that the simulation can produce a reasonable approximation to $h_{pq}(t)$, thus we can calculate $H_{pq}(\omega)$. The measured mouthpiece pressure when blowing a note can be calculated from signal theory, which says that

$$p_m(t) = h_{pq}(t) * q_m(t), \tag{D.1}$$

where the ** denotes a convolution in time. In the frequency domain, this equation becomes

$$P_m(\omega) = H_{pq}(\omega)Q_m(\omega), \tag{D.2}$$

and since we know $P_m(\omega)$ and also $H_{pq}(\omega)$, we can get $Q_m(\omega)$ and hence its time function $q_m(t)$. Note that $p_m(t)$ is periodic, so we can use an Fourier transform based analysis. $q_m(t)$ will be periodic as well, but of course $h_{pq}(t)$ will have a length of many periods before the signal dies out. This much longer duration means that $H_{pq}(\omega)$ will be almost continuous in frequency. All this stuff will come out in the analysis, for which a number of decisions will have to be made. It really requires a signal-based frame of mind [52].

Appendix E

Derivation of Energy Simplification from Section 3.2.1

In this appendix, we will derive the energy expression (3.18) from section 3.2.1 in the thesis. Recall that we had the following system of equations

$$\frac{D\rho}{Dt} + \rho\nabla \cdot \vec{u} = 0, \tag{E.1}$$

$$\rho\frac{D\vec{u}}{Dt} = -\nabla \cdot p, \tag{E.2}$$

$$\rho c_p \frac{DT}{Dt} - \alpha T\frac{Dp}{Dt} = 0, \tag{E.3}$$

$$\alpha = -\frac{1}{\rho}(\frac{\partial\rho}{\partial T})_p = \frac{1}{T}, \tag{E.4}$$

$$P = \rho RT. \tag{E.5}$$

We now want to use the above equations to derive one partial differential equation that will describe the propagation of small amplitude sound waves. To begin, we substitute $T = \frac{p}{\rho R}$, $\gamma = \frac{c_p}{c_v}$ into the energy equation (E.3) to obtain

$$\rho c_p \frac{DT}{Dt} - \alpha T\frac{Dp}{Dt} = 0 \tag{E.6}$$

This can further be simplified to obtain

$$\rho\frac{Dp}{Dt} - \gamma p\frac{D\rho}{Dt} = 0. \tag{E.7}$$

To find (E.7), substitute $T = \frac{p}{\rho R}$ into (E.6) to obtain

$$\rho c_p \frac{\rho^2}{\rho^2}\frac{D}{Dt}\left(\frac{p}{\rho R}\right) - \alpha\left(\frac{p}{\rho R}\right)\frac{Dp}{Dt} = 0. \tag{E.8}$$

Expanding, and factoring $\frac{Dp}{Dt}$ gives

$$\rho c_p\left[\frac{1}{\rho R}\frac{Dp}{Dt} - \frac{p}{\rho^2 R}\frac{D\rho}{Dt}\right] - \alpha\frac{p}{\rho T}\frac{Dp}{Dt} = 0, \tag{E.9}$$

$$\frac{Dp}{Dt}\left(\frac{\rho c_p}{\rho} - \frac{\gamma p}{\rho}\right) - \frac{\rho p c_p}{\rho^2}\frac{D\rho}{Dt} = 0 \tag{E.10}$$

If we multiply by ρ and then substitute $\alpha = \frac{1}{T}$ into (E.10), we obtain

$$\rho\frac{Dp}{Dt}\left(c_p - \frac{p}{\rho T}\right) - p c_p\frac{D\rho}{Dt} = 0 \tag{E.11}$$

Substitute $R = \frac{p}{\rho T}$ into (E.11) as well as $c_p + c_v = R$ to find

$$\rho\frac{Dp}{Dt}c_v - p c_p\frac{D\rho}{Dt} = 0. \tag{E.12}$$

Finally, using the fact that $\gamma = \frac{c_p}{c_v}$, we find

$$\rho c_p\frac{DT}{Dt} - \gamma T\frac{Dp}{Dt} = 0, \tag{E.13}$$

as desired.

Appendix F

Derivation of Dimension Factor from Section 5.2.5

Consider the trumpet bell depicted in figure F.1, where the diameter of the bell is denoted by s (which is approximately 13 cm) and the radius of the bore is denoted by R (which is approximately 0.75 cm). Assuming that the sound wave has axial symmetry as it exits the bell, we can assume that the shape of sound pressure waveform will be the same across the arc denoted L. The radius of the arc will be denoted by r (which is approximately 8 cm) and the angle (between the arc and horizontal line centered in the trumpet bell) will be denoted as θ_0. The angle θ_0 can be found by considering the geometry of the problem. In particular,

$$\sin\theta_0 = \frac{s}{2r},$$

which approximately gives $\theta_0 = 0.9484$ radians or 54.43 degrees.

We want to estimate the area of the curved wave front (that is propagating out of the bell) between the second and third dimension. Let us first consider this approximation in two dimensions. The area of the circular bore (denoted by A_b) can be expressed as $A_b = \pi R^2$. However, for the two dimensional simulation, this area (denoted by A_s) must be approximated by a rectangle; in particular, $A_s = W2R$, where $W = \frac{A_b}{2R} = \frac{R\pi}{2}$. To determine the arc length of the entire two dimensional sector drawn in the diagram, denoted by $2L$, recall that when θ is in radians

$$2L = 2\int_0^{\theta_0} r d\theta = 2r\theta_0. \tag{F.1}$$

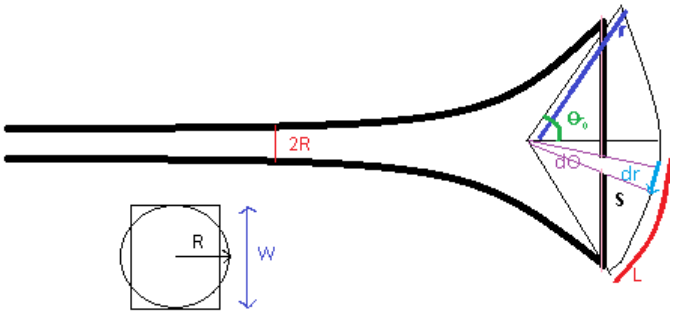

Figure F.1: Trumpet bell in two dimensions. Notice that in order to approximate the bore with radius R, we would have to use a square with height W.

Therefore, the area of the bell in two dimensions, denoted by A_2, can be written as

$$A_2 = 2LW = 2Wr\theta_0. \tag{F.2}$$

Now considering the analogous problem in three dimensions, the area at the end of the cap, denoted by A_3, can be found by integrating a slice of our sector (as shown in the picture in purple)

$$A_3 = 2\int_0^{\theta_0} 2\pi r^2 \sin(\theta) d\theta = 2\pi r^2[1 - \cos(\theta_0)]. \tag{F.3}$$

Notice that as $\theta_0 \to \pi$, $A_3 \to 4\pi r^2$ as one would expect. If we now consider the ratio $\frac{A_2}{A_3}$, we obtain the following

$$\begin{aligned} \frac{A_2}{A_3} &= \frac{2Wr\theta_0}{2\pi r^2[1 - \cos(\theta_0)]}, \\ &= \frac{R\theta_0}{2r[1 - \cos(\theta_0)]}, \\ &\approx 0.1066. \end{aligned} \tag{F.4}$$

Since in reality a wave front exiting the bell of a trumpet will do so with a certain amount of energy, we will assume that this energy is conserved between the second and third dimension. Thus, by conservation of energy we have

$$
\begin{aligned}
A_3 p_3^2 &= A_2 p_2^2, \\
\left(\frac{p_2}{p_3}\right) &= \sqrt{\frac{A_3}{A_2}}, \\
\frac{p_2}{p_3} &\approx 3.1.
\end{aligned}
\tag{F.5}
$$

Therefore, we speculate that neglecting the third dimension in our simulations could produce an amplitude that is 3.1 times larger than it should be.

Bibliography

[1] Acheson, David J. (**2009**). *Elementary Fluid Dynamics* (Clarendon, Oxford).

[2] Adachi, S. (**2009**) 'Principles of Sound Production in Wind Instruments,' Acoustic Society and Technology **25.5**, 400-05.

[3] Backus, J., Hundley, T. C. (**1971**). 'Harmonic generation in the trumpet,' J. Acoust. Soc. Am. **49**, 509-519.

[4] Babuska, I., B.Q. Guo (**1992**). 'The h, p and h-p version of the finite element method: basis theory and applications,' Advances in Engineering Software, **15**, Issue 3-4.

[5] Benade, A. H. (**1900**). *Fundamentals of Musical Acoustics* (Dover Publications, New York)

[6] Benade, A. H., and D.H. Keefe (**1983**). 'Wave propagation in strongly curved ducts,' J. Acoust. Soc. Am. **74**, 320-332.

[7] Beranek, L. (**1986**). *Acoustics* (Published by the American Institute of Physics for the Acoustical Society of America, New York, NY)

[8] Blackstock, D. T., Hamilton, M. F., and Pierce, A. D. (**1998**). *Nonlinear Acoustics*, edited by M. F. Hamilton and D. T. Blackstock (Academic, San Diego).

[9] Bilbao, S. (**2012**). Personal conversation, *University of Edinburgh*.

[10] Billingham, J., and A. C. K. (**2001**). *Wave Motion*. (Cambridge UP, Cambridge)

[11] Cabelli, A. (**1979**). 'The Acoustic Characteristics of Duct Bends.' J. Sound and Vibration **68**, 369-88.

[12] Campbell D. M. (**1999**). 'Nonlinear dynamics of musical reed and brass wind instruments,' Contemporary Physics. **114**, 415-431.

[13] Cockburn, B. (**2003**). 'Discontinuous galerkin methods.' ZAMM Journal of Applied Mathematics and Mechanics **83**, 731-754.

[14] Cockburn, B., Karniadakis, G., and Chi-Wang Shu. (**2000**). 'The development of discontinuous Galerkin methods.' UMSI research report/University of Minnesota (Minneapolis, Mn).

[15] Gilbert, J., Campbell, D. M., Myers, A., and Pyle, R. W. (**2007**). 'Differences between brass instruments arising from variations in brassiness due to nonlinear propagation,' ISMA.

[16] *Music and Computers.* $< www.music.columbia.edu/cmc/musicandcomputers/ >$.

[17] Churchhill, R. V. (**1963**). *Fourier Series and Boundary Value Problems*, 2nd ed. (McGraw-Hill Inc., New York).

[18] Connor, D. (**2012**). Personal conversation, *University of Waterloo.*

[19] Elliott, S.J., and J.M. Bowsher (**1982**). 'Regeneration in brass wind instrument' J. Sound and Vibration, **83**, 181-217.

[20] Enflo, B. O., and Hedberg, C. M. (**2002**). *Theory of Nonlinear Acoustics in Fluids* (Kluwer Academic, Dordrecht).

[21] Feynman, R. (**1900**). *The Feynman Lectures on Physics* (California).

[22] Fletcher, N.H. (**1998**). 'The nonlinear physics of musical instruments' Rep. Prog. Phys. **62**, 723-765.

[23] Fletcher, N. H., and A. Tarnopolsky. (**1998**). 'Blowing pressure, power, and spectrum in trumpet playing,' J. Acoust. Soc. Am. **105**, 874-881.

[24] Fletcher, N. H., and Rossing, T. D. (**1991**). *The Physics of Musical Instruments* (Springer-Verlag, New York), pp. 183-194.

[25] French, A. P. (**1971**). *Vibrations and Waves* (W.W Norton and Company, New York).

[26] Gilbert, J., Dalmont, J., and Guimezanes, T. (**2005**). 'Nonlinear wave propagation in woodwinds,' Forum Acusticum, Budapest, 1369-1372.

[27] Godlewski, E., Raviart, P. A. (**1996**). *Numerical Approximation of Hyperbolic Systems of Conservation Laws*, Volume 118 (Springer, New York).

[28] Haberman, R. (**2004**). *Applied Partial Differential Equations with Fourier Series and Boundary Value Problems* (Pearson Prentice Hall, Upper Saddle River, N.J).

[29] Hirschberg, A. J., Gilbert, J., Msallam, R., and Wijnands, A. P. J. (**1995**). 'Shock waves in trombones,' J. Acoust. Soc. Am. **99**, 1754-1758.

[30] Hirschberg, A. J., Gilbert, J., and Wijnands, A. P. J. (**1994**). 'Musical aero-acoustics of the clarinet,' J. De Physique. **44**, 559-568.

[31] Hopkin, B. (**1996**). *Musical Instrument Design Practical Information for Instrument Making* (New York).

[32] Johns Hopkins University, http://www.jhu.edu, Maryland.

[33] Kausel, W., and Moore, T. (**2010**). 'Influence of wall vibrations on the sound of brass wind instruments', Universitat fur Musik und darstellende Kunst Weiin, 1-46.

[34] Krivadonova, L. (**2012**). Personal conversation, *University of Waterloo.*

[35] Kundu, P. K., Cohen, I. M. (**2008**). *Fluid Mechanics*, 4th ed. (Elsevier Inc., London, UK).

[36] Liepmann, H. W., and A. Roshko. (**2001**). *Elements of Gasdynamics* (Dover Publications, Mineola, NY).

[37] *Math Works* $< http://www.mathworks.com/ >$.

[38] Munson, B. R., Donald F. Y., and Theodore H. O. (**2005**). *Fundamentals of Fluid Mechanics* (Wiley, New York).

[39] Naugolnykh, K., and L. A. Ostrovskii. (**1998**). *Nonlinear Wave Processes in Acoustics.* (Cambridge University Press, Cambridge) .

[40] Nederveen, C. J. (**1998**). 'Influence of a toroidal bend on wind instrument turning,' J. Acoust. Soc. Am. **104**, 1616-1626.

[41] Official NASA website.

[42] Olson, H. F. (**1980**). *Music, Physics and Engineering.* 2nd ed. (Dover Publications,New York).

[43] Pandya, B. H., Settles, G. S., and Miller, J. D. (**2003**). 'Schlieren imaging of shock waves in a trumpet,' J. Acoust. Soc. Am. **114**, 3363-3367.

[44] Pyle, R. (**2010**). *The influence of mouthpiece cup shape on brassiness* (University of Music and Performing Arts Wienna, Austria).

[45] Qin, R. (**2012**). Personal conversation, *University of Waterloo.*

[46] Rayleigh, J. W. S., and Robert B. Lindsay. (**1976**). *The Theory of Sound, Volume One Unabridged Second Revised Edition* (Dover Publications, Minneapolis).

[47] Rayleigh, J. W. S., and Robert B. Lindsay. (**1976**). *The Theory of Sound, Volume Two (Dover Classics of Science and Mathematics)* (Dover Publications, Minneapolis).

[48] Rendon, P. L., Narezo, D., Bustamante, F. O., and Lopez, A. P. (**2009**). 'Nonlinear progressive waves in a slide trombone resonator,' J. Acoust. Soc. Am. **127**, 1096-1103.

[49] Schlichting, Hermann. (**1979**). *Boundary Layer Theory*, 7th ed. (McGraw-Hill Book, New York).

[50] 'Sound.' *ThinkQuest < library.thinkquest.org/C*005705/*English/sound/history.htm >*

[51] Thompson, M. W., and Strong, W. J. (**2001**). 'Inclusion of wave steepening in a frequency-domain model of trombone sound production,' J. Acoust. Soc. Am. **110**, 556-562.

[52] Vanderkooy, J. (**2012**). Personal conversation, *University of Waterloo.*

[53] Waite, M. (**2012**). AMATH 663 class, *University of Waterloo.*

[54] Warburton, T., and Hesthaven, J. S. (**2008**). *Nodal Discontinuous Galerkin Methods: Algorithms, Analysis, and Applications* (Springer, New York).

[55] Wolfe, J. 'Brass Instrument Acoustics An Introduction'. *Brass Instrument (lip Reed) Acoustics: An Introduction. < www.phys.unsw.edu.au/jw/brassacoustics.html > .*